

# Spectroscopic characterization of a series of aryl Schiff bases and their potential use for targeting DNA

Master's thesis in Master Programme of Nanotechnology

SMARAGDA-MARIA ARGYRI



MASTER'S THESIS 2019

# Spectroscopic characterization of a series of aryl Schiff bases and their potential use for targeting DNA

Master thesis in Master Programme of Nanotechnology

SMARAGDA-MARIA ARGYRI



Department of Chemistry and Chemical Engineering  
*Division of Chemistry and Biochemistry*  
Wilhelmsson Group  
CHALMERS UNIVERSITY OF TECHNOLOGY  
Gothenburg, Sweden 2019

Spectroscopic characterization of a series of aryl Schiff bases and their potential use for targeting DNA  
Master thesis in Master Programme of Nanotechnology

© SMARAGDA-MARIA ARGYRI, 2019.

Supervisor and Examiner: Marcus Wilhelmsson, Department of Chemistry and Chemical Engineering

Master's Thesis 2019  
Department of Chemistry and Chemical Engineering  
Division of Chemistry and Biochemistry  
Wilhelmsson Group  
Chalmers University of Technology  
SE-412 96 Gothenburg  
Telephone +46 31 772 1000

Cover: Representative isomerization spectrum of compound **8**, 15  $\mu\text{M}$ , 5%DMSO (left down), general chemical structure of compounds utilized in this study (middle) and simplified general structure of a DNA nucleotide (up right) designed *via* ChemDraw Pro 12.1 Software.

Typeset in L<sup>A</sup>T<sub>E</sub>X  
Gothenburg, Sweden 2019

Spectroscopic characterization of a series of aryl Schiff bases and their potential use for targeting DNA

Smaragda-Maria Argyri

Department of Chemistry and Chemical Engineering

Division of Chemistry and Biochemistry

Chalmers University of Technology

## Abstract

Schiff bases are a class of chemical compounds that are considered promising therapeutic agents, mainly due to their antimicrobial [1, 2], antioxidant [2, 3], and anticancer [4, 5] properties. Also, structural modifications can easily be attained, *via* straightforward condensation reactions with ketones or aldehydes. [2], [5] The therapeutic properties are attributed to the imine functional group ( $-C=N-$ ), but also to subsequent functional groups attached to the Schiff bases, such as: methyl ( $-CH_3$ ), carbonyl ( $C=O$ ), hydroxyl ( $-OH$ ), amine ( $-NH_2$ ) and other functional groups, [Hodnett, Ernest M., and William J. Dunn. 1970 [6]. Additionally, different structural characteristics of the compounds (*e.g.* size, charge and flatness of the surface etc.) have been studied [7–9]. However, the mechanism of action has not yet been determined. [10] Many researchers connect the biological activity to possible DNA binding interactions [2], [4], [11–14], which was the starting point of this study. The Institute of Nanoscience and Nanotechnology of the National Centre of Scientific Research (NCSR) “Demokritos”, Athens, Greece, generously provided a series of Schiff bases. The DNA interactions of these compounds were to be studied in order to determine their potential as DNA-targeting probes [10] or drugs. To achieve this, UV-vis spectroscopy, fluorescence spectroscopy and linear dichroism were utilized. During the experiments it was observed that the compounds undergo a chemical transformation when the chemical environment changes polarity. The effect that this transformation has on the DNA binding properties of this class of compounds is something that has not been documented in the literature before. So, besides the potential DNA binding, the transformation kinetics, the thermodynamical equilibrium and the chemical structure of the compounds, *via* spectroscopic techniques as well as NMR spectroscopy (H-NMR, C-NMR, and HSQC-NMR) were performed. The NMR analysis suggests that a *trans* to *cis* isomerization (with respect to the  $C=N$  double-bond) occurs upon going from a less polar (DMSO) to a more polar (EtOH) solvent. This result is also in line with the spectroscopic evaluation. Linear dichroism spectroscopy showed very slow and weak binding, likely *via* intercalation. Based on these results we propose that the *trans* isomer is the DNA-binding isomeric form and that the slow binding kinetics are attributed to the isomeric distribution in aqueous solution being shifted significantly towards the non-DNA binding *cis*-form.

Keywords: DNA binding, *cis* - *trans* isomerization, DNA ligands, UV-vis spectroscopy, Fluorescence, Linear Dichroism.



# Acknowledgements

Ἐν βυθῷ γάρ ἡ ἀλήθεια.  
-Δημόκριτος (470-370 π.Χ.)

First and foremost I would like to express my gratitude to my thesis supervisor and examiner Dr. Marcus Wilhelmsson for giving me the opportunity to work as part of his research group. Thank you for sharing your expertise and for allowing me to learn from my mistakes. I am also grateful for the daily support and effort provided by Dr. Jesper Nilsson. Thank you for the encouragement and for believing in me. It has been amazing working with you.

I would also like to thank the research group of Dr. Papadopoulos Kyriakos, Institute of Nanoscience and Nanotechnology, NCSR “Demokritos”, Athens, Greece and especially Dr. Marios Krokidis for coming in contact and being open in this collaboration. This project would not have been executed without the generous contribution of the compounds.

Acknowledgement should be attributed to Maria Gunnarsson for the assistance she provided during the execution and evaluation of NMR spectroscopy measurements and results. Thank you for taking the time and for sharing your knowledge and experience. And thank you Per Lincoln for the fruitful discussion regarding DNA binding.

Finally, I would like to express my gratitude to my family for the life lessons, the encouragement and for believing in me even in the toughest of moments. Of course, to all the friends I made here in Sweden, I would to say thank you, for all the valuable memories and the way we grew bigger together. Oh! And thanks Davide!

Tack alla så mycket!

Smaragda-Maria Argyri, Gothenburg, 06 2019



# Contents

<b>List of Figures</b>	<b>xi</b>
<b>List of Tables</b>	<b>xvii</b>
<b>List of Abbreviations</b>	<b>xix</b>
<b>1 Introduction</b>	<b>1</b>
1.1 DNA structure . . . . .	1
1.2 DNA binding . . . . .	3
1.3 Schiff Bases . . . . .	5
1.3.1 Keto-enol tautomerism . . . . .	7
1.3.2 Cis-trans isomerization . . . . .	7
1.4 Aim and Objectives . . . . .	8
<b>2 Theory</b>	<b>9</b>
2.1 Spectroscopy . . . . .	9
2.2 Jablonski diagram . . . . .	9
2.2.1 Absorption . . . . .	10
2.2.2 Fluorescence . . . . .	10
2.2.3 Linear dichroism . . . . .	11
2.3 DNA binding . . . . .	11
2.4 Activation Energy . . . . .	12
<b>3 Materials and Methods</b>	<b>13</b>
3.1 Compounds . . . . .	13
3.1.1 Stock solution preparation . . . . .	14
3.2 Buffer preparation . . . . .	14
3.3 DNA preparation . . . . .	14
3.4 UV-Vis absorption instrumentation . . . . .	14
3.5 Fluorescence spectroscopy instrumentation . . . . .	14
3.6 Nuclear Magnetic Resonance (NMR) . . . . .	15
3.7 Linear Dichroism . . . . .	15
<b>4 Results and Discussion</b>	<b>17</b>
4.1 Schiff base solubility in up to 5% DMSO . . . . .	17
4.2 Emission of Schiff bases . . . . .	18
4.3 Initial screen for DNA binding . . . . .	19

4.4	Molar absorptivity . . . . .	20
4.5	Kinetics of molecular transition upon dilution into buffer . . . . .	21
4.6	Solvent effects . . . . .	23
4.7	Nuclear Magnetic Resonance . . . . .	24
4.7.1	<sup>1</sup> H-NMR of Schiff base <b>15</b> in different solvents . . . . .	25
4.7.2	<sup>13</sup> C-NMR of Schiff base <b>15</b> in different solvents . . . . .	25
4.7.3	Heteronuclear Single Quantum Coherence (HSQC) of Schiff base <b>15</b> in different solvents . . . . .	26
4.8	Activation energy of <i>trans-cis</i> -transformation of <b>15</b> when going from DMSO to buffer . . . . .	27
4.9	DNA binding of <b>15</b> . . . . .	28
4.9.1	Kinetics of DNA binding of <b>15</b> studied with fluorescence spectroscopy . . . . .	29
4.9.2	DNA binding of <b>15</b> studied with linear dichroism . . . . .	29
4.9.3	Ethidium bromide displacement . . . . .	31
<b>5</b>	<b>Conclusion</b> . . . . .	<b>33</b>
5.1	Future work . . . . .	33
<b>A</b>	<b>Appendix</b> . . . . .	<b>I</b>
A.1	Schiff bases . . . . .	I
A.2	UV-Vis spectra of compounds in 0.2% DMSO . . . . .	II
A.3	Compounds not Soluble in 5% DMSO . . . . .	VII
A.4	Absorption Kinetics . . . . .	VIII
A.5	Absorption Emission . . . . .	XIII
A.6	Molar absorptivity . . . . .	XIV
A.7	Nuclear Magnetic Resonance . . . . .	XIV
A.8	DNA binding . . . . .	XVII
A.8.0.1	Emission Kinetics of compound <b>15</b> . . . . .	XVII
A.8.1	Linear Dichroism Spectra . . . . .	XIX

# List of Figures

1.1	Chemical structure of nucleotide, here exemplified by deoxyadenosine monophosphate. . . . .	1
1.2	Chemical structure of DNA nucleotides . . . . .	2
1.3	3D model of DNA structure [15] . . . . .	3
1.4	Main non-covalent DNA binding modes [16] . . . . .	4
1.5	General chemical structure of imines . . . . .	6
1.6	Keto-enol tautomerism . . . . .	7
1.7	Cis-trans tautomerism . . . . .	8
2.1	Jablonski diagram illustrating electronic transitions in a molecule . .	10
2.2	a) LD spectroscopy illustration, b) oriented sample . . . . .	11
3.1	Chemical Structures of the compounds utilized in this study . . . . .	13
4.1	Absorption (red line) and emission (black line) spectra of compound <b>14</b> , 15 $\mu\text{M}$ , 0.2% <i>DMSO</i> . . . . .	18
4.2	Absorption spectrum of <b>15</b> (14.7 $\mu\text{M}$ , 5% <i>DMSO</i> in 50 <i>mM</i> Tris-HCl (100 <i>mM</i> NaCl) buffer) with and without DNA (50 $\mu\text{M}$ ) present. Note that the spectrum of <b>15</b> without DNA was collected before the thermal equilibrium had established. . . . .	19
4.3	Isothermal kinetics of compound <b>15</b> , 20 $\mu\text{M}$ , in 50 <i>mM</i> Tris-HCl (100 <i>mM</i> NaCl) and 5% <i>DMSO</i> . . . . .	20
4.4	Absorption with respect to concentration . . . . .	21
4.5	Molecular transition of <b>15</b> (20 $\mu\text{M}$ ) in 0.1% <i>DMSO</i> monitored using UV-vis spectroscopy at room temperature ( <i>ca.</i> 22°C) immediately after compound addition from a concentrated <i>DMSO</i> stock into aqueous buffer. Left panel: Temporal spectral evolution. Right panel: Absorption at 336 <i>nm</i> (black squares) as a function of time. A first-order exponential fit (red line) rendered a time constant ( $\tau = 3.2 \text{ min}$ ) for the reaction. . . . .	22
4.6	Molecular transition of <b>15</b> (20 $\mu\text{M}$ ) in 50 <i>mM</i> Tris-HCl (100 <i>mM</i> NaCl), 5% <i>DMSO</i> monitored using UV-vis spectroscopy at room temperature ( <i>ca.</i> 22°C) immediately after compound addition from a concentrated <i>DMSO</i> stock into aqueous buffer. Left panel: Temporal spectral evolution. Right panel: Absorption at 336 <i>nm</i> (black squares) as a function of time. A first-order exponential fit (red line) rendered a time constant ( $\tau = 6.8 \text{ min}$ ) for the reaction. . . . .	22

---

4.7	Molecular transition of <b>15</b> (50 $\mu\text{M}$ ) in Acetonitrile monitored using UV-vis spectroscopy at room temperature ( <i>ca.</i> 22°C) immediately after compound addition from a concentrated DMSO stock into the solvent ([DMSO] = 0.5%). Left panel: Absorption spectra (no changes were recorded over time). Right panel: Absorption at 350 nm (black squares) as a function of time. . . . .	23
4.8	Molecular transition of <b>15</b> (50 $\mu\text{M}$ ) in Ethanol monitored using UV-vis spectroscopy at room temperature ( <i>ca.</i> 22°C) immediately after compound addition from a concentrated DMSO stock into the solvent ([DMSO] = 0.5%). Left panel: Temporal spectral evolution. Right panel: Absorption at 350 nm (black squares) as a function of time. . . . .	23
4.9	Molecular transition of <b>15</b> (50 $\mu\text{M}$ ) in ultra purified, MQ-water (not Tris-HCl buffer) monitored using UV-vis spectroscopy at room temperature ( <i>ca.</i> 22°C) immediately after compound addition from a concentrated DMSO stock into the solvent ([DMSO] = 0.5%). Left panel: Temporal spectral evolution. Right panel: Absorption at 350 nm (black squares) as a function of time. . . . .	24
4.10	Proton NMR comparison of compound <b>15</b> in two different solvents . . . . .	25
4.11	Carbon NMR comparison of compound <b>15</b> in two different solvents . . . . .	26
4.12	HSQC-NMR of compound <b>15</b> in DMSO (red) and ethanol (green) . . . . .	27
4.13	Arrhenius plot of compound <b>15</b> utilized for the determination of the activation energy $E_a$ from the slope of equation 2.7 . . . . .	28
4.14	Left: Emission intensity spectrum of pre-equilibration of compound <b>15</b> , and at different time points after addition of ctDNA. Right: Emission kinetics spectrum of adding compound <b>15</b> first, C=15 $\mu\text{M}$ . . . . .	29
4.15	Left: LD spectra of solutions with 200 $\mu\text{M}$ ctDNA and 100 $\mu\text{M}$ of compound <b>15</b> after different times. Right: Magnified image of LD spectra illustrated on the left panel, wavelength range from 320 nm to 500 nm . . . . .	30
4.16	Ethidium bromide displacement from DNA upon adding compound <b>15</b> . . . . .	31
A.1	Absorption spectrum of compound <b>1</b> , 10 $\mu\text{M}$ at 0.2% DMSO . . . . .	II
A.2	Absorption spectrum of compound <b>5</b> , 10 $\mu\text{M}$ at 0.2% DMSO . . . . .	II
A.3	Absorption spectrum of compound <b>8</b> , 10 $\mu\text{M}$ at 0.2% DMSO . . . . .	III
A.4	Absorption spectrum of compound <b>9</b> , 10 $\mu\text{M}$ at 0.2% DMSO . . . . .	III
A.5	Absorption spectrum of compound <b>12</b> , 10 $\mu\text{M}$ at 0.2% DMSO . . . . .	IV
A.6	Absorption spectrum of compound <b>14</b> , 10 $\mu\text{M}$ at 0.2% DMSO . . . . .	IV
A.7	Absorption spectrum of compound <b>17</b> , 10 $\mu\text{M}$ at 0.2% DMSO . . . . .	V
A.8	Absorption spectrum of compound <b>23</b> , 10 $\mu\text{M}$ at 0.2% DMSO . . . . .	V
A.9	Absorption spectrum of compound <b>24</b> , 10 $\mu\text{M}$ at 0.2% DMSO . . . . .	VI
A.10	Absorption spectrum of compound <b>26</b> , 10 $\mu\text{M}$ at 0.2% DMSO . . . . .	VI
A.11	Absorption spectrum of compound <b>28</b> , 10 $\mu\text{M}$ at 0.2% DMSO . . . . .	VII
A.12	Absorption spectrum of compound <b>23</b> , 20 $\mu\text{M}$ at 5% DMSO . . . . .	VII
A.13	Absorption spectrum of compound <b>24</b> , 15 $\mu\text{M}$ at various percentages of DMSO . . . . .	VIII

- A.14 Molecular transition of compound **1** (10  $\mu\text{M}$ ) in 5% DMSO monitored using UV-vis spectroscopy at room temperature (*ca.* 22°C) immediately after compound addition from a concentrated DMSO stock into 50 *mM* Tris-HCl (100 *mM* NaCl) buffer. Left panel: Temporal spectral evolution. Right panel: Absorption at 353 *nm* (black squares) as a function of time. A first-order exponential fit (red line) rendered a time constant ( $\tau = 18.301 \text{ min}$ ) for the reaction. . . . . VIII
- A.15 Molecular transition of compound **5** (10  $\mu\text{M}$ ) in 5% DMSO monitored using UV-vis spectroscopy at room temperature (*ca.* 22°C) immediately after compound addition from a concentrated DMSO stock into 50 *mM* Tris-HCl (100 *mM* NaCl) buffer. Left panel: Temporal spectral evolution. Right panel: Absorption at 322 *nm* (black squares) as a function of time. A first-order exponential fit (red line) rendered a time constant ( $\tau = 9.963 \text{ min}$ ) for the reaction. . . . . IX
- A.16 Molecular transition of compound **8** (10  $\mu\text{M}$ ) in 5% DMSO monitored using UV-vis spectroscopy at room temperature (*ca.* 22°C) immediately after compound addition from a concentrated DMSO stock into 50 *mM* Tris-HCl (100 *mM* NaCl) buffer. Left panel: Temporal spectral evolution. Right panel: Absorption at 343 *nm* (black squares) as a function of time. A first-order exponential fit (red line) rendered a time constant ( $\tau = 21.3751 \text{ min}$ ) for the reaction. . . . . IX
- A.17 Molecular transition of compound **9** (10  $\mu\text{M}$ ) in 5% DMSO monitored using UV-vis spectroscopy at room temperature (*ca.* 22°C) immediately after compound addition from a concentrated DMSO stock into 50 *mM* Tris-HCl (100 *mM* NaCl) buffer. Left panel: Temporal spectral evolution. Right panel: Absorption at 345 *nm* (black squares) as a function of time. A first-order exponential fit (red line) rendered a time constant ( $\tau = 17.473 \text{ min}$ ) for the reaction. . . . . X
- A.18 Molecular transition of compound **12** (10  $\mu\text{M}$ ) in 5% DMSO monitored using UV-vis spectroscopy at room temperature (*ca.* 22°C) immediately after compound addition from a concentrated DMSO stock into 50 *mM* Tris-HCl (100 *mM* NaCl) buffer. Left panel: Temporal spectral evolution. Right panel: Absorption at 340 *nm* (black squares) as a function of time. A first-order exponential fit (red line) rendered a time constant ( $\tau = 11.972 \text{ min}$ ) for the reaction. . . . . X
- A.19 Molecular transition of compound **13** (10  $\mu\text{M}$ ) in 0.1% DMSO monitored using UV-vis spectroscopy at room temperature (*ca.* 22°C) immediately after compound addition from a concentrated DMSO stock into 50 *mM* Tris-HCl (100 *mM* NaCl) buffer. Left panel: Temporal spectral evolution. Right panel: Absorption at 369 *nm* (black squares) as a function of time. A first-order exponential fit (red line) rendered a time constant ( $\tau = 4.094 \text{ min}$ ) for the reaction. . . . . XI

- A.20 Molecular transition of compound **13** ( $10 \mu\text{M}$ ) in 5% DMSO monitored using UV-vis spectroscopy at room temperature (*ca.*  $22^\circ\text{C}$ ) immediately after compound addition from a concentrated DMSO stock into  $50 \text{ mM}$  Tris-HCl ( $100 \text{ mM}$  NaCl) buffer. Left panel: Temporal spectral evolution. Right panel: Absorption at  $369 \text{ nm}$  (black squares) as a function of time. A first-order exponential fit (red line) rendered a time constant ( $\tau = 8.515 \text{ min}$ ) for the reaction. . . . . XI
- A.21 Molecular transition of compound **17** ( $15 \mu\text{M}$ ) in 5% DMSO monitored using UV-vis spectroscopy at room temperature (*ca.*  $22^\circ\text{C}$ ) immediately after compound addition from a concentrated DMSO stock into  $50 \text{ mM}$  Tris-HCl ( $100 \text{ mM}$  NaCl) buffer. Left panel: Temporal spectral evolution. Right panel: Absorption at  $319 \text{ nm}$  (black squares) as a function of time. A first-order exponential fit (red line) rendered a time constant ( $\tau = 9.743 \text{ min}$ ) for the reaction. . . . . XII
- A.22 Molecular transition of compound **26** ( $10 \mu\text{M}$ ) in 5% DMSO monitored using UV-vis spectroscopy at room temperature (*ca.*  $22^\circ\text{C}$ ) immediately after compound addition from a concentrated DMSO stock into  $50 \text{ mM}$  Tris-HCl ( $100 \text{ mM}$  NaCl) buffer. Left panel: Temporal spectral evolution. Right panel: Absorption at  $282 \text{ nm}$  (black squares) as a function of time. A first-order exponential fit (red line) rendered a time constant ( $\tau = 10.592 \text{ min}$ ) for the reaction. . . . . XII
- A.23 Molecular transition of compound **28** ( $10 \mu\text{M}$ ) in 5% DMSO monitored using UV-vis spectroscopy at room temperature (*ca.*  $22^\circ\text{C}$ ) immediately after compound addition from a concentrated DMSO stock into  $50 \text{ mM}$  Tris-HCl ( $100 \text{ mM}$  NaCl) buffer. Left panel: Temporal spectral evolution. Right panel: Absorption at  $276 \text{ nm}$  (black squares) as a function of time. A first-order exponential fit (red line) rendered a time constant ( $\tau = 14.951 \text{ min}$ ) for the reaction. . . . . XIII
- A.24 Proton NMR integration of peaks . . . . . XIV
- A.25 Carbon NMR chemical shift maximized . . . . . XV
- A.26 Left panel: Emission kinetics adding DNA prior to compound **15** addition (*i.e.* "DNA first"),  $15 \mu\text{M}$ , exciting at  $\lambda_{exc} = 393 \text{ nm}$  and recording emission at  $\lambda_{em} = 512 \text{ nm}$ . Right panel: Emission spectra at: time 0 (before the emission kinetics recording started, black line),  $120 \text{ min}$  after the emission kinetics initiated (red line) and after  $228 \text{ min}$  (endpoint, blue line). Emission peak at  $\lambda_{em} = 512 \text{ nm}$  . . . XVII

- A.27 Left panel: Emission spectra: *i*) black line: only compound **15** was present in 50 mM Tris HCl (100 mM NaCl) buffer. Emission peak at  $\lambda_{em} = 512 \text{ nm}$ , *ii*) red line: only compound **15** in buffer after thermodynamical equilibrium was established ( $t = 185 \text{ min}$ , Shift in emission peak is observed from  $\lambda_{em} = 512 \text{ nm}$  to  $\lambda_{em} = 501 \text{ nm}$ , *iii*) blue line: 200  $\mu\text{M}$  of DNA was added. No changes in emission intensity are observed. Emission peak at  $\lambda_{em} = 501 \text{ nm}$ , *iv*) after linear dichroism spectroscopy took place (approximately 200 min after DNA was added in solution. Emission peak at  $\lambda_{em} = 501 \text{ nm}$ . Right panel: Emission kinetics adding compound **15**, 100  $\mu\text{M}$  prior to DNA addition, exciting at  $\lambda_{exc} = 393 \text{ nm}$  and recording at  $\lambda_{em} = 512 \text{ nm}$  . XVII
- A.28 Left panel: Emission kinetics adding 200  $\mu\text{M}$  DNA, prior to 100  $\mu\text{M}$  (black line) and *ca.* 85  $\mu\text{M}$  (red line) of compound **15** addition. Exciting at  $\lambda_{exc} = 393 \text{ nm}$  and recording at  $\lambda_{em} = 512 \text{ nm}$ . The experiment was performed twice to confirm the repeatability of the results. The same pattern in emission intensity changes is recorded, as an initial increase and afterwards a gradual decrease in intensity is observed, until the thermodynamical equilibrium is established after *ca.* 100 min. Right panel: Emission intensity spectra of the two samples. The black and red lines correspond to the sample with concentration equal to 100  $\mu\text{M}$  of **15**, at time 0 (before the emission kinetics were initiated) and 230 min after the kinetics were initiated and the thermodynamical equilibrium was established (endpoint), respectively. Shift in emission peak from  $\lambda_{em} = 512 \text{ nm}$  to  $\lambda_{em} = 501 \text{ nm}$  and decrease in emission intensity are observed. The blue and green lines correspond to the sample with concentration equal to approximately 85  $\mu\text{M}$  of **15**, at time 0 (before the emission kinetics were initiated) and 140 min after the kinetics were initiated and the thermodynamical equilibrium was established (endpoint), respectively. Shift in emission peak from  $\lambda_{em} = 512 \text{ nm}$  to  $\lambda_{em} = 501 \text{ nm}$  and decrease in emission intensity are observed. . . . . XVIII
- A.29 Absorption and LD spectra of compound **15**, 100  $\mu\text{M}$  adding 200  $\mu\text{M}$  DNA prior to compound addition. Left panel: Shift in absorption is observed 2 days after the sample was prepared. Right panel: Magnified image of LD spectra illustrated on the left panel, wavelengths range from 320 nm to 410 nm . . . . . XIX
- A.30 Absorption and LD spectra of compound **5**, 15  $\mu\text{M}$ , in Tris-HCl buffer, 5% DMSO and 200  $\mu\text{M}$  of DNA . . . . . XIX
- A.31 Absorption and LD spectra of compound **8**, 15  $\mu\text{M}$ , in Tris-HCl buffer, 5% DMSO and 200  $\mu\text{M}$  of DNA . . . . . XX
- A.32 Absorption and LD spectra of compound **9**, 15  $\mu\text{M}$ , in Tris-HCl buffer, 5% DMSO and 200  $\mu\text{M}$  of DNA . . . . . XX
- A.33 Absorption and LD spectra of compound **13**, 15  $\mu\text{M}$ , in Tris-HCl buffer, 5% DMSO and 200  $\mu\text{M}$  of DNA . . . . . XXI
- A.34 Absorption and LD spectra of compound **28**, 15  $\mu\text{M}$ , in Tris-HCl buffer, 5% DMSO and 200  $\mu\text{M}$  of DNA . . . . . XXI



# List of Tables

4.1	Absorption values of compound <b>15</b> at absorption peak ( $\lambda = 398 \text{ nm}$ ) in different concentrations . . . . .	21
4.2	Ethidium bromide displacement of compound <b>15</b> comparison with literature . . . . .	32
A.1	Chemical name and Molecular weight of compounds used . . . . .	I
A.2	Fluorescent properties of all compounds . . . . .	XIII
A.3	Molar absorptivity values for compounds <b>9, 14, 17 26, 28</b> . . . . .	XIV
A.4	Carbon and HSQC NMR peak values for compound <b>15</b> in DMSO . .	XV
A.5	Carbon and HSQC NMR peak values for compound <b>15</b> in ethanol . .	XVI



# List of Abbreviations

<b>Co(II)</b>	Cobalt cation ( $\text{Co}^{2+}$ )
<b>ctDNA</b>	Calf thymus DNA
<b>Cu(II)</b>	Copper cation ( $\text{Cu}^{2+}$ )
<b>DMSO</b>	Dimethyl sulphoxide
<b>DNA</b>	Deoxyribonucleic acid
<b>dsDNA</b>	Double strand DNA
<b>HPLC</b>	High Performance Liquid Chromatography
<b>HSQC</b>	Heteronuclear Single Quantum Coherence
<b>IR</b>	Infrared
$K_a$	Association constant
<b>LD</b>	Linear Dichroism
<b>Mo(IV)</b>	Molybdenum cation ( $\text{Mo}^{2+}$ )
<b>MQ-water</b>	Milli-Q water, © Merck KGaA
<b>MW</b>	Molecular weight
<b>Ni(II)</b>	Nickel cation ( $\text{Ni}^{2+}$ )
<b>NMR</b>	Nuclear Magnetic Resonance
<b>NOESY</b>	Nuclear Overhauser Effect Spectroscopy
<b>Pd(II)</b>	Palladium cation ( $\text{Pd}^{2+}$ )
<b>ppm</b>	Parts per milion
<b>Pt(II)</b>	Platinum cation ( $\text{Pt}^{2+}$ )
<b>RNA</b>	Ribonucleic acid
<b>Ru</b>	Ruthenium
<b>Vis</b>	Visible
<b>UV</b>	Ultraviolet
<b>Zn(II)</b>	Zinc cation ( $\text{Zn}^{2+}$ )
<b>Å</b>	Ångström



# 1

## Introduction

In living organisms, all the information related to the biological functions responsible for the maintenance of life is encoded in the genome. [17] Deoxyribonucleic acid (DNA) is a self-replicating macromolecule that carries all the information necessary for the formation of the building blocks of life, *i.e.* ribonucleic acid (RNA) and proteins. Various small molecules have the ability to interact with DNA, proteins and/or other biomolecules, acting as inhibitors, activators and/or labels and probes. Investigating the biological mechanisms and function of these small molecules is essential for drug and probe development.

### 1.1 DNA structure

DNA is a macromolecule consisting of a double helix made up of a sequence of nucleotides. Each nucleotide consists of a phosphate group, a sugar group (deoxyribose) and a nitrogenous species, more commonly known as a DNA base (Figure 1.1). The sugar and phosphate group create a repeating pattern that forms the DNA backbone, while the DNA sequence is determined by the particular order of DNA bases.

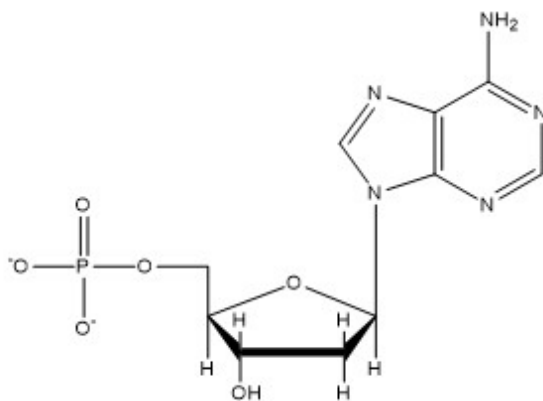


**Figure 1.1:** Chemical structure of nucleotide, here exemplified by deoxyadenosine monophosphate.

There are four different DNA bases: adenine (A), thymine (T), cytosine (C) and guanine (G) (Figure 1.2). In so called Watson-Crick base-pairing, adenine binds selectively *via* hydrogen bonds to thymine (A-T) and cytosine selectively with guanine (C-G), creating a specific set of DNA base-pairs. [18] The bases are aromatic,

heterocyclic molecules with hydrophobic properties, while the external part, consisting of the sugar-phosphate backbone, exhibits hydrophilicity due to its net negative charge. The complementarity between A and T as well as G and C is essential for the DNA double strand formation and replication, processes that are vital in for example cell division. [17]

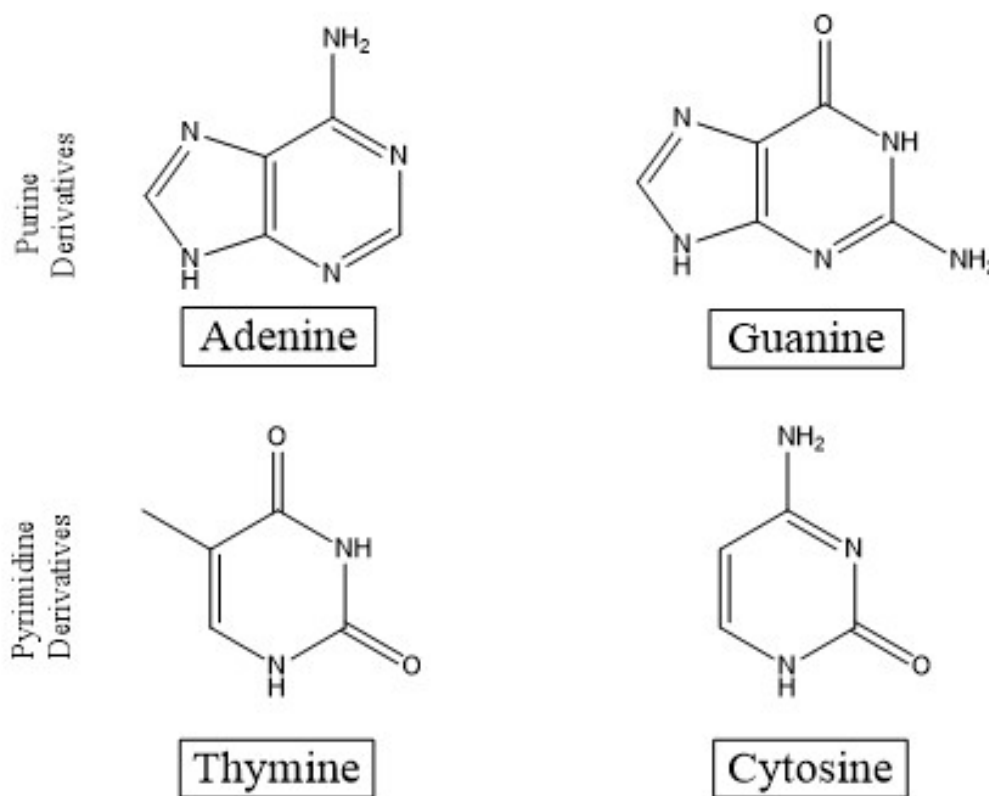


**Figure 1.2:** Chemical structure of DNA nucleotides

The most abundant form of double strand DNA (dsDNA) was first described by Watson and Crick, and is known as B-form DNA. According to the proposed model, it exhibits a right-handed double helical conformation, consisting of 10 base pairs per turn. The rotation angle is  $36^\circ$  per base pair, while there is a vertical rise of  $3.4 \text{ \AA}$  per base pair. The helical diameter is ca.  $23.7 \text{ \AA}$ . [19] Due to the asymmetry originating from the geometry of the base pairs, dsDNA presents two grooves on the exterior of the helix, that differ both in depth and width. The wider groove is called the major groove whilst the narrower is called the minor groove.

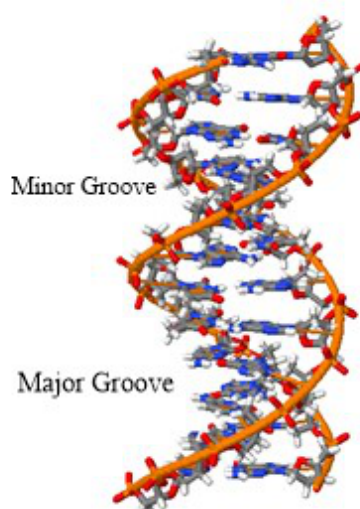


**Figure 1.3:** 3D model of DNA structure [15]

## 1.2 DNA binding

The study of DNA interactions with small molecules can provide important information regarding the potential of the molecule to be utilized *e.g.* as drugs or DNA fluorescent probes. Investigations on the thermodynamic equilibrium state and binding kinetics of the DNA binding agents can provide information regarding the structure and dynamics of DNA, as well as details regarding the binding and function of the ligand. For instance, in the case of slow binding kinetics, intermediate binding sites may be uncovered. [20]

Small molecules can bind to DNA either *via* covalent or non-covalent interactions. Covalent DNA binding leads to a permanent modification of the double stranded DNA *via* cross-linking, either by linking the nucleotides directly (*e.g.* the photocrosslinking drug psoralen [21]), or by first inserting into the dsDNA and then cross-linking the DNA bases (*e.g.* Mytomycin C and Aflatoxin B1 [21]). By changing the DNA conformation, the transcription as well as other DNA dependent processes are affected, typically leading to cell death. Small molecules typically exhibit very low selectivity, which leads to significant cytotoxicity also towards healthy cells. [21]

Typically, four non-covalent binding modes are distinguished for DNA: major groove binding, minor groove binding, electrostatic binding, and intercalation (mode 1, 2, 3, and 4 in Figure 1.4, respectively).

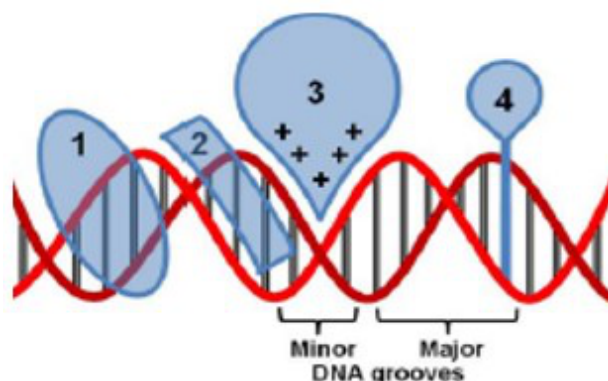


**Figure 1.4:** Main non-covalent DNA binding modes [16]

The term *major groove binding* refers to the interactions of small molecules with the larger groove site of DNA. A clear example of non-covalent interaction with DNA is Ditercalinium, which is a compound derived by the natural product ellipticine. It causes structural changes to the DNA, such as unwinding and widening of the major and minor grooves. [16] In other cases, compounds can interact non-covalently with the major groove of DNA, but cause non-reversible changes to DNA for instance by DNA cleavage, alkylation, or other mechanisms. [22] Examples of natural major groove binding agents that exhibit this behavior are: Neocarzinostatin, Azinomycin and Leinamycin. This is attributed to the formation of intermediate products that are activated in the presence of DNA. [16]

*Minor groove binding* is the result of molecules that bind non-covalently on the minor groove of DNA. This type of DNA binding agents may interact *via* van der Waals forces with the minor groove walls or *via* non-specific electrostatic interactions. [23] A typical example of minor groove DNA binding agents is netropsin [16] which presents a selectivity towards AT bases, with which it may also interact covalently *via* hydrogen bond formation. Other examples of minor groove binders are: distamycin, netropsin, chromomycin and actinomycin D. [16]

*Electrostatically binding* compounds typically have cationic functional groups that interact electrostatically with the negatively charged DNA backbone. Metal complexes of compounds with antibacterial, anticancer, antiviral, or other biological properties are typical examples of this type of DNA binding agents. Some of the most commonly utilized metals are: Co(II) [24–26], Cu(II) [27–29], Ni(II), [30–32] Pd(II), [31, 33, 34] Pt(II) [31, 35, 36], Mo(IV) [31, 37] and Zn(II) [38].

*Intercalation* refers to the non-covalent insertion of compounds in between the DNA bases and leads to stabilization of the DNA double strand. This can be detected for instance *via* a DNA Thermal shift assay, in which the denaturation temperature of DNA with and without the compound are determined and compared. As denaturation temperature of DNA is defined as the temperature at which, under standard conditions, 50% of the DNA double strand is separated into single strands [39], also known as melting temperature. In case the melting temperature is increased by

more than 5°C then this is an indication of intercalation.

Another technique that determines whether the binding mode of a compound is *via* interaction, is called *ethidium bromide displacement assay*. Ethidium bromide is a characteristic example of interacting DNA binding agent. In this technique, ethidium bromide is added to a DNA solution and the emission spectrum is collected [da Silva, 2017 [12]]. Then a known concentration of the compound under investigation is added to the solution and the emission spectrum is collected again. In case the emission is decreased, it is an indication that the ethidium bromide has been displaced by the compound. Afterwards, more titration steps can be followed up until the point the emission intensity is no longer decreased, indicating an equilibrium between the DNA binding places.

A special case of intercalation which has been widely studied with Ruthenium (Ru) complexes, is known as *threading interaction*. This binding mode is attributed to the very slow and strong binding kinetics that for instance some Ru complexes exhibit. [40] These characteristics classify these complexes as very promising drugs and for that reason research has taken place to a great extent, especially in cancer treatment. [41–43]

It should be noted however that although DNA binding experiments are able to provide important information regarding the thermodynamical equilibrium state of the reaction, there is a possibility that a compound may present cytotoxicity *in vivo* without necessarily exhibiting DNA interactions (*e.g.* prodrugs and nuclear receptors). Thus, it is found important to raise interest regarding molecular studies in order to develop deeper understanding of the activity and mechanisms of small molecules *in vivo*.

### 1.3 Schiff Bases

A family of compounds that has attracted the interest of many researchers is Schiff bases. These compounds have a wide variety of applications in organic, inorganic (*e.g.* as catalysts, corrosion inhibitors etc. and analytical chemistry. [10] They are considered versatile pharmacophores due to the multiple cytotoxicity properties they exhibit, such as: anticancer, antioxidant, antidepressant, anthelmintic, analgesic antimicrobial, anticonvulsant and other [10]. These properties are attributed to the azomethine functional group ( $-\text{C}=\text{N}-$ ), however, the mechanism of action is still not completely clear. Many researchers consider DNA binding as the mechanism behind their cytotoxicity [18, 19, 44], [16, 21–23] for that reason DNA binding investigations *in vitro* are the main tools for the study of these molecules.

Schiff bases, named after the German-Italian chemist Hugo Schiff (1834 – 1915), are chemical compounds that are characterized by an imine group ( $-\text{C}=\text{N}-$ ). As mentioned above, they exhibit a wide number of properties and applications that are attributed to their functional group, but also to subsequent functional groups attached to the Schiff bases, such as: methyl ( $-\text{CH}_3$ ), carbonyl ( $\text{C}=\text{O}$ ), hydroxyl ( $-\text{OH}$ )

OH), amine ( $-\text{NH}_2$ ) and other functional groups, [Hodnett, Ernest M., and William J. Dunn. 1970 [6]. In the study performed by Hodnett, Ernest M., and William J. Dunn. 1970 [6], the structure and the substituent groups present in Schiff bases was correlated to the anticancer activity of the compounds. Overall, it is reported that aldehyde group leads to induced anticancer activity compared to an amine group. An interesting observation is that anticancer activity is favored in the case the substituent group leads to electron withdrawal from the ring. According to the authors this could be either due to increased structural stability of the Schiff base, or to the possible attachment of the compounds to receptor sites.

In this thesis, the main interest is given to aryl Schiff bases and for that reason, in this subchapter, research related only to these compounds is presented. In this work, particular attention has also been given to publications related to chemical transitions that these compounds undergo, such as keto-enol tautomerism and cis-trans isomerization, depending on the chemical environment or UV irradiation, respectively.

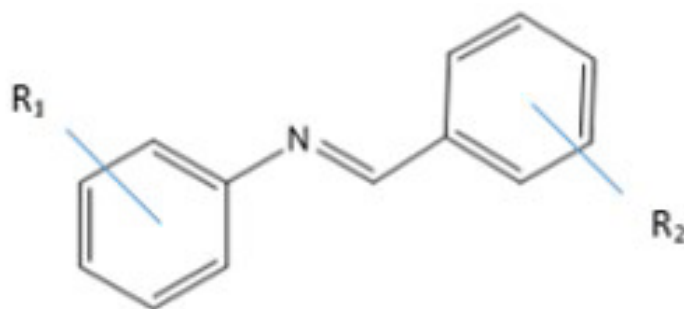


**Figure 1.5:** General chemical structure of imines

According to the review article written by Kajal, Anu, *et al.* 2013 [10], *in vivo* experiments have been performed in various cell lines, examining the biological properties of Schiff bases. These compounds have successfully exhibited antimicrobial, antidyslipidemic, anthelmintic, antitubercular, antidepressant, anticonvulsant, anti-inflammatory, antitumor, antioxidant, antiviral, antihypertensive and antidiabetic activity. Classifying this class of compounds as versatile pharmacophores. [10]

Dileepan, AG Bharathi, *et al.* 2018 [2], report Schiff bases derived by Isatin as antimicrobial and antioxidant agents. The activity of the compounds is correlated to DNA binding *via* intercalation. The binding constants reported belong to the range of  $10^5$  to  $10^4 M^{-1}$ . The cytotoxicity assays resulted in strong inhibition of bacterial growth and potential for improvement of antibacterial drugs are concluded.

All the compounds included in this study are novel, besides compound number **15** (view Figure 3.1 in page 13). This compound has been widely studied and it is used as a reference. According to Souza, Ana O. de, *et al.* 2007 [45], this compound appears to have effective antimicrobial activity. It was tested against *M. tuberculosis* H37Rv and it exhibited Minimum Inhibitory Concentration (MIC)

of 8  $\mu\text{mol/L}$ . Additionally low cytotoxicity was found against J774 macrophages, as at concentration of 1,000  $\mu\text{mol/L}$ , led to 20% of cell death. Da Silva Cleiton M, *et al.* 2017 [12], examined the cytotoxicity and selectivity in a wide variety of cell lines. Compound **15** exhibited high selectivity and cytotoxicity towards MCF-7 breast cancer cell line and U-251 MG brain cancer cell line. The DNA binding of the compound was also examined, and a correlation between biological activity and DNA interaction was proposed. The DNA binding mode was proposed to be intercalation.

Demirci, Selami, *et al.* 2017 [46], report DNA interactions and suggest DNA cleavage as a possible mechanism responsible for the biological activity of the compounds. The Schiff bases studied exhibited anticancer activity against prostate cancer cell lines.

### 1.3.1 Keto-enol tautomerism

Tautomerism refers to the rapid back and forth structural shift of molecules that differ in a hydrogen atom or a double bond. [47] In the case of ketones, this transition usually takes place due to the protonation of the C=O bond from an  $\alpha$  hydrogen (*i.e.* Hydrogen connected to the carbon next to the C=O carbon. More than one  $\alpha$  hydrogens may be present), in acidic solutions. [48] The protonation leads to the breaking of the C=O double bond and the creation of an enol group (-OH) as well as a C=C double bond (Figure 1.6). The two tautomers are called *keto* and *enol*, tautomers respectively. This transition is important in the carbonyl chemistry and research regarding Schiff bases has also taken place.

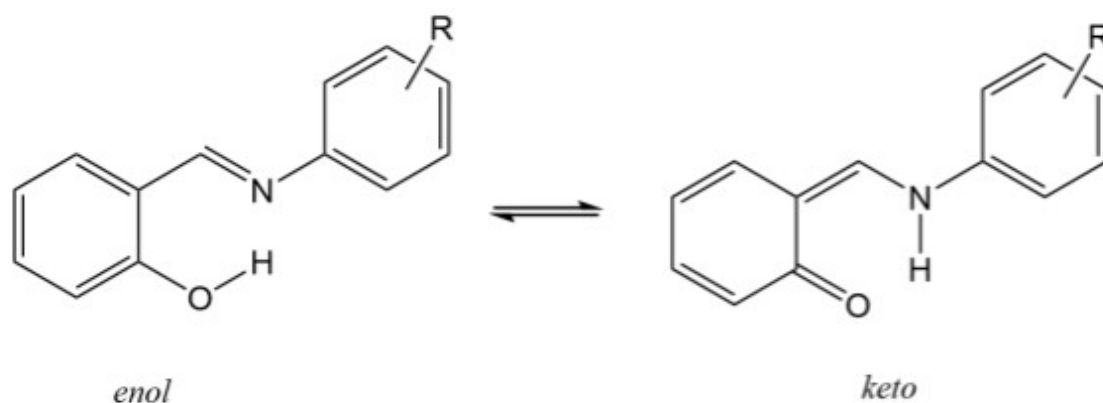


**Figure 1.6:** Keto-enol tautomerism

### 1.3.2 Cis-trans isomerization

Another structural transition that has been observed regarding Schiff bases is cis-trans isomerism. Coelho J, *et al.* 2013 [49] studied this transition in a series of Schiff bases that have the same general structure as the ones studied in this thesis (Figure 1.7). It is reported that the cis-trans isomerization can be induced by UV light,

leading to the formation of cis form. Whereas, in the absence of light the compound return to the original trans form. The transition kinetics were recorded to be slow, thus the observation at room temperature was possible. [49]

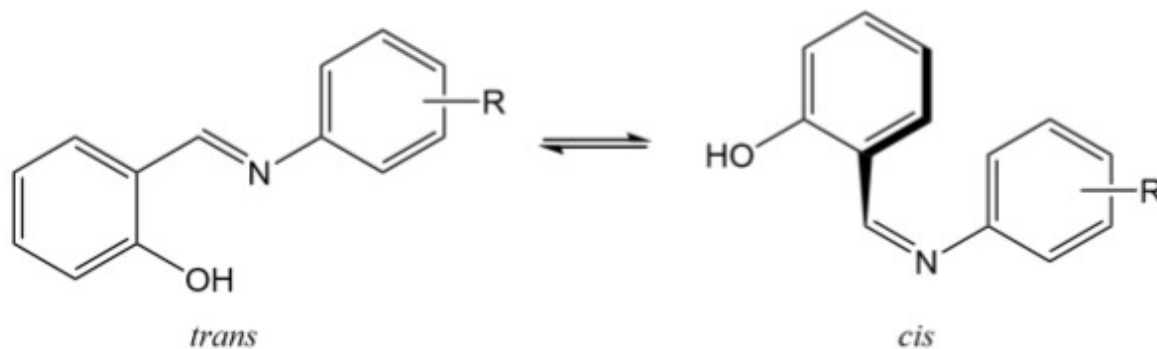


**Figure 1.7:** Cis-trans tautomerism

## 1.4 Aim and Objectives

The initial objective of this thesis was focused on the *in vitro* DNA binding study of thirteen Schiff bases (View Table A.1 in Appendix) by using calf thymus DNA (ct DNA). For that reason spectroscopic techniques are utilized (UV-vis spectroscopy, eclipse spectroscopy and linear dichroism). During the execution of the experiments it was observed that a chemical transition takes place when the compounds are introduced from the 100%DMSO stock solutions into 50mM Tris-HCl (100mM NaCl). For that reason, besides the potential DNA binding, the structure of the compounds is studied *via* NMR ( $^1\text{H}$ -NMR,  $^{13}\text{C}$ -NMR and HSQC-NMR). This set new objectives, such as determining the type of transition that takes place and investigating whether the compounds interact with the DNA by any means. These studies aimed towards the determination of the potential DNA binding mode, as well as the strength of the interaction between the compounds and the DNA. As this information can define the possibility of the compounds to be utilized as drugs or DNA probes.

# 2

## Theory

### 2.1 Spectroscopy

Spectroscopy refers to a number of techniques (*e.g.* IR, UV, NMR) that study the interactions between electromagnetic radiation and matter in a quantitative and a qualitative way. Since ancient times, vision and electromagnetic radiation in the form of light have triggered the human mind. The energy that light carries is described by the formula:

$$E = hc\tilde{\nu} = \frac{hc}{\lambda} \quad (2.1)$$

Where:

- h: Planck's constant ( $6.626 * 10^{-34} \text{ m}^2\text{kg/s}$ )
- c: speed of light in vacuum ( $299,792,458 \text{ m/s}$ )
- $\tilde{\nu}$ : spatial frequency of wave [ $\text{sec}^{-1}$ ]
- $\lambda$ : wavelength of wave [ $\text{nm}$ ]

This formula indicates the wave-particle duality of light, meaning that light propagates in quanta (*i.e.* small packages of energy – photons), but also as a harmonic wave with the electric and the magnetic components perpendicular to each other. The harmonic wave is characterized by the wavelength, which determines the energy it carries.

### 2.2 Jablonski diagram

When a molecule absorbs energy from light in the ultraviolet (UV) or visible part of the spectrum, different electronic transitions may occur. The Jablonski diagram (Figure 2.1) provides a graphical description of the possible transitions between quantized energy states in a molecule. Two classes of electronic states can be defined: singlets and triplets. In the singlet state (S), the electrons have opposite spins and transitions between different singlet states is spin-allowed. When a molecule returns to the ground state from an excited singlet state, it can do so non-radiatively or radiatively (*i.e.* by emitting light). In the case of radiative relaxation, the process is called fluorescence. The intramolecular non-radiative transitions are typically categorized as vibrational relaxation, internal conversion, and inter-system crossing. In addition, intermolecular reactions can depopulate the excited states. This is typically called “quenching” and for a fluorescent molecule it leads to a decrease of the observed fluorescence intensity.

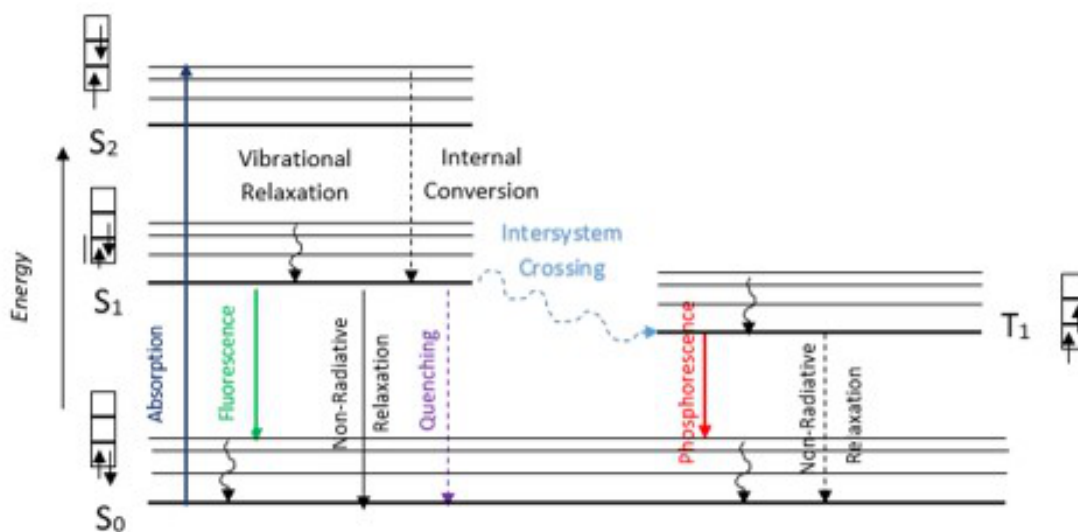


**Figure 2.1:** Jablonski diagram illustrating electronic transitions in a molecule

### 2.2.1 Absorption

The absorption spectrum in the UV and visible region can be utilized to determine the concentration of a chemical compound in solution, according to Beer-Lambert law:

$$A(\lambda) = C * \epsilon(\lambda) * l \quad (2.2)$$

Where:

- $A(\lambda)$ : Absorption at specific wavelength,  $\lambda$  [*a.u.*]
- $c$ : Concentration of substance of interest [M]
- $\epsilon(\lambda)$ : Molar absorptivity coefficient at specific wavelength,  $\lambda$  [ $M^{-1}cm^{-1}$ ]
- $l$ : Path length of the cuvette [cm]

### 2.2.2 Fluorescence

Fluorescent molecules, also known as fluorophores, absorb light at specific wavelengths and emit light at longer wavelengths after a short period of time, known as the fluorescence lifetime. [50] In case these molecules have the ability to bind to DNA they may have potential to be utilized as DNA dyes. Fluorophores have a key role in bioimaging studies of DNA, cells and organisms as they may have the ability to provide important information regarding the DNA structure, [51] the characteristics of cells membranes [52], the expression of genes [53], and other biological activities. Some examples of fluorescence techniques utilized for that purpose are laser scanning confocal microscopy, time-correlated single photon counting (TCSPC), and Förster resonance energy transfer (FRET).

In this thesis, only fluorescence emission spectroscopy was utilized, which is a technique that records the emission spectrum when exciting at a specific wavelength.

That way the fluorescent intensity of the molecules of interest and potential differences in fluorescence when DNA is present, can be investigated.

### 2.2.3 Linear dichroism

Flow-oriented linear dichroism (LD) is a steady-state spectroscopy technique that can be utilized to study macromolecular samples, such as DNA. According to this technique, molecules that are oriented in solution, using for instance a Couette cell, are probed with linearly polarized light, with the polarization angles perpendicular to each other and to the direction of light propagation. [54] The difference in absorption between the two polarizations defines the LD signal according to:

$$LD = A_{\parallel} - A_{\perp} \quad (2.3)$$

In solution, molecules are typically randomly oriented. Thus, when no flow is applied, the overall LD signal is zero. In the case were oriented DNA interacts with small molecules, two binding modes can be described.

- If  $A_{\parallel} > A_{\perp}$  then  $LD > 0$ . In this case the majority of compound is parallel to the flow, thus it binds in the grooves of DNA.
- If  $A_{\perp} > A_{\parallel}$  then  $LD < 0$ . In this case the majority of compound is perpendicular to the flow, thus the binding mode is intercalation.

The LD technique provides high quality results that can easily be interpreted. However, it is not a wide-spread technique as it requires orientation equipment that is currently not available in most biophysical labs. [54]

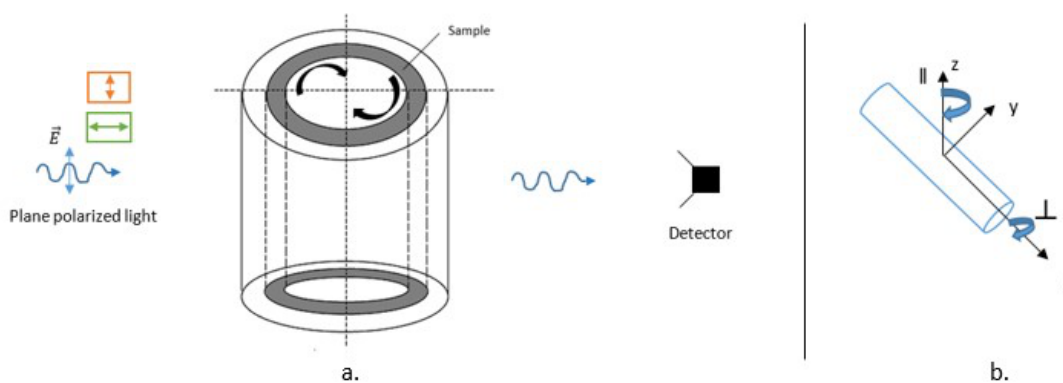
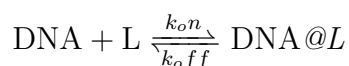


**Figure 2.2:** a) LD spectroscopy illustration, b) oriented sample

## 2.3 DNA binding

When DNA-binding ligands interact with DNA in a non-covalent manner, the molecules reversibly associate and dissociate from the binding sites of DNA.



The rate of ligands binding on DNA is expressed by the formula as:

$$\frac{d[DNA@L]}{dt} = k_{on}[DNA] * [L] - k_{off}[DNA@L] \quad (2.4)$$

Where,

- $[L]$ : concentration of ligands (binding agents) free in solution  $[M]$
- $[DNA]$ : concentration of DNA free in solution  $[M]$
- $[DNA@L]$ : concentration of ligands bound on DNA  $[M]$
- $k_{on}$ : association rate  $[sec^{-1}]$
- $k_{off}$ : dissociation rate  $[sec^{-1}]$

At equilibrium, the rate of ligands associate and dissociate from DNA are constant. Thus, the binding constant ( $K_{eq}$ ) at equilibrium is defined as:

$$\frac{d[DNA@L]}{dt} = 0 \quad (2.5)$$

$$K_{eq} = \frac{k_{on}}{k_{off}} = \frac{[DNA@L]}{[DNA][L]} \quad (2.6)$$

## 2.4 Activation Energy

In the case that a chemical reaction or structural transition (*e.g.* isomerization) takes place, the energy that is required to activate the reaction can be determined by plotting the van Hoff's diagram. This is based to the Arrhenius law:

$$\ln(k) = \ln(A) - \frac{E_a}{RT} \quad (2.7)$$

Where,

- $k$ : rate constant  $[sec^{-1}]$ , for first order reaction
- $A$ : Arrhenius factor  $[sec^{-1}]$ , for first order reaction
- $E_a$ : activation energy  $[J/mol]$
- $R$ : gas constant  $[8.314462 J^*K^{-1}*mol^{-1}]$
- $T$ : temperature  $[K]$

By plotting the  $\ln(k)$  with respect to  $1/T$ , the activation energy  $E_a$  can be calculated by the slope of the graph, which will be equal to  $E_a/R$ .

# 3

## Materials and Methods

### 3.1 Compounds

The dry compounds were received as a generous contribution by the research group of Dr. Papadopoulos Kyriakos, Institute of Nanoscience and Nanotechnology, NCSR “Demokritos”, Athens, Greece (Figure 3.1 and Table A.1). Prior to use, the samples were stored in the dark at room temperature (ca. 22°C).

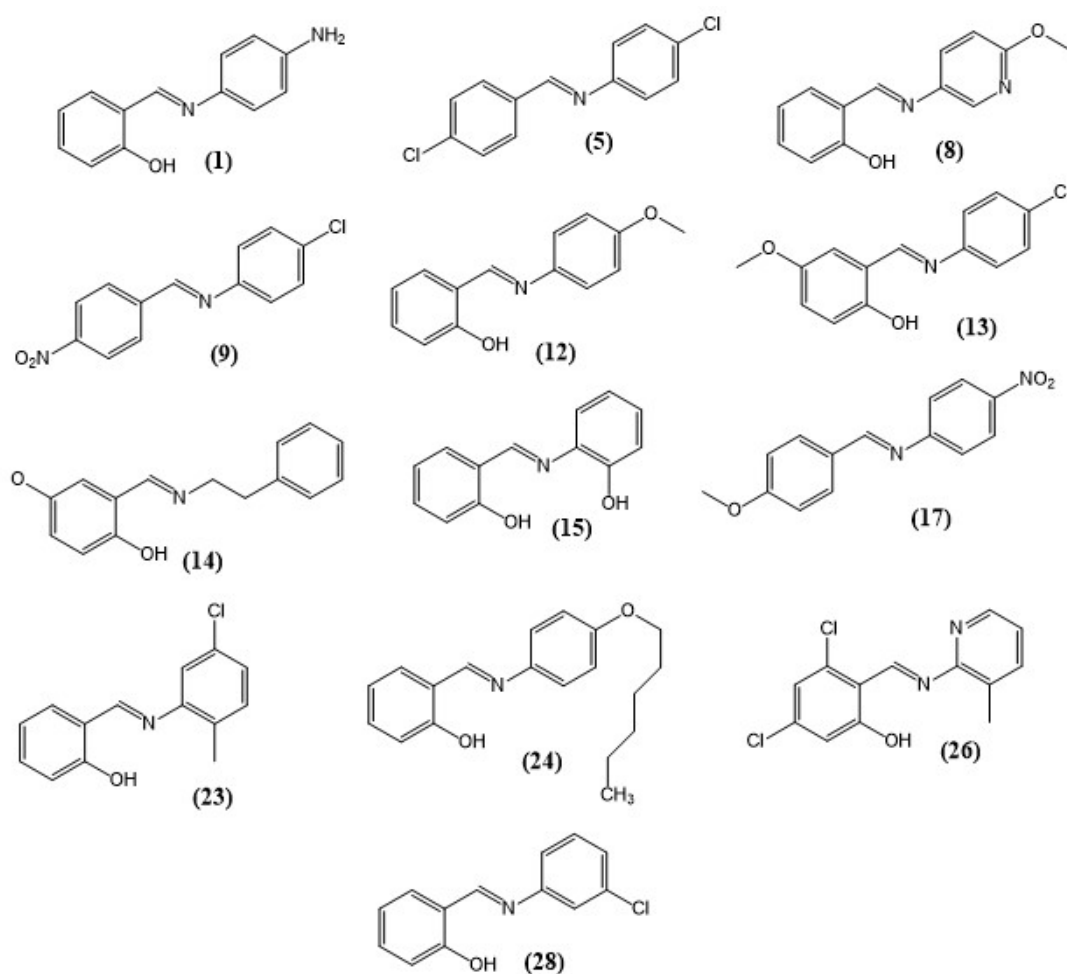


**Figure 3.1:** Chemical Structures of the compounds utilized in this study

#### 3.1.1 Stock solution preparation

Stock solutions (10 *mM*) were prepared by weighing approximately 2.5 *mg* of each dry compound and dissolving them in the appropriate amount of dimethyl sulphoxide (DMSO). To accelerate the dissolution process, a Vortex device was used. All compounds appeared to be soluble in DMSO. No unsolvable particles could be observed when the solutions were prepared. However, after 3 months of storage at 5°C, compound **1** appeared to have formed some precipitates. From the 10 *mM* stock solution, a further diluted 300  $\mu$ *M* stock solution was prepared and used as a working solution throughout the project. All DMSO stock solutions were stored at 5°C.

#### 3.2 Buffer preparation

The buffer solution used was a 50 *mM* Tris buffer containing 100 *mM* NaCl. To prepare it, a 10X concentrated buffer solution was first prepared by dissolving Tris-HCl (13.222 *g*, 0.0839 *mol*), Tris-Base (1.943 *g*, 0.0160 *mol*), and NaCl (11.690 *g*, 0.2000 *mol*) in mQ water. The pH of this solution was found to be 7.44 at 22.2°C. Finally, the 1X buffer used in the experiments were prepared by diluting the 10X buffer ten times using mQ water. The 10X and 1X buffers were stored in 5°C throughout the project.

#### 3.3 DNA preparation

Calf thymus DNA (ctDNA, Sigma-Aldrich) in solid form, was added to the 1X buffer and subjected to mild agitation overnight. The resulting solution was clear. The concentration of the solution was determined *via* UV-vis spectroscopy to be 2.53 *mM*. This DNA stock solution was stored in 5°C throughout the project.

#### 3.4 UV-Vis absorption instrumentation

Three different instruments were used for the UV-Visible absorption measurements: Varian Cary 50, Varian Cary 4000 and Varian Cary 5000. The same parameter set-up was used for all instruments: Scan rate: 600 *nm/min*, Scan range: 200 *nm* – 700 *nm*. A sample-matching solvent baseline was recorded and subtracted for all measurement. Two different types of quartz cuvettes were used: one with dimensions 1.0 *cm* × 0.4 *cm* and one with dimensions 1 *cm* × 1 *cm*. The second one was only used for the determination of the molar extinction coefficient ( $\epsilon$ ) of the compounds. The pathway (*l*) of the cuvette used was 1 *cm* for all measurements unless stated otherwise.

#### 3.5 Fluorescence spectroscopy instrumentation

A Varian Cary Eclipse fluorescence spectrometer was used for the emission spectroscopy measurements. The scanning rate applied was 600 *nm/min*. Slit widths, excitation wavelength, and scanning wavelengths varied depending the compound.

### 3.6 Nuclear Magnetic Resonance (NMR)

For the NMR measurements a 2 M stock solution was prepared by diluting 49.00mg of compound **15** ( $MW = 213.08 \text{ g/mol}$ ) in 114.98  $\mu\text{L}$  of deuterated DMSO. After using Vortex no undissolved particles could be observed. From that stock solution two samples were prepared with the aim to investigate whether there are two chemical structures in solutions that differ in polarity preference. The concentration of both samples was 0.5 M of compound **15**. One sample was present in 100% deuterated DMSO (relative polarity 0.444), while the other sample solution consisted of 5% deuterated DMSO and 95% deuterated ethanol (relative polarity 0.654). [55]

Three different NMR experiments were performed for the examination of the structures of compound **15**: 1D  $^1\text{H}$ , 1D  $^{13}\text{C}$  and 2D  $^1\text{H}$ - $^{13}\text{C}$  Heteronuclear Single Quantum Coherence (HSQC) spectroscopy. The latter mentioned is a 2 dimensional (2D) and more sensitive technique that is a product of the combined proton and carbon NMR spectrums. In HSQC analysis each proton ( $^1\text{H}$ ) can be assigned to the covalently bonded carbon and the chemical structure of a compound can be more easily predicted and interpreted. During the experimental procedures standard parameters were used. Regarding H NMR 8 scans were performed and the relaxation time applied was 1sec. For  $^{13}\text{C}$  the relaxation time applied was 3sec and 128 scans were performed. The frequency of deuterated DMSO was utilized as a reference frequency (lock frequency) for both samples.

The software used for the processing and presentation of the results is MestReNova x64.

### 3.7 Linear Dichroism

The instrument used for LD was an Applied Photophysics Chirascan spectrometer. A custom built Couette cell with a total pathlength of 1  $m\text{M}$ , was used. Three consecutive technical replicates were collected for each rotational speed: 0  $rpm$ , 300  $rpm$ , and 500  $rpm$ . With zero rotation, the molecules in solution are randomly oriented and, as a result, the LD should be zero. However, due to different instrumental parameters such as the relative wavelength- and polarization-sensitivity of the detector, the measured LD at zero rotation is non-zero. For that reason, the zero rotation is used as a baseline for all flow-oriented measurements.



# 4

## Results and Discussion

As mentioned in the introductory chapter 1, according to the literature, Schiff bases have been reported to interact with DNA. However, as will be discussed here in this project this observation was not that straightforward.

We started out by merely mixing calf thymus DNA (ctDNA) and the various Schiff bases to investigate if interaction could easily be detected using UV-vis absorption. We examined the ability of the molecules to bind to DNA by adding a high quantity of ctDNA into a solution where buffer, DMSO (at 5% - a concentration considered to be the highest acceptable in DNA-binding studies) and compound were present. Significant changes in the Schiff base absorption region were observed that for most compounds suggested extensive aggregation and/or changes to the Schiff base itself (example spectrum given in Appendix page VII). Specifically, changes in the absorption spectra were observed when the compounds were added from a 100% DMSO stock solution to the buffer. These initial results suggest, not unexpectedly, that most of the Schiff bases are significantly hydrophobic in nature and possibly also form other species when changing solvent from DMSO to more polar ones. Thus, we needed to perform more detailed research on the Schiff bases only to distinguish between effects resulting from changes due to the compounds themselves and their possible DNA binding.

Due to the existing publications, compound **15** was later chosen to be studied in more detail, for example, *via* NMR for the compound itself and *via* linear dichroism for its DNA-binding. Due to the large volume of experimental results produced for this thesis, only compound **15** is presented in this Chapter. The results of the other compounds can be found in the Appendix from page II to page XXI.

### 4.1 Schiff base solubility in up to 5% DMSO

Due to the initial observation of aggregation or presence of various species of Schiff base in buffer solution we set out to study the solubility of compound in water-based solutions. The solubility of compounds was examined to determine the minimum percentage of DMSO needed in the studies of the compounds in buffered solutions. As mentioned above, the stock solutions of the compounds were kept in DMSO. The concentrations of the compounds utilized for these experiments were within the range of 10  $\mu M$  to 20  $\mu M$ . As evidenced by no (or very little) scattering in absorption, compounds **8**, **12**, **13**, **14**, **15**, **17** and **28** exhibited the highest solubility, being able to solubilize even in 0.1 to 0.2% DMSO (Figure 4.5 and Appendix II). For the

rest of compounds, 2 – 5% *DMSO* was needed, except for compounds **1**, **23** and **24** which at 5% *DMSO* exhibited scattering in the wavelength region between 550 *nm* and 700 *nm*. This indicates that half of the compounds exhibit very high solubility in buffer. Taking into account the proper solubility and the number of publications available regarding compound **15** that show antibacterial and anticancer properties [12], we chose to study this compound and its DNA-binding in more detail (see below).

## 4.2 Emission of Schiff bases

Before investigating compound **15** in more detail, we decided to study the fluorescence properties of the Schiff bases. For that purpose steady-state emission measurements of the compounds dissolved in 5% *DMSO* and 95% 50 *mM* Tris-HCl (100 *mM* NaCl) were performed (Figure 4.1). Overall, all Schiff bases except **12**, **17** and **23** were emissive.

It should be noted that these measurements were collected as a first investigation of the properties of the compounds. As will be presented later, we found out that the compounds undergo a structural transition that changes the absorption spectrum and as a result also the emission. Hence, the emission found here correspond to the mixture of two isomers in solution present initially in the solvent before any transition to the final state has taken place. The percentage of each isomer in solution can be determined *e.g.* by a chromatographic technique known as High Performance Liquid Chromatography (HPLC). This technique is able to separate the two isomers and estimate the quantity of each in solution. A table with the fluorescence properties of the compounds can be found in the Appendix A.2.

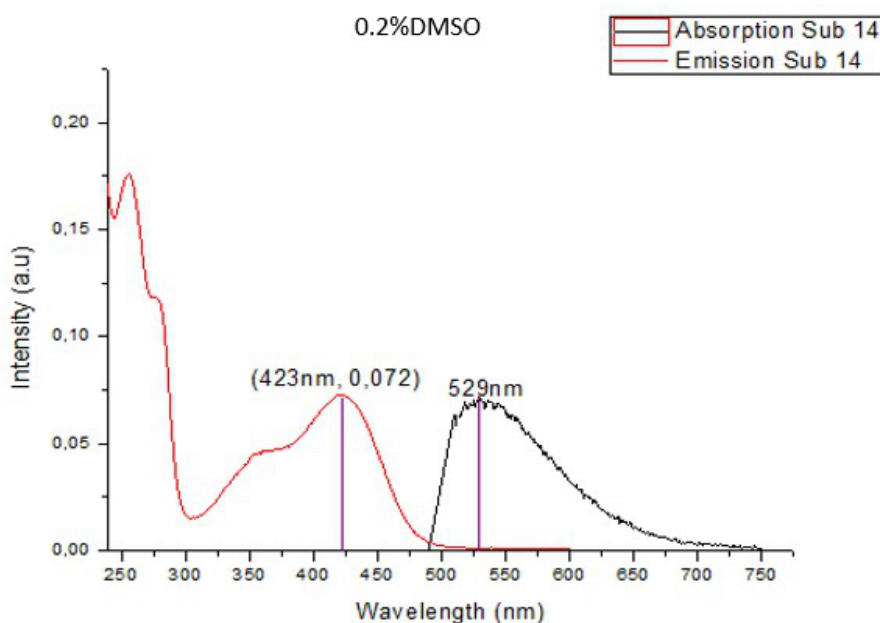


**Figure 4.1:** Absorption (red line) and emission (black line) spectra of compound **14**, 15  $\mu\text{M}$ , 0.2% *DMSO*

### 4.3 Initial screen for DNA binding

All compounds were screened for potential DNA binding by observing changes in absorption upon adding a small volume (*ca.* 50  $\mu\text{L}$ ) from the DMSO compound stock to a large volume (*ca.* 950  $\mu\text{L}$ ) of DNA in buffer. The DNA was present in a 3.4-fold excess (*ca.* 50  $\mu\text{M}$  of DNA to 14.7  $\mu\text{M}$  of compound) and the final DMSO concentration was 4.9%. As shown in Figure 4.2, a clear change in the absorption and emission spectra was seen. This observation was initially thought to be an indication of DNA binding attributed to the presence of bound and unbound compound in solution.

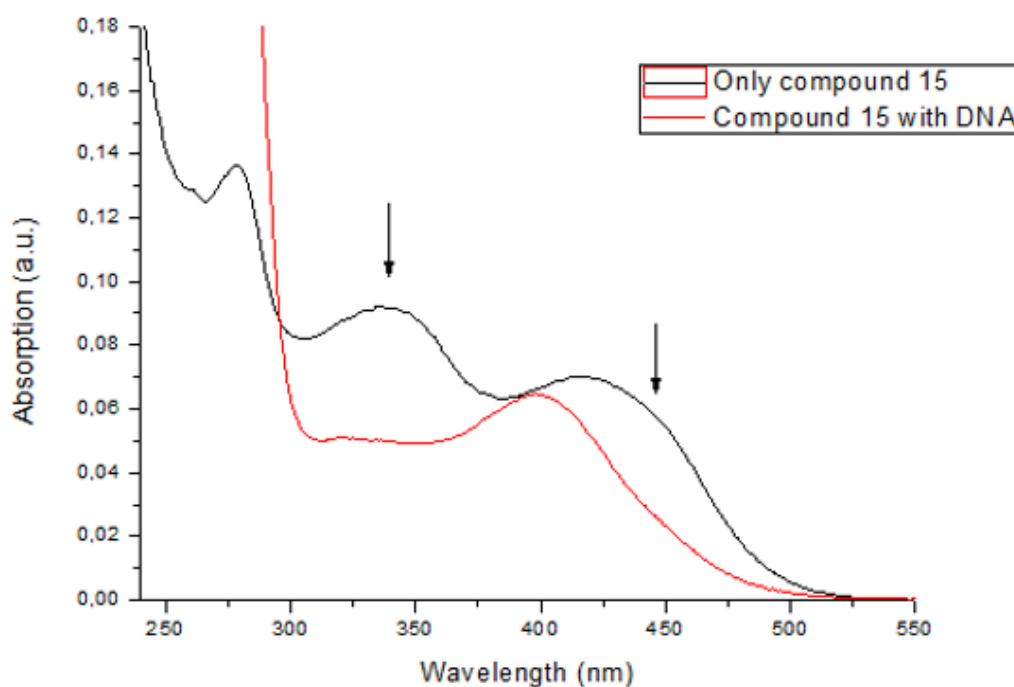


**Figure 4.2:** Absorption spectrum of **15** (14.7  $\mu\text{M}$ , 5% DMSO in 50 *mM* Tris-HCl (100 *mM* NaCl) buffer) with and without DNA (50  $\mu\text{M}$ ) present. Note that the spectrum of **15** without DNA was collected before the thermal equilibrium had established.

However, changes in the absorption spectrum were observed also when the compound DMSO stock was added to buffer without DNA was present (Figure 4.3). This prompted us to investigate the behavior of the compounds alone in solution before moving on with further DNA binding studies.

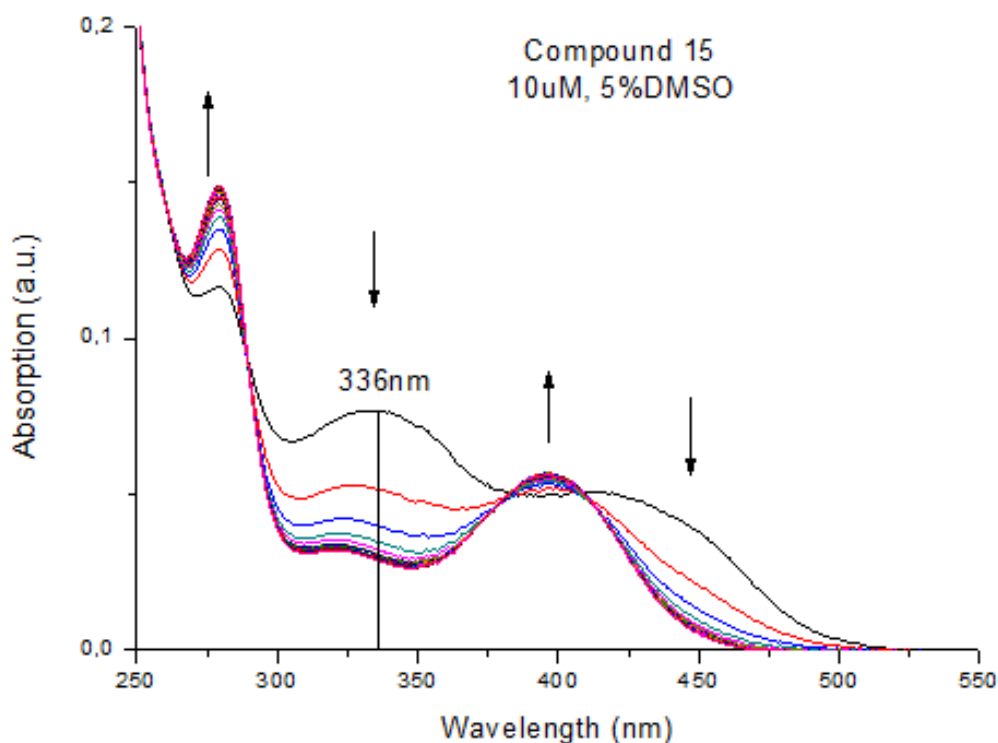


**Figure 4.3:** Isothermal kinetics of compound **15**, 20  $\mu\text{M}$ , in 50  $m\text{M}$  Tris-HCl (100  $m\text{M}$  NaCl) and 5%DMSO

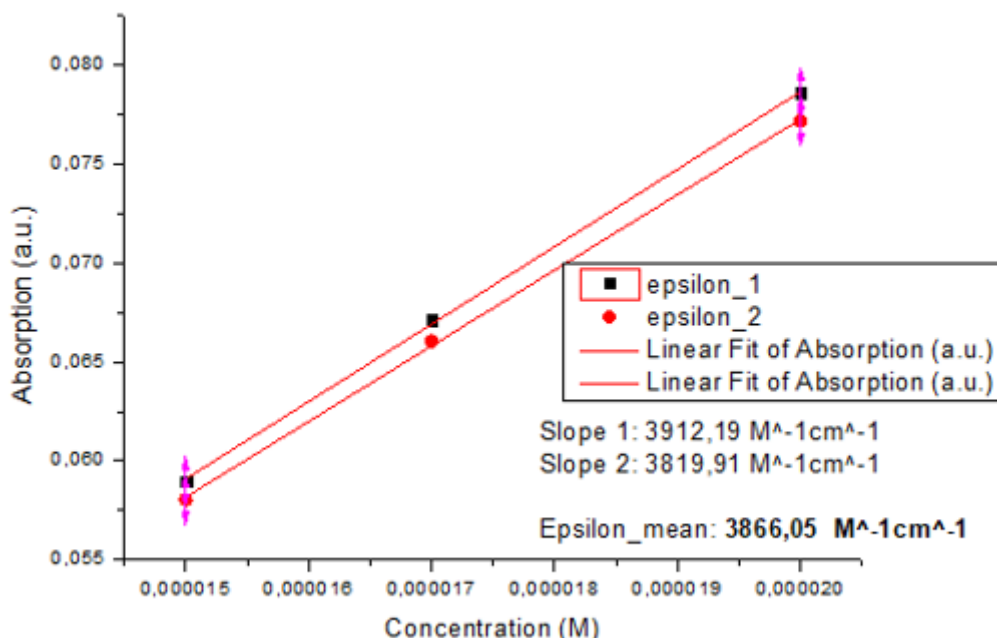
#### 4.4 Molar absorptivity

The molar absorptivity ( $\epsilon$ ) of compounds **9**, **14**, **15**, **17**, **26**, and **28** was determined in 5% DMSO in buffer. This selection was motivated by the compounds exhibiting 1) adequate solubility in buffer, 2) fluorescent properties, and 3) a clearly distinguishable interaction with DNA, as judged by changes in absorption or emission upon DNA addition. The binding potential (criterion 3 above) at this point of the project was however misjudged, as the spectral changes of the compounds itself was mistaken for DNA binding. Nevertheless, the molar absorptivity of compound **15** is presented below, while the corresponding data for the other compounds can be found in the Appendix. To determine the molar absorptivity of the compounds, a 20  $\mu\text{M}$  solution was prepared as described above and showed in Figure 4.4. Absorption spectra were then collected over time in room temperature until no further changes could be observed in the absorption. After this, the 20  $\mu\text{M}$  solution was diluted down to 17  $\mu\text{M}$  and then to 15  $\mu\text{M}$  and spectra were collected at each concentration. The measurements were repeated twice and the results are shown in Table 4.1.

**Table 4.1:** Absorption values of compound **15** at absorption peak ( $\lambda = 398 \text{ nm}$ ) in different concentrations

Concentration ( $\mu\text{M}$ )	Absorption (sample 1) (a.u.)	Absorption (sample 2) (a.u.)
15	0.05897	0.05804
17	0.0671	0.06603
20	0.07857	0.07718

By plotting the absorption *vs.* concentration, the molar absorptivity is calculated as the slope of the linear fit, as shown in Figure 4.4. The absorptivity was thus determined to be  $3900 \text{ M}^{-1}\text{cm}^{-1}$  for compound **15**.

**Figure 4.4:** Absorption with respect to concentration

## 4.5 Kinetics of molecular transition upon dilution into buffer

The molecular transition characteristics of the Schiff bases upon going from the less polar DMSO solution to aqueous solution was evaluated using UV-vis spectroscopy. Each compound was studied at room temperature (*ca.*  $22^\circ\text{C}$ ) immediately after adding a small volume of the DMSO stock solution to  $50 \text{ mM}$  Tris-HCl ( $100 \text{ mM}$

## 4. Results and Discussion

NaCl), by collecting absorption spectra over time. Both 0.1% and 5% DMSO preparations were studied. The experiment was terminated when no more significant changes in absorption were observed.

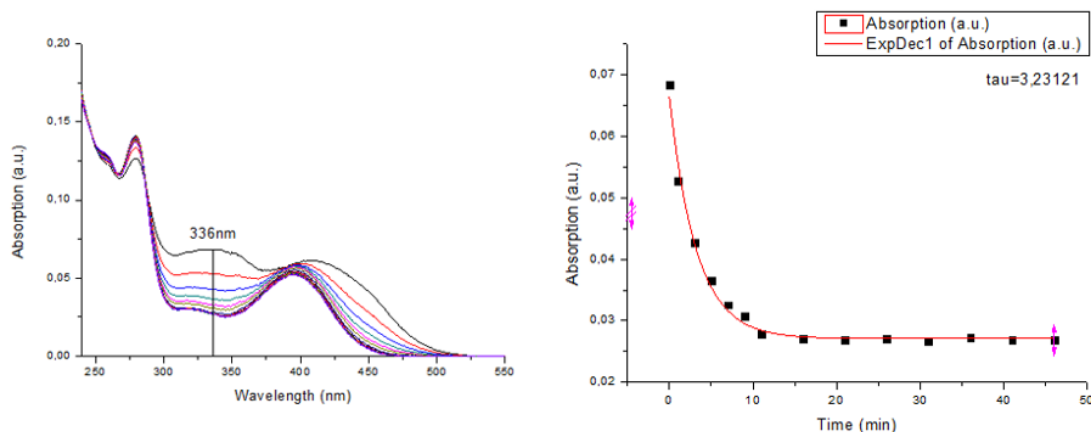


**Figure 4.5:** Molecular transition of **15** ( $20 \mu\text{M}$ ) in 0.1% DMSO monitored using UV-vis spectroscopy at room temperature (*ca.*  $22^\circ\text{C}$ ) immediately after compound addition from a concentrated DMSO stock into aqueous buffer. Left panel: Temporal spectral evolution. Right panel: Absorption at  $336 \text{ nm}$  (black squares) as a function of time. A first-order exponential fit (red line) rendered a time constant ( $\tau = 3.2 \text{ min}$ ) for the reaction.

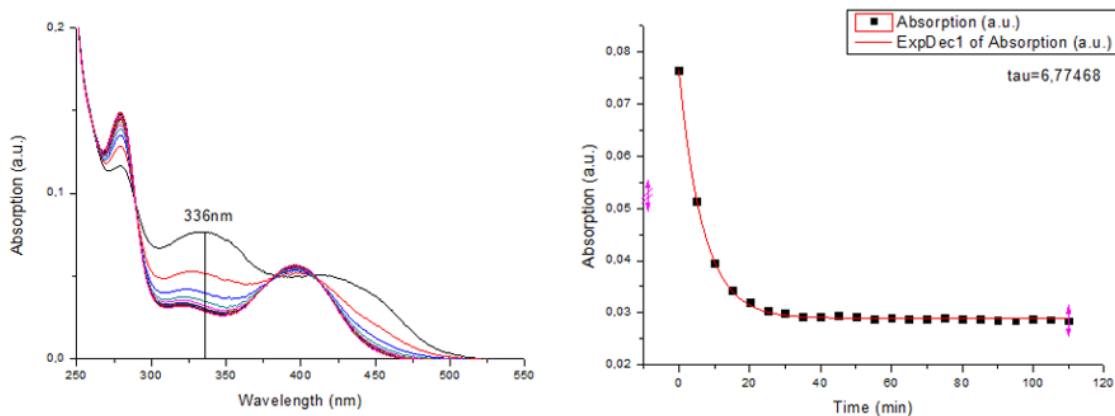


**Figure 4.6:** Molecular transition of **15** ( $20 \mu\text{M}$ ) in  $50 \text{ mM}$  Tris-HCl ( $100 \text{ mM}$  NaCl), 5% DMSO monitored using UV-vis spectroscopy at room temperature (*ca.*  $22^\circ\text{C}$ ) immediately after compound addition from a concentrated DMSO stock into aqueous buffer. Left panel: Temporal spectral evolution. Right panel: Absorption at  $336 \text{ nm}$  (black squares) as a function of time. A first-order exponential fit (red line) rendered a time constant ( $\tau = 6.8 \text{ min}$ ) for the reaction.

In figures 4.5 and 4.6, isosbestic points, *i.e.* wavelengths at which the absorption does not change with time, can be observed at  $252 \text{ nm}$ ,  $288 \text{ nm}$ ,  $389 \text{ nm}$ , and  $409 \text{ nm}$ . This is a strong indication that the chemical transformation involves not more than two states.

## 4.6 Solvent effects

In an attempt to learn more about the nature of this transition, the kinetic behavior of compound **15** was studied in three solvents with increasingly polar nature: acetonitrile, ethanol, and methanol, having polarities (relative to water) of 0.46, 0.65, and 0.76, respectively. [55] This was done by collecting absorption spectra over time following addition of a small volume ( $5 \mu\text{L}$ ) of DMSO stock solution ( $10 \text{ mM}$ ) to a large volume of the solvent ( $950 \mu\text{L}$ ). Thus, in the cuvette the DMSO content was 0.5% and the concentration of the compound was  $50 \mu\text{M}$ .

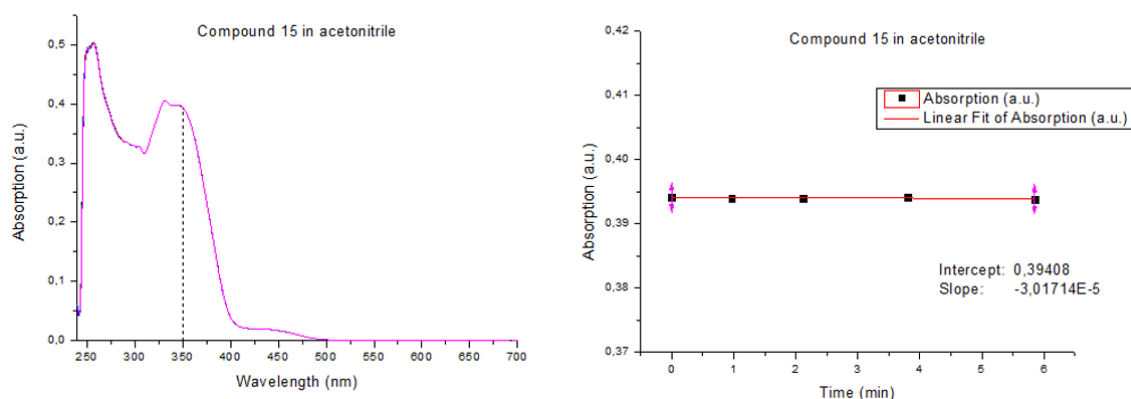


**Figure 4.7:** Molecular transition of **15** ( $50 \mu\text{M}$ ) in Acetonitrile monitored using UV-vis spectroscopy at room temperature (*ca.*  $22^\circ\text{C}$ ) immediately after compound addition from a concentrated DMSO stock into the solvent ( $[\text{DMSO}] = 0.5\%$ ). Left panel: Absorption spectra (no changes were recorded over time). Right panel: Absorption at  $350 \text{ nm}$  (black squares) as a function of time.

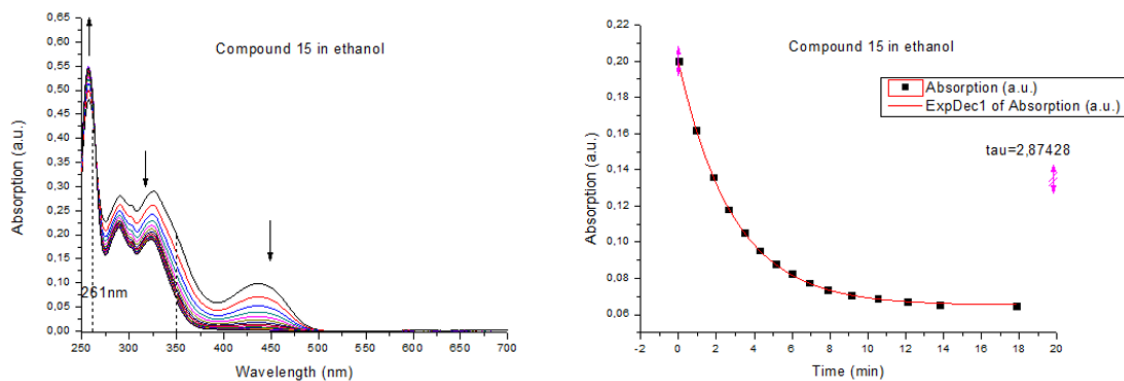


**Figure 4.8:** Molecular transition of **15** ( $50 \mu\text{M}$ ) in Ethanol monitored using UV-vis spectroscopy at room temperature (*ca.*  $22^\circ\text{C}$ ) immediately after compound addition from a concentrated DMSO stock into the solvent ( $[\text{DMSO}] = 0.5\%$ ). Left panel: Temporal spectral evolution. Right panel: Absorption at  $350 \text{ nm}$  (black squares) as a function of time.

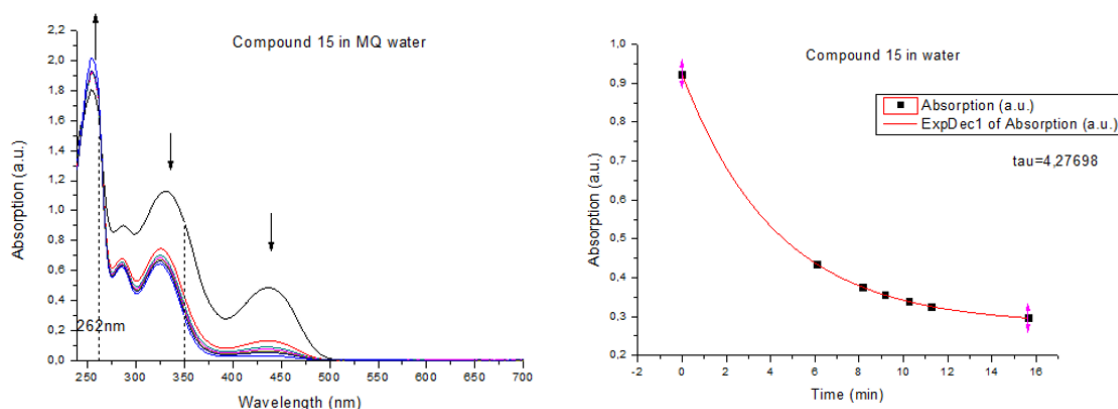


**Figure 4.9:** Molecular transition of **15** ( $50 \mu\text{M}$ ) in ultra purified, MQ-water (not Tris-HCl buffer) monitored using UV-vis spectroscopy at room temperature (*ca.*  $22^\circ\text{C}$ ) immediately after compound addition from a concentrated DMSO stock into the solvent ( $[\text{DMSO}] = 0.5\%$ ). Left panel: Temporal spectral evolution. Right panel: Absorption at  $350 \text{ nm}$  (black squares) as a function of time.

It was observed that when **15** was added to acetonitrile which is closest in polarity to DMSO ( $0.46$  *vs.*  $0.44$ , respectively [55]), no significant changes were detected over time. However, for ethanol and water, changes in absorption spectrum over time were observed. An isosbestic point was found close to  $261 \text{ nm}$  (Figure 4.8) and  $262 \text{ nm}$  (Figure 4.9) in ethanol and in water, respectively. It was observed that compound **15** reaches thermal equilibrium faster in ethanol (time constant =  $2.9 \text{ min}$ ) compared to water (time constant =  $4.3 \text{ min}$ ). This does not fit the hypothesis that a more polar surrounding accelerates the reaction, which suggests that additional factors influences these kinetics.

Nevertheless, the manifestation of the spectral changes in the two polar solvents water and ethanol, but not in the comparatively less polar solvents DMSO and acetonitrile could support the hypothesis that two chemical forms that differ in polarity are present in solution. Specifically, in the case of *cis-trans* isomerization, the *cis*-form has higher polarity compared to the *trans*-form. Thus, the *cis*-form is more favored in a more polar solvent compared to the *trans*-form. As ethanol is less polar compared to water, the difference of polarity between DMSO and ethanol *vs.* DMSO and water is smaller and could result in differences in rates of transformation. Also, effects like hydrogen bonding ability of solvent could potentially affect the rate of transformation.

## 4.7 Nuclear Magnetic Resonance

The chemical structure of compound **15** was examined *via* Nuclear Magnetic Resonance spectroscopy. The results acquired from  $^1\text{H}$ ,  $^{13}\text{C}$  and  $^1\text{H}$ - $^{13}\text{C}$  HSQC spectroscopy are presented bellow.

#### 4.7.1 $^1\text{H}$ -NMR of Schiff base **15** in different solvents

In Figure 4.10 the  $^1\text{H}$ -NMR spectra of the compound in DMSO and ethanol, respectively, are shown. There are significant differences between the spectra in the two solvents. The differences most likely is a result of changes in shifts due to the different solvents but also, importantly, due to a conformational difference of the compound in the two solvents. An important difference in the number of peaks is observed for the signals between 7.4 ppm and 7.3 ppm. Specifically, there are four and five peaks present for the sample in DMSO and ethanol, respectively. The number of peaks corresponds to the number of non-equivalent protons present in the chemical structure. Thus, this change is an indication of a structural difference between the two solvents, originating from the different chemical environments in the two solvents used.

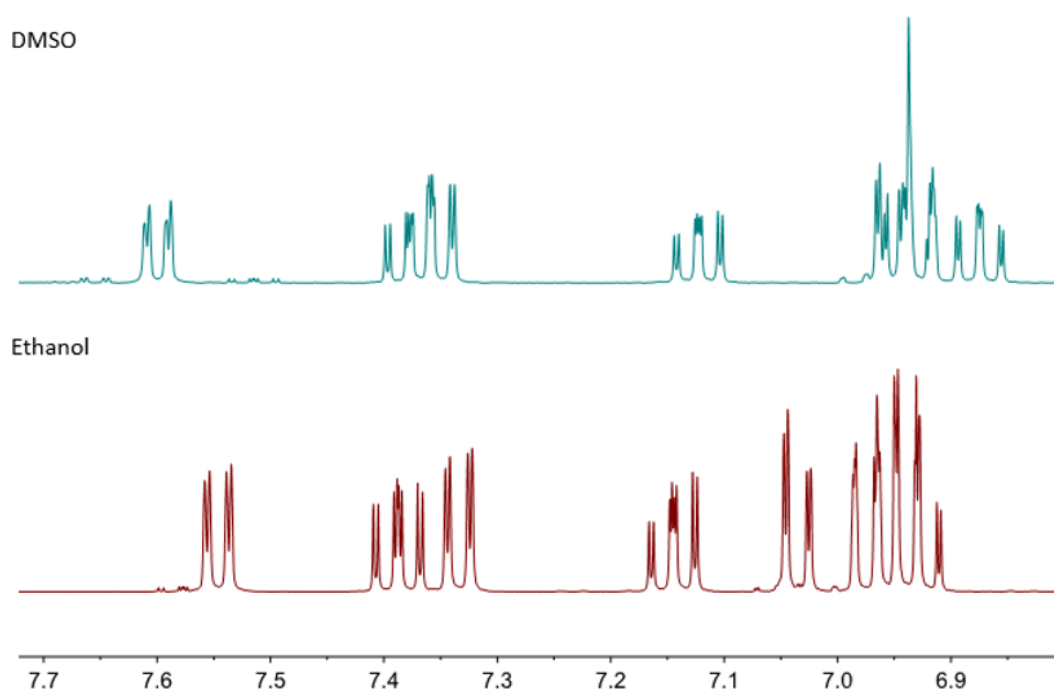


**Figure 4.10:** Proton NMR comparison of compound **15** in two different solvents

The complete setup of peaks between 7.7 ppm and 6.8 ppm correspond to the signals from the aromatic hydrogens. By integrating the area under the peaks the number of protons present in the specific signal can be determined. According to the values calculated by the software MestReNova x64, nine protons were found in both samples (Appendix A.24). This means that the protons, apart from the ones in the -OH-group, present in the aromatic structures are all found in the  $^1\text{H}$ -NMR and were neither reduced nor increased due to the solvent.

#### 4.7.2 $^{13}\text{C}$ -NMR of Schiff base **15** in different solvents

In figure 4.11, the  $^{13}\text{C}$  NMR signals are presented. For one of the peaks it is observed that there is a chemical shift from 161 ppm (sample in DMSO) to 163 ppm (sample

in ethanol). The chemical shift can be the result of either a conformational change, or an effect that the solvent environment has to the resonance signal. [55] It is highly plausible that the observed chemical shift is an indication of a structural change. However, to confirm and be certain about the validity of this observation HSQC-NMR, a 2D-NMR technique was performed.

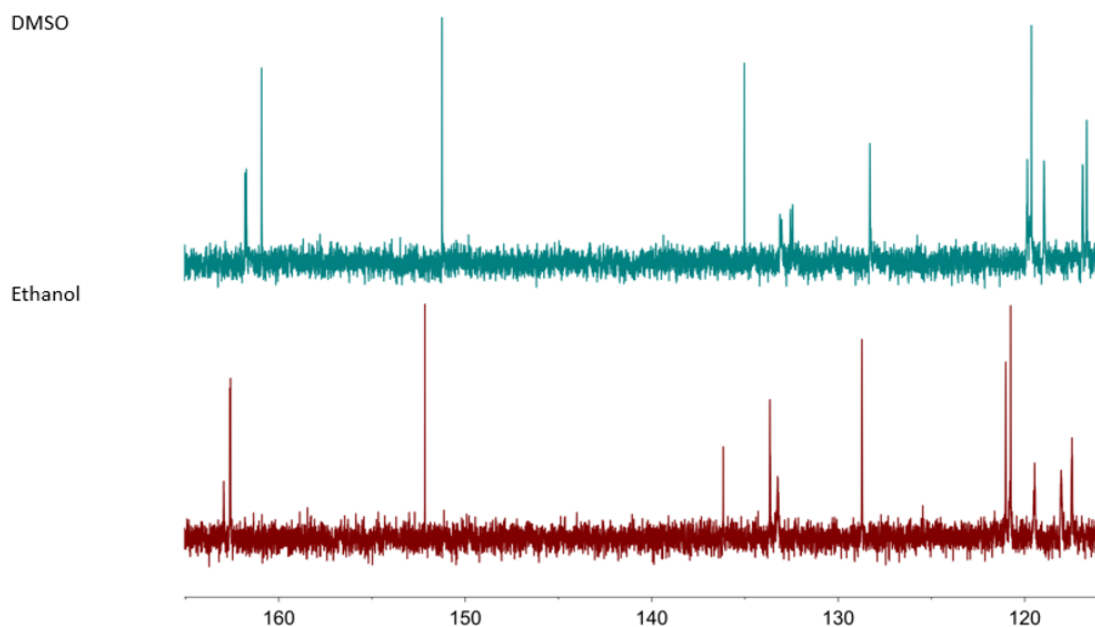


**Figure 4.11:** Carbon NMR comparison of compound **15** in two different solvents

### 4.7.3 Heteronuclear Single Quantum Coherence (HSQC) of Schiff base **15** in different solvents

The results of HSQC-NMR spectroscopy of **15** in both DMSO and EtOH are shown in Figure 4.12. In the x- and y-axis the chemical shifts in ppm of  $^1\text{H}$ -NMR and C-NMR are depicted, respectively. The red circles correspond to the signals produced by the sample in DMSO and the green ones to the sample present in ethanol.

In tables A.4 and A.5 in Appendix the exact values of the DMSO and ethanol samples, respectively are shown. Overall, it is observed that an upfield shift is induced for the  $^1\text{H}$  peaks while a downfield shift is induced for the  $^{13}\text{C}$  peaks when compound **15** is present in Ethanol. This is an indication of magnetic shielding of  $^1\text{H}$ 's and a magnetic deshielding of the  $^{13}\text{C}$ 's, caused by increased electron density in the chemical structure.  $^1\text{H}$ - $^{13}\text{C}$  HSQC can only observe carbons with protons attached to it, while quaternary carbons are lacking in the spectrum. Therefore, it could be confirmed that the peak at 161 ppm in DMSO move to 163 ppm in ethanol since this peak was absent in the  $^1\text{H}$ - $^{13}\text{C}$  HSQC spectrum in both solvents. From the structural predications presented below it is suggested that this peak is assigned to one of the carbons with a hydroxyl groups attached to it. The alteration in solvent, going from DMSO to ethanol, could be the explanation for the observed chemical shift change. In other words, the different chemical environments obtained in the

different solvent could be the reason for a change in conformation, here appearing as a change in chemical shift, but needs to be confirmed by *e.g.* evaluation of the interactions between protons close in space which can be observed in a Nuclear Overhauser Effect Spectroscopy (NOESY) experiment.

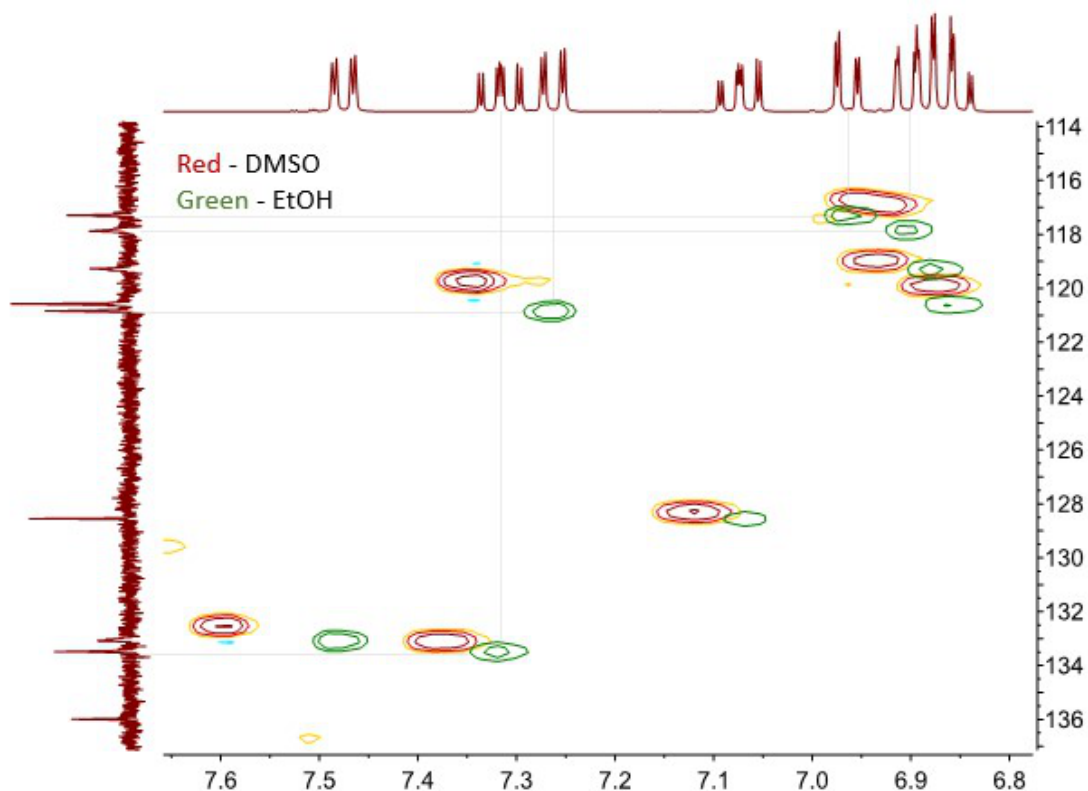


**Figure 4.12:** HSQC-NMR of compound **15** in DMSO (red) and ethanol (green)

## 4.8 Activation energy of *trans-cis*-transformation of **15** when going from DMSO to buffer

For the evaluation of the activation energy of the isomerization reaction, the rate constant for reaching the thermodynamic equilibrium at three different temperatures (20°C, 30°C and 40°C) were determined. The transition was studied when going from 100% DMSO to a buffer solution where the rest concentration of DMSO was 0.1%. The isomerization process was studied using the change in absorption of the compound at a wavelength where the variation in absorption as an effect of the transition is profound (312 nm, see Figure 4.5). This change in absorptive properties were then plotted as an effect of time. The data fit to a 1st order exponential decay, which together with the isosbestic point verifies the existence of no more than two states. As expected the time needed for the transition to take place was shorter with increased temperature. The rate constant ( $k$ ) is related to the exponential time constant ( $\tau$ ) as:

$$k = \frac{1}{\tau} \quad (4.1)$$

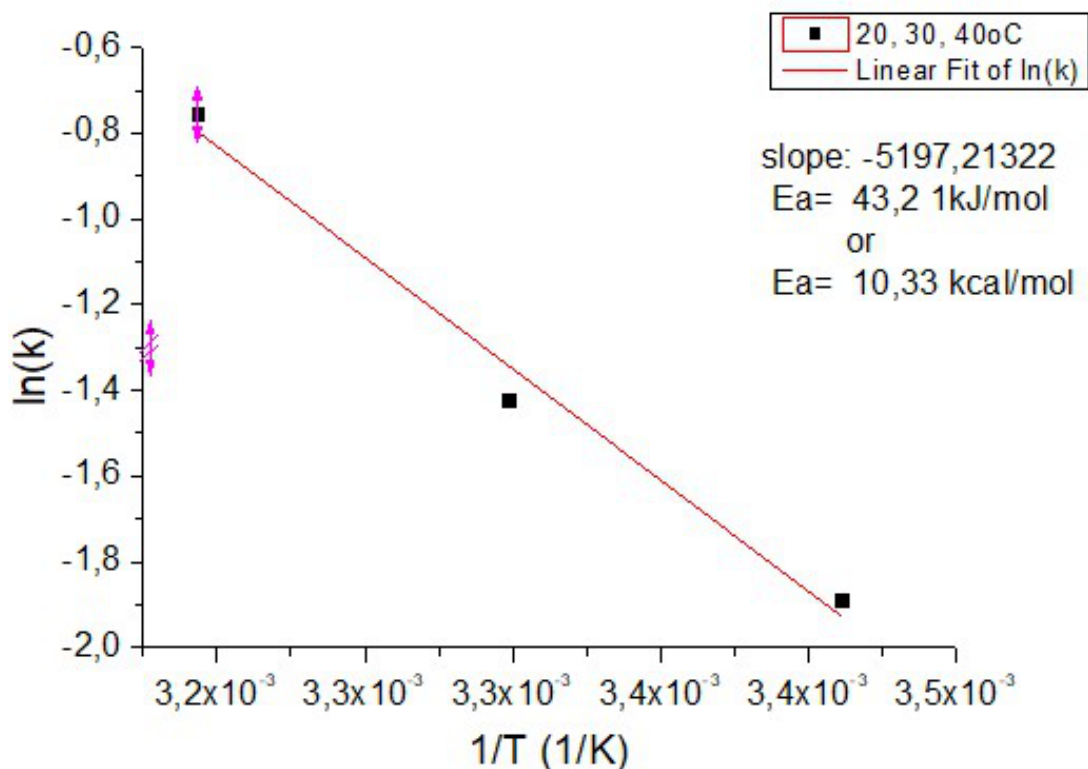


**Figure 4.13:** Arrhenius plot of compound **15** utilized for the determination of the activation energy  $E_a$  from the slope of equation 2.7

As shown in the Arrhenius evaluation of the process in Figure 4.13 the reaction has an activation energy of 43.2 kJ/mol, *i.e.* 10.33 kcal/mol. This value is reasonably well in line with literature values that are reported to be between 13 kcal/mol and 18 kcal/mol [49, 56].

## 4.9 DNA binding of 15

The DNA binding of compounds **5**, **8**, **9**, **13**, **15** and **28** was examined using UV-Visible spectroscopy and linear dichroism. Herein, only the results for compound **15** are presented and the rest can be found in the Appendix. Having established that the *cis*-form of **15** is the thermodynamically stable form in buffer we focused first on the addition of this form to DNA not to have two kinetic processes overlaid in our investigations.

### 4.9.1 Kinetics of DNA binding of **15** studied with fluorescence spectroscopy

Compound **15** was excited at wavelength  $\lambda_{\text{exc}}=393$  nm and the emission intensity was collected over time at the emission peak wavelength,  $\lambda_{\text{em}}=512$  nm. The excitation wavelength was chosen to be close to the isosbestic point at  $\lambda_{\text{iso}}=389$  nm, as this means that the changes seen in emission is only an effect of changed quantum yield and not an effect of changes in absorptivity. The sample with compound **15** was pre-equilibrated to reach its *cis*-form before the addition of DNA and starting the measurements. In this experiment 15  $\mu\text{M}$  of compound **15** in buffer (5% DMSO) was pre-equilibrated whereafter ctDNA was added. First, emission spectra at various times, with and without DNA were collected by exciting at  $\lambda_{\text{exc}}=393\text{nm}$  (Figure 4.14 (right)). In an additional experiment, the change in emission over time by exciting at wavelength  $\lambda_{\text{exc}} = 393\text{nm}$  and observing the emission at  $\lambda_{\text{em}} = 512$  nm was performed. We measured the emission of the pre-equilibration of **15** up until no significant changes in the emission was observed (Figure 4.14 (left),  $t = 200$  min). Thereafter, approximately 195  $\mu\text{M}$  of ctDNA (100  $\mu\text{L}$ ) was added to the solution and the emission kinetics were collected for an additional 4.5 hours.

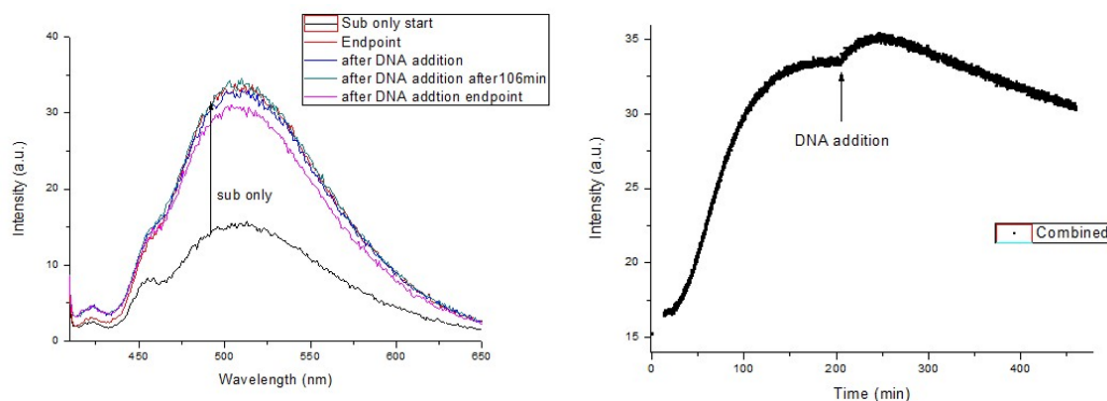


**Figure 4.14:** Left: Emission intensity spectrum of pre-equilibration of compound **15**, and at different time points after addition of ctDNA. Right: Emission kinetics spectrum of adding compound **15** first,  $C=15 \mu\text{M}$

It can be observed that the emission intensity doubled during the *trans-cis*-transition, indicating a higher quantum yield of the *cis*-form. After the addition of DNA, the emission intensity increased slightly more during the course of approximately 0.5 h and then it started to linearly decrease. The former could be an indication of DNA binding and the latter could be a consequence of photo-degradation due to the long irradiation of the compound. By studying the DNA binding process by adding compound **15** to DNA (and not the other way around as studied above) similar results were found (see Appendix from page XVII to page XVIII).

### 4.9.2 DNA binding of **15** studied with linear dichroism

DNA binding of compound **15** was studied using linear dichroism spectroscopy. Linear dichroism and UV-visible absorption spectra were collected daily for up to

3 days, while keeping the samples at room temperature, to examine whether any changes are observed. To examine the stability of DNA under those conditions, a sample which consisted of only 200  $\mu\text{M}$  ctDNA in buffer (5% DMSO) was stored at the same conditions and spectra were also collected daily for up to 3 days (Appendix).

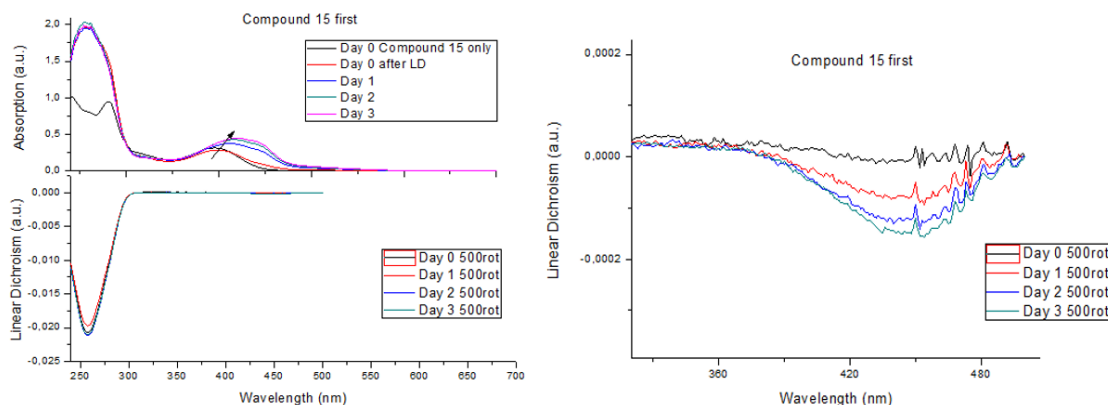
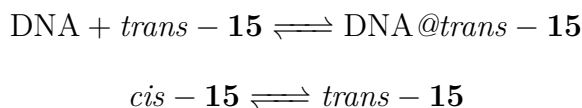


**Figure 4.15:** Left: LD spectra of solutions with 200  $\mu\text{M}$  ctDNA and 100  $\mu\text{M}$  of compound **15** after different times. Right: Magnified image of LD spectra illustrated on the left panel, wavelength range from 320  $\text{nm}$  to 500  $\text{nm}$

As can be seen in Figure 4.15 (left), there is a change in absorption spectrum over time and by magnifying the LD signal (Figure 4.15 (right)) a weak change is also observed between the wavelengths 360  $\text{nm}$  and 500  $\text{nm}$  where compound **15** has its low energy absorption band. According to LD-theory the negative signal suggests binding angles above  $55^\circ$  and approaching perpendicular orientation relative to the DNA helix axis, thus indicating an intercalative mode of binding. In comparison to the transformation kinetics (Figure 4.3) the change in absorption spectrum of **15** seems to follow the opposite pattern. Thus, it is plausible that the DNA forces compound **15** into the *trans* form, *i.e.* binds only the *trans*-form and therefore slowly enriches this species. However, the binding kinetics is very slow. It takes up to 3 days to observe merely minute changes in absorption and LD signal. The reason is attributed to the fact that the *cis-trans* equilibrium is heavily pushed towards the *cis*-form in free solution and a very slow transformation between the two states. Specifically, this means that two chemical equilibria take place in solution:



The first chemical reaction is pushed towards the right, *i.e.* has a low free energy for the DNA-bound *trans*-form. As *trans* is bound to DNA less *trans* form is found free in solution. Thus, the equilibrium of the second chemical interaction is pushed towards the right to compensate for the lost *trans*-form free in solution. As a result, more *cis*-form free in solution is transformed into *trans*, which subsequently binds to DNA up until an overall equilibrium has been established.

When we studied the same phenomenon instead adding compound to DNA we found similar behavior as described above (see Appendix A.29). Overall, we find DNA binding of the Schiff base **15**. However, it appears to be much weaker than the values reported in literature ( $K_a = 10^{-4}M^{-1} - 10^{-6}M^{-1}$ ) [57] and, also, the binding process appears to be much slower.

### 4.9.3 Ethidium bromide displacement

As was mentioned in Chapter 1, ethidium bromide is a common DNA intercalator that can be used to examine whether a compound interacts with DNA *via* intercalation. This is achieved by a competition assay where ethidium bromide is added in a solution with brine and DNA. Thereafter, a high amount of the compound of interest is added and the change in ethidium bromide emission intensity is recorded. This study has previously been performed on DNA and **15** by da Silva *et al.* 2017 [12], showing a decrease in intensity by 10.2% when 30  $\mu M$  of compound **15** was added in Tris HCl 20 *mM* (NaCl 100 *mM*) and 1.6  $\mu M$  of ethidium bromide. In our ethidium bromide displacement experiment we chose conditions that resembled the ones in the previous study. However, as can be seen in Figure 4.16, no significant difference was observed by adding 10  $\mu M$  of compound **15**. When slowly increasing concentration of compound **15** to 100  $\mu M$  slight changes to the ethidium bromide emission started to appear (see Figure 4.16 and Table 4.2).

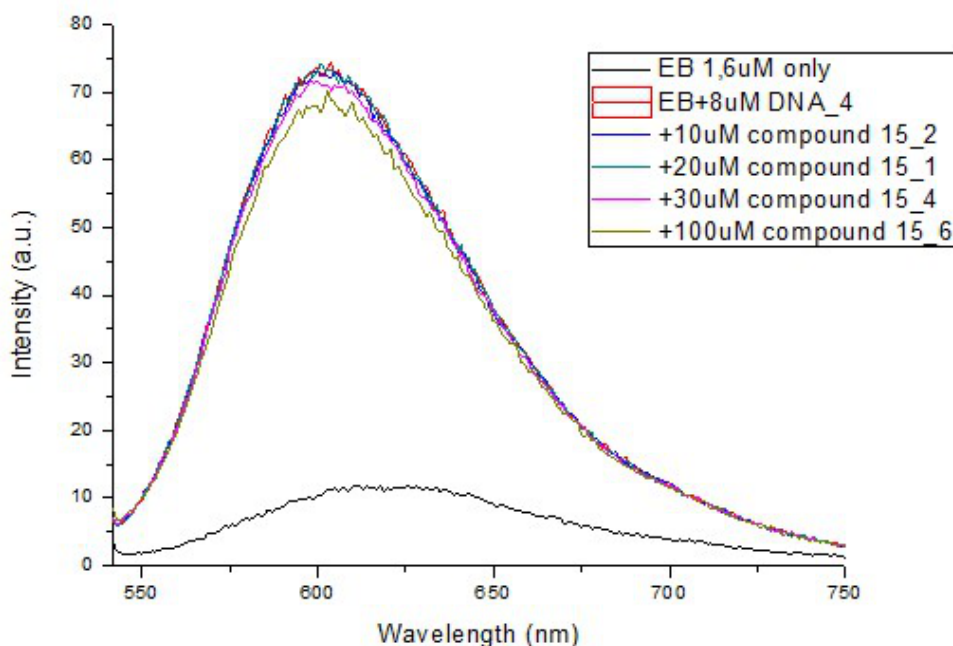


**Figure 4.16:** Ethidium bromide displacement from DNA upon adding compound **15**

Specifically, a 2.6% decrease in fluorescence was calculated from the spectra above for 30  $\mu M$  of **15** added. For 100  $\mu M$  of compound **15** a 5.9% decrease in emission was noted. This is still a lower value compared to the one reported by da Silva *et*

#### 4. Results and Discussion

---

*al.* 2017 [12]. Even though we cannot repeat the results by da Silva *et al.* 2017 [12], the emission decrease that we find still is well in line with the suggestion from the linear dichroism that **15** in its *trans*-form, although weakly and slowly, intercalates into DNA.

**Table 4.2:** Ethidium bromide displacement of compound **15** comparison with literature

Compound Concentration ( $\mu\text{M}$ )	Emission Intensity (a.u.)	% Fluorescent decrease	Literature da Silva <i>et al.</i> 2017 [12]
0	73.4	-	-
30	71.5	2.6	10.2
100	69.1	5.9	-

# 5

## Conclusion

This research aimed to identify the absorption and fluorescence properties, as well as the potential DNA binding of a number of Schiff bases provided by NSCR "Demokritos". It appears that the compounds exhibit very slow and weak DNA binding that did not allow the determination of the association constant ( $K_a$ ). Most of the compounds had high to moderate solubility in 5% DMSO which allows biological studies. Additionally, compounds **1**, **8**, and **26** exhibited satisfactory fluorescent properties, thus they may have potential to be utilized as probes. The chemical transition observed in all compounds may be attributed to *cis-trans* isomerization transition. This is highly supported by the UV/Vis spectroscopy and the activation energy results, as the values were in close proximity to the literature, in regard to compound **15**. The two isomers appear to differ in polarity preference. Specifically, *trans* isomer appears to be favored in solvents with lower polarity compared to the *cis* isomer. The LD and UV-vis spectra of compound **15** suggest that DNA induces a slow transition back to the *trans*-form, over time. The mode of binding appears to be *via* intercalation, however, the binding constant is found to be much weaker compared to the values suggested by the literature. Additionally, regarding compound **15** the results of the Ethidium Bromide Displacement assay provided by da Silva *et al.* 2017 [12] were not reproducible, since much lower decrease in emission intensity is recorded in the experiments performed in this thesis.

### 5.1 Future work

Based on these conclusions, it is suggested to continue the study of the remaining compounds, to examine whether the same isomerization transition occurs and evaluate the binding mode and potential as DNA binding agents. It is also suggested to perform High Performance Liquid Chromatography (HPLC) to determine the percentage of each isomer in solution depending on the solvent in which they are present. That way the structural evaluation and the evaluation of fluorescence and binding properties can be improved. Additionally, it is suggested to repeat the emission kinetics, as the temperature might increase the transition rate or effect the binding kinetics. Another binding technique that could be applied is thermal shift assay. According to this technique the melting temperature of DNA is measured in presence and absence of compound. In case the temperature difference of these two measurements is greater than 5°C, then intercalation is considered to be the binding mode, as the temperature increase is attributed to the fact that *via* intercalation the dsDNA becomes more stable. Overall, according to the literature these compounds appear to have therapeutic properties, however, based on the results of

## 5. Conclusion

---

this thesis they do not seem to be attributed to DNA binding as it is very weak. Thus, a detailed biological study is suggested to take place in the future, to estimate the biological activity of these compounds. Currently, cytotoxicity assays are performed at NCSR “Demokritos” of the novel compounds to estimate their anticancer properties against glioblastoma cell lines.

# Bibliography

- [1] Cleiton M Da Silva, Daniel L da Silva, Luzia V Modolo, Rosemeire B Alves, Maria A de Resende, Cleide VB Martins, and Ângelo de Fátima. Schiff bases: A short review of their antimicrobial activities. *Journal of Advanced research*, 2(1):1–8, 2011.
- [2] AG Bharathi Dileepan, T Daniel Prakash, A Ganesh Kumar, P Shameela Rajam, V Violet Dhayabaran, and R Rajaram. Isatin based macrocyclic schiff base ligands as novel candidates for antimicrobial and antioxidant drug design: In vitro dna binding and biological studies. *Journal of Photochemistry and Photobiology B: Biology*, 183:191–200, 2018.
- [3] Pattan Sirajuddin Nayab, Istikhar A Ansari, and Mohammad Shahid. New phthalimide-appended schiff bases: Studies of dna binding, molecular docking and antioxidant activities. *Luminescence*, 32(5):829–838, 2017.
- [4] Mahnaz Ariyaeifar, Hadi Amiri Rudbari, Mehdi Sahihi, Zahra Kazemi, Abolghasem Abbasi Kajani, Hassan Zali-Boeini, Nazanin Kordestani, Giuseppe Bruno, and Sajjad Gharaghani. Chiral halogenated schiff base compounds: green synthesis, anticancer activity and dna-binding study. *Journal of Molecular Structure*, 1161:497–511, 2018.
- [5] Pritam Ghosh, Additi Roy Chowdhury, Sourav Kr Saha, Meenakshi Ghosh, Mrinal Pal, Naresh Chandra Murmu, and Priyabrata Banerjee. Synthesis and characterization of redox non-innocent cobalt (iii) complexes of a o, n, o donor ligand: Radical generation, semi-conductivity, antibacterial and anticancer activities. *Inorganica Chimica Acta*, 429:99–108, 2015.
- [6] Ernest M Hodnett and William J Dunn. Structure-antitumor activity correlation of some schiff bases. *Journal of Medicinal Chemistry*, 13(4):768–770, 1970.
- [7] X-J Tan, L-Y Zhang, Y-K Sun, and X-M Zhou. Synthesis, structure and antiproliferative and optical activities of two new biphenyl-derived schiff bases. *Acta Crystallographica Section C: Structural Chemistry*, 75(2), 2019.
- [8] Hui Wang, Mingyue Jiang, Fangli Sun, Shujun Li, Chung-Yun Hse, and Chunde Jin. Screening, synthesis, and qsar research on cinnamaldehyde-amino acid schiff base compounds as antibacterial agents. *Molecules*, 23(11):3027, 2018.
- [9] Francisco M García-Valle, Vanessa Tabernerero, Tomás Cuenca, Jesús Cano, and Marta EG Mosquera. Aluminates with fluorinated schiff bases: Influence

- of the alkali metal–fluorine interactions in structure stabilization. *Molecules*, 23(12):3108, 2018.
- [10] Anu Kajal, Suman Bala, Sunil Kamboj, Neha Sharma, and Vipin Saini. Schiff bases: a versatile pharmacophore. *Journal of Catalysts*, 2013, 2013.
- [11] A Xavier and N Srividhya. Synthesis and study of schiff base ligands. *IOSR Journal of Applied Chemistry*, 7(11):06–15, 2014.
- [12] Cleiton M da Silva, Marina M Silva, Fabiano S Reis, Ana Lúcia TG Ruiz, João E de Carvalho, Josué CC Santos, Isis M Figueiredo, Rosemeire B Alves, Luzia V Modolo, and Ângelo de Fátima. Studies on free radical scavenging, cancer cell antiproliferation, and calf thymus dna interaction of schiff bases. *Journal of Photochemistry and Photobiology B: Biology*, 172:129–138, 2017.
- [13] Arezoo Jamshidvand, Mehdi Sahihi, Valiollah Mirkhani, Majid Moghadam, Iraj Mohammadpoor-Baltork, Shahram Tangestaninejad, Hadi Amiri Rudbari, Hadi Kargar, Reza Keshavarzi, and Sajjad Gharaghani. Studies on dna binding properties of new schiff base ligands using spectroscopic, electrochemical and computational methods: influence of substitutions on dna-binding. *Journal of Molecular Liquids*, 253:61–71, 2018.
- [14] R Vikneswaran, Muhamad Syamir Syafiq, Naser Eltaher Eltayeb, Mohd Naquuddin Kamaruddin, Subramaniam Ramesh, and Rosiyah Yahya. A new thio-schiff base fluorophore with copper ion sensing, dna binding and nuclease activity. *Spectrochimica Acta Part A: Molecular and Biomolecular Spectroscopy*, 150:175–180, 2015.
- [15] DNA. <https://proteopedia.org/wiki/index.php/DNA>, Journal: DNA - Proteopedia, life in 3D.
- [16] Ali A Almaqwashi, Thayaparan Paramanathan, Ioulia Rouzina, and Mark C Williams. Mechanisms of small molecule–dna interactions probed by single-molecule force spectroscopy. *Nucleic acids research*, 44(9):3971–3988, 2016.
- [17] LM Wilhelmsson. *Recognition and visualization of nucleic acids*. PhD thesis, Chalmers University of Technology, 2003.
- [18] DNA - STRUCTURE. <https://www.chemguide.co.uk/organicprops/aminoacids/dna1.html>, Jim Clark, DNA - structure, 2007.
- [19] B form DNA. <https://www.genscript.com/molecular-biology-glossary/8673/B-form-DNA>, GenScript.
- [20] Dinshaw Patel, Keith R Fox, David Rusling, Tom Brown, Yves Pommier, Christophe Marchand, Christian Bailly, Bengt NordÚn, Peter E Nielsen, Natalie Dias, et al. *Sequence-specific DNA binding agents*. Royal Society of Chemistry, 2007.
- [21] Maolin Wang, Yuanyuan Yu, Chao Liang, Aiping Lu, and Ge Zhang. Recent advances in developing small molecules targeting nucleic acid. *International journal of molecular sciences*, 17(6):779, 2016.
- [22] Paris L Hamilton and Dev P Arya. Natural product dna major groove binders. *Natural product reports*, 29(2):134–143, 2012.

- 
- [23] Antonino Lauria, Alessandra Montalbano, Paola Barraja, Gaetano Dattolo, and Anna Maria Almerico. Dna minor groove binders: an overview on molecular modeling and qsar approaches. *Current medicinal chemistry*, 14(20):2136–2160, 2007.
- [24] Raman Dhivya, Sellamuthu Kathiresan, Murugesan Vigneshwar, Jothi Ranjani, Jeyaprakash Rajendhran, Nattamai SP Bhuvanesh, and Jamespandi Annaraj. Bioactive mono/bis (carboxyamide) based co (ii), ni (ii) and cu (ii) complexes: Synthesis, characterization, dna binding and anticancer potentials. *Applied Organometallic Chemistry*, 33(1):e4660, 2019.
- [25] M Shahnawaz Khan, Mohd Khalid, M Shahwaz Ahmad, Musheer Ahmad, Mo Ashafaq, Rizwan Arif, M Shahid, et al. Synthesis, spectral and crystallographic study, dna binding and molecular docking studies of homo dinuclear co (ii) and ni (ii) complexes. *Journal of Molecular Structure*, 1175:889–899, 2019.
- [26] Bing-Fan Long, Qin Huang, Shu-Long Wang, Yan Mi, Meng-Fan Wang, Ting Xiong, Shu-Cong Zhang, Xian-Hong Yin, and Fei-Long Hu. Five new cobalt (ii) complexes based on indazole derivatives: synthesis, dna binding and molecular docking study. *Journal of Coordination Chemistry*, pages 1–19, 2019.
- [27] Farasha Sama, Mukul Raizada, Mo Ashafaq, M Naqi Ahamad, I Mantasha, Khushboo Iman, M Shahid, Rizwan Arif, Naseer A Shah, Hatem AM Saleh, et al. Synthesis, structure and dna binding properties of a homodinuclear cu (ii) complex: An experimental and theoretical approach. *Journal of Molecular Structure*, 1176:283–289, 2019.
- [28] Zhenzhen Li, Qian Zhang, Hua Liu, Guangying Wang, and Jiacheng Liu. Dna binding and in vitro antineoplastic activity of neotype water-soluble cu (ii)-complexes based on fluorinated benzoylhydrazone porphyrin ligands. *Dyes and Pigments*, 163:647–655, 2019.
- [29] Manjuri Kumar, Sidhali Uday Parsekar, Natarajan Duraipandy, Manikantan Syamala Kiran, and Aditya P Koley. Synthesis, dna binding and in vitro cytotoxicity studies of a mononuclear copper (ii) complex containing n2s (thiolate) cu core and 1, 10-phenanthroline as a coligand. *Inorganica Chimica Acta*, 484:219–226, 2019.
- [30] Kalyanmoy Jana, Somnath Das, Horst Puschmann, Subhas Chandra Debnath, Aparna Shukla, Arun K Mahanta, Maidul Hossain, Tithi Maity, and Bidhan Chandra Samanta. Supramolecular self-assembly, dna interaction, antibacterial and cell viability studies of cu (ii) and ni (ii) complexes derived from nnn donor schiff base ligand. *Inorganica Chimica Acta*, 487:128–137, 2019.
- [31] Rania G Mohamed, Fatma M Elantabli, Ayman A Abdel Aziz, H Moustafa, and Samir M El-Medani. Synthesis, characterization, nlo properties, antimicrobial, ct-dna binding and dft modeling of ni (ii), pd (ii), pt (ii), mo (iv) and ru (i) complexes with nos schiff base. *Journal of Molecular Structure*, 1176:501–514, 2019.
- [32] Animesh Pradhan, Shobhraj Haldar, Krishnasis Basu Mallik, Mrinmoy Ghosh,

- Manindranath Bera, Nayim Sepay, Dieter Schollmeyer, Sumanta Kumar Ghatak, Sanchita Roy, and Sandip Saha. Mixed phenoxo and azido bridged dinuclear nickel (ii) and copper (ii) compounds with n, n, o-donor schiff bases: Synthesis, structure, dna binding, dft and molecular docking study. *Inorganica Chimica Acta*, 484:197–205, 2019.
- [33] Animesh Pradhan, Shobhraj Haldar, Krishnasis Basu Mallik, Mrinmoy Ghosh, Manindranath Bera, Nayim Sepay, Dieter Schollmeyer, Sumanta Kumar Ghatak, Sanchita Roy, and Sandip Saha. Mixed phenoxo and azido bridged dinuclear nickel (ii) and copper (ii) compounds with n, n, o-donor schiff bases: Synthesis, structure, dna binding, dft and molecular docking study. *Inorganica Chimica Acta*, 484:197–205, 2019.
- [34] Ariadni Zianna, George D Geromichalos, Antonios G Hatzidimitriou, Evdoxia Coutouli-Argyropoulou, Maria Lalia-Kantouri, and George Psomas. Palladium (ii) complexes with salicylaldehyde ligands: Synthesis, characterization, structure, in vitro and in silico study of the interaction with calf-thymus dna and albumins. *Journal of inorganic biochemistry*, 194:85–96, 2019.
- [35] Gokcen Eren, Esra Emerce, Leyla Acik, Betul Aydin, and Fatma Gumus. A novel trans-pt (ii) complex bearing 2-acetoxymethylbenzimidazole as a non-leaving ligand (trans-[pt (ambi) 2cl2]): Synthesis, antiproliferative activity, dna interaction and molecular docking studies compared with its cis isomer (cis-[pt (ambi) 2cl2]). *Journal of Molecular Structure*, 1184:512–518, 2019.
- [36] Keke Chai, Yihui Jiang, Tianzhi Han, Junlong Niu, Liushuang Yao, Haiyu Zhang, Min Zeng, Li Zhang, Xuemin Duan, and Jintao Wang. Synthesis, dna binding, topoisomerase i inhibition and antiproliferation activities of three new binuclear terpyridine platinum (ii) complexes. *Polyhedron*, 157:124–130, 2019.
- [37] Ph Pengkiliya Devi, Francis AS Chipem, Ch Brajakishor Singh, and RK Lonibala. Complexation of 2-amino-3-(4-hydroxyphenyl)-n'-[(2-hydroxyphenyl)methylene] propane hydrazide with mn (ii), co (ii), ni (ii), cu (ii) and zn (ii) ions: Structural characterization, dft, dna binding and antimicrobial studies. *Journal of Molecular Structure*, 1176:7–18, 2019.
- [38] Khalid Mahmood, Waleed Hashmi, Hammad Ismail, Bushra Mirza, Brendan Twamley, Zareen Akhter, Isabel Rozas, and Robert J Baker. Synthesis, dna binding and antibacterial activity of metal (ii) complexes of a benzimidazole schiff base. *Polyhedron*, 157:326–334, 2019.
- [39] Xiaofang Wang, Hyun Jeong Lim, and Ahjeong Son. Characterization of denaturation and renaturation of dna for dna hybridization. *Environmental health and toxicology*, 29, 2014.
- [40] Cleiton M da Silva, Marina M Silva, Fabiano S Reis, Ana Lúcia TG Ruiz, João E de Carvalho, Josué CC Santos, Isis M Figueiredo, Rosemeire B Alves, Luzia V Modolo, and Ângelo de Fátima. Studies on free radical scavenging, cancer cell antiproliferation, and calf thymus dna interaction of schiff bases. *Journal of Photochemistry and Photobiology B: Biology*, 172:129–138, 2017.
- [41] L Marcus Wilhelmsson, Fredrik Westerlund, Per Lincoln, and Bengt Nordén.

- Dna-binding of semirigid binuclear ruthenium complex  $\delta$ ,  $\delta$ - $[\mu$ -(11, 11'-bidppz)(phen)  $4\text{Ru}_2$ ]  $4+$ : Extremely slow intercalation kinetics. *Journal of the American Chemical Society*, 124(41):12092–12093, 2002.
- [42] Jessica D Knoll and Claudia Turro. Control and utilization of ruthenium and rhodium metal complex excited states for photoactivated cancer therapy. *Coordination chemistry reviews*, 282:110–126, 2015.
- [43] Gaetano Mangiapia, Gerardino D'Errico, Luca Simeone, Carlo Irace, Aurel Radulescu, Antonio Di Pascale, Alfredo Colonna, Daniela Montesarchio, and Luigi Paduano. Ruthenium-based complex nanocarriers for cancer therapy. *Biomaterials*, 33(14):3770–3782, 2012.
- [44] major groove. <https://medical-dictionary.thefreedictionary.com/majorgroove>, Farlex, The Free Dictionary.
- [45] Ana O de Souza, Fabio Galetti, Célio L Silva, Beatriz Bicalho, Márcia M Parma, Sebastião F Fonseca, Anita J Marsaioli, Angela CLB Trindade, Rossimíriam P Freitas Gil, Franciglauber S Bezerra, et al. Antimycobacterial and cytotoxicity activity of synthetic and natural compounds. *Química Nova*, 30(7):1563–1566, 2007.
- [46] Selami Demirci, Ayşegül Doğan, Neşe Başak Türkmen, Dilek Telci, Albert A Rizvanov, and Fikrettin Şahin. Schiff base-ploxamer p85 combination demonstrates chemotherapeutic effect on prostate cancer cells in vitro. *Biomedicine & Pharmacotherapy*, 86:492–501, 2017.
- [47] Michael B Smith and Jerry March. *March's advanced organic chemistry: reactions, mechanisms, and structure*. John Wiley & Sons, 2007.
- [48] S. Kalsi P. *Organic Reactions and Their Mechanisms (3rd Edition)*, chapter 2.15.1 Keto-Enol Tautomerism. New Academic Science, 2018.
- [49] Paulo J Coelho, M Cidália R Castro, and M Manuela M Raposo. Reversible trans-cis photoisomerization of new pyrrolidene heterocyclic imines. *Journal of Photochemistry and Photobiology A: Chemistry*, 259:59–65, 2013.
- [50] Jan Slavík et al. *Fluorescence microscopy and fluorescent probes*. Springer, 1996.
- [51] Karl Börjesson, Søren Preus, Afaf H El-Sagheer, Tom Brown, Bo Albinsson, and L Marcus Wilhelmsson. Nucleic acid base analog fret-pair facilitating detailed structural measurements in nucleic acid containing systems. *Journal of the American Chemical Society*, 131(12):4288–4293, 2009.
- [52] Hui Liu, Yumin Du, Xiaohui Wang, and Liping Sun. Chitosan kills bacteria through cell membrane damage. *International journal of food microbiology*, 95(2):147–155, 2004.
- [53] Renu A Heller, Mark Schena, Andrew Chai, Dari Shalon, Tod Bedilion, James Gilmore, David E Woolley, and Ronald W Davis. Discovery and analysis of inflammatory disease-related genes using cDNA microarrays. *Proceedings of the National Academy of Sciences*, 94(6):2150–2155, 1997.

- [54] Alison Rodger, Bengt Nordén, et al. *Circular dichroism and linear dichroism*, volume 1. Oxford University Press, USA, 1997.
- [55] Christian Reichardt and Thomas Welton. *Solvents and solvent effects in organic chemistry*. John Wiley & Sons, 2011.
- [56] SA Houlden and IG Csizmadia. The geometry and electronic structure of substituted schiff's bases. *Tetrahedron*, 25(5):1137–1153, 1969.
- [57] Eva M Talavera, Pablo Guerrero, Francisco Ocana, and Jose M Alvarez-Pez. Photophysical and direct determination of binding constants of ethidium bromide complexed to e. coli dna. *Applied spectroscopy*, 56(3):362–369, 2002.

# A

## Appendix

### A.1 Schiff bases

**Table A.1:** Chemical name and Molecular weight of compounds used

Compound	Chemical name	Molecular Weight [g/mol]
1	2-(((E)-(4-aminophenylimino)methyl)phenol	212.09
5	(E)-N-(4-chlorobenzylidene)-4-chlorobenzenamine	250.12
8	2-((E)-(6-methoxypyridin-3-ylimino)methyl)phenol	228.09
9	(E)-N-(4-nitrobenzylidene)-4-chlorobenzenamine	260.68
12	2-((E)-(4-methoxyphenylimino)methyl)phenol	227.26
13	2-(((E)-(4-chlorophenylimino)methyl)-4-methoxyphenol	261.06
14	4-methoxy-2-((E)-(phenethylimino)methyl)-3,5-dichlorophenol	255.31
15	(E)-2-(2-hydroxybenzylideneamino)phenol	213.08
17	(E)-N-(4-methoxybenzylidene)-4-nitrobenzenamine	256.26
23	2-((E)-(5-chloro-2-methylphenylimino)methyl)phenol	245.70
24	2-((E)-(4-(hexyloxy)phenylimino)methyl)phenol	297.39
26	2-((E)-(3-methylpyridin-2-ylimino)methyl)-3,5-dichlorophenol	281.14
28	2-((E)-(3-chlorophenylimino)methyl)phenol	231.68

## A.2 UV-Vis spectra of compounds in 0.2% DMSO

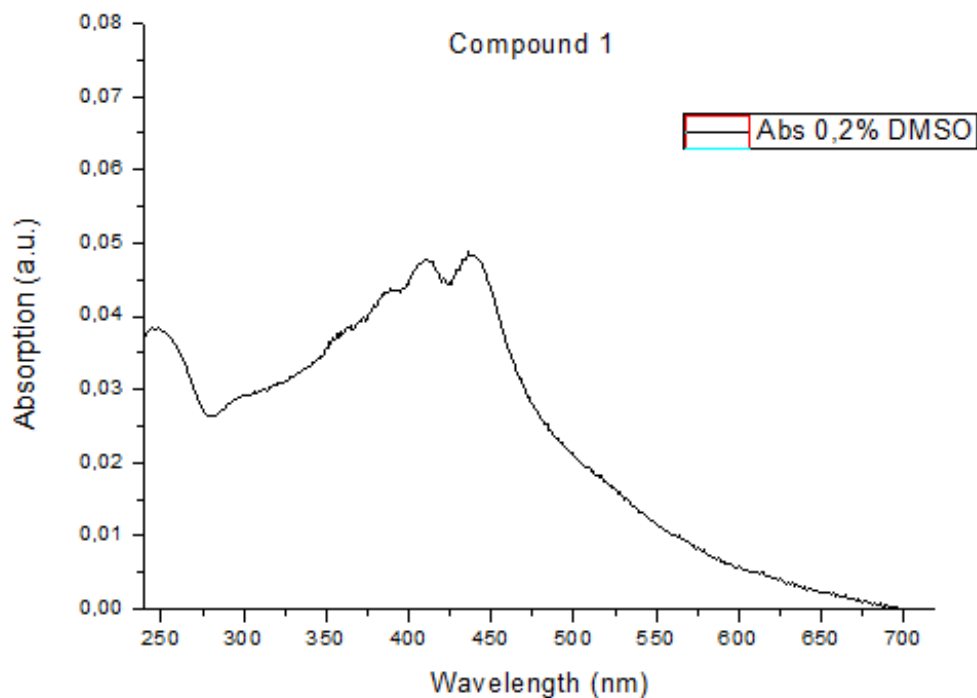


Figure A.1: Absorption spectrum of compound 1, 10  $\mu$ M at 0.2% DMSO

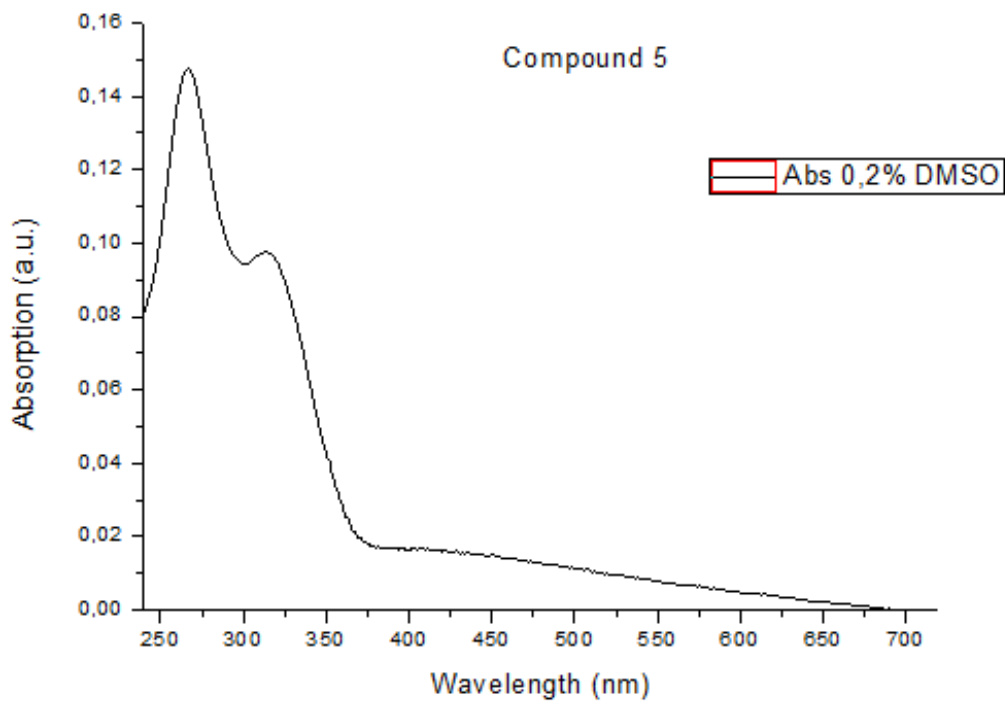


Figure A.2: Absorption spectrum of compound 5, 10  $\mu$ M at 0.2% DMSO

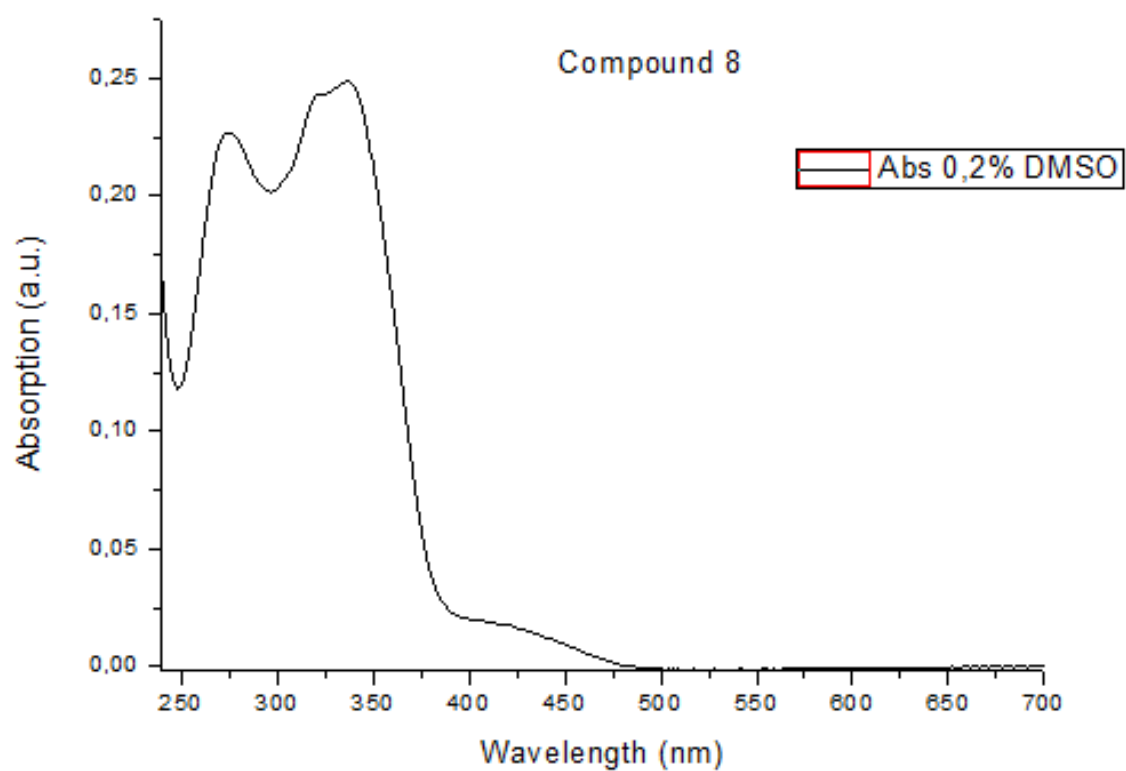


Figure A.3: Absorption spectrum of compound 8, 10  $\mu\text{M}$  at 0.2% DMSO

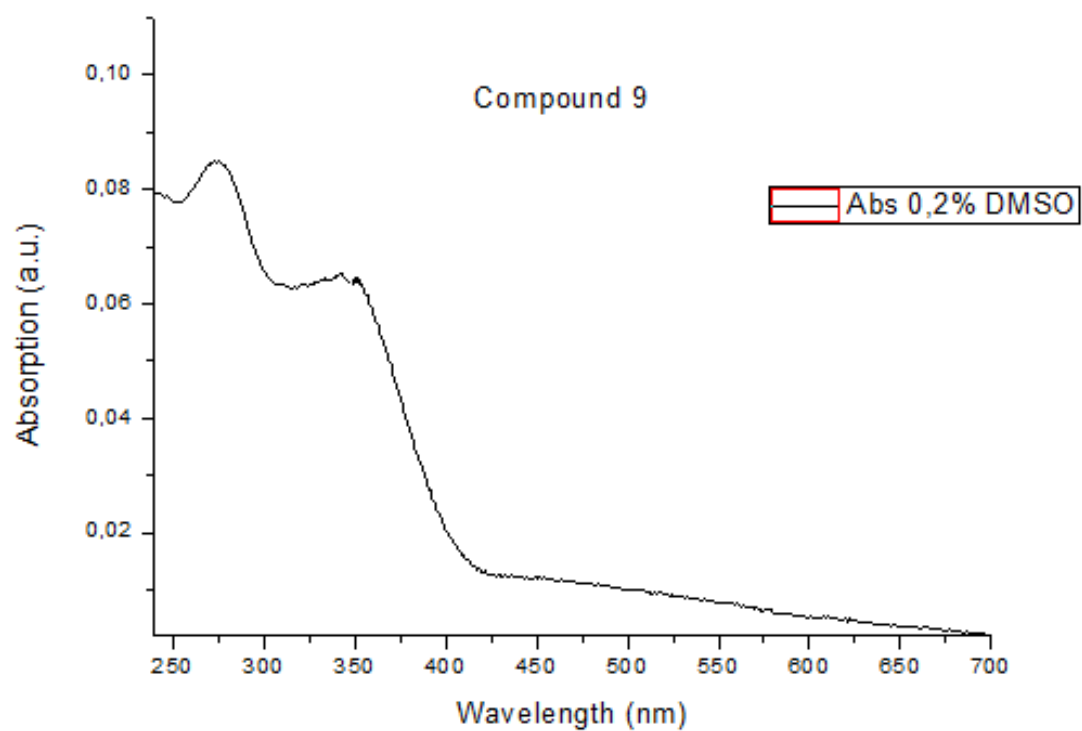


Figure A.4: Absorption spectrum of compound 9, 10  $\mu\text{M}$  at 0.2% DMSO

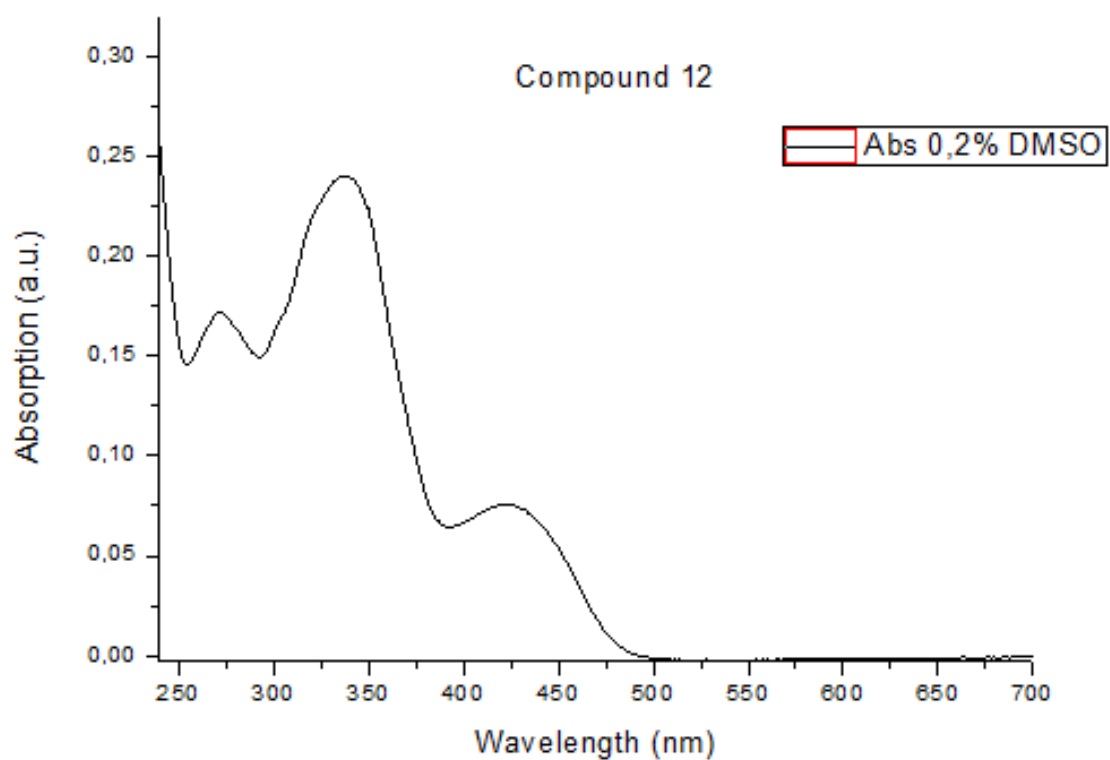


Figure A.5: Absorption spectrum of compound 12, 10  $\mu$ M at 0.2% DMSO

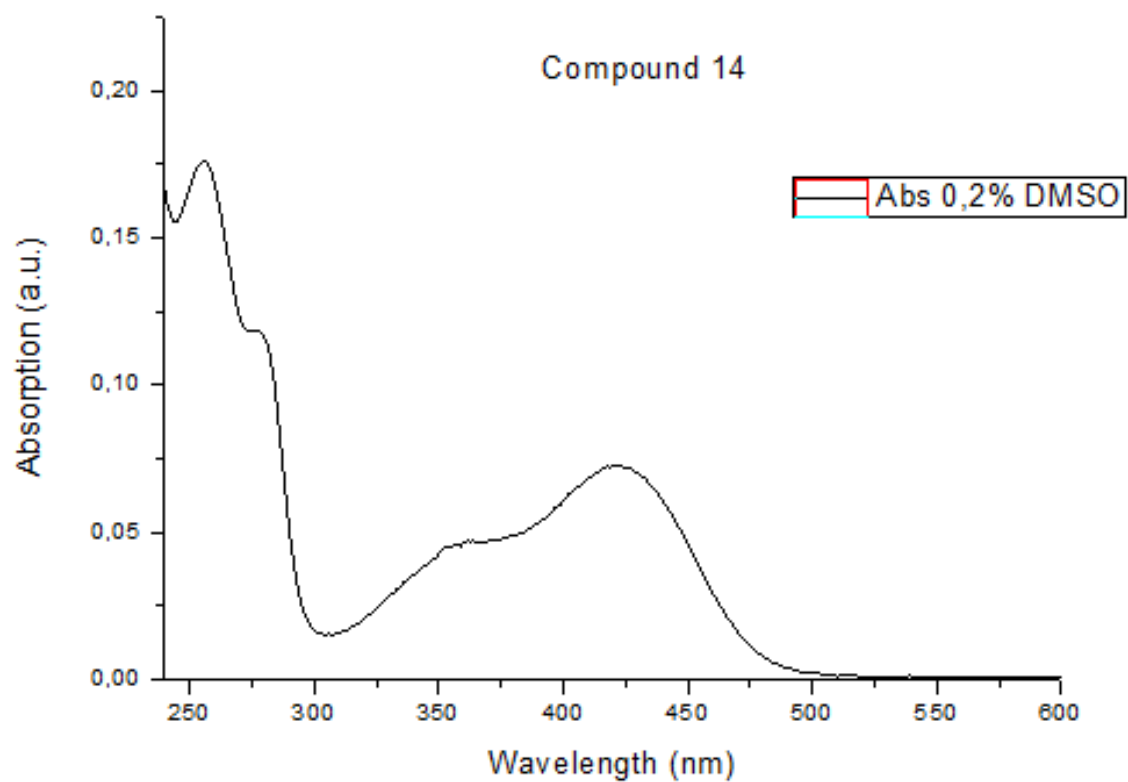


Figure A.6: Absorption spectrum of compound 14, 10  $\mu$ M at 0.2% DMSO

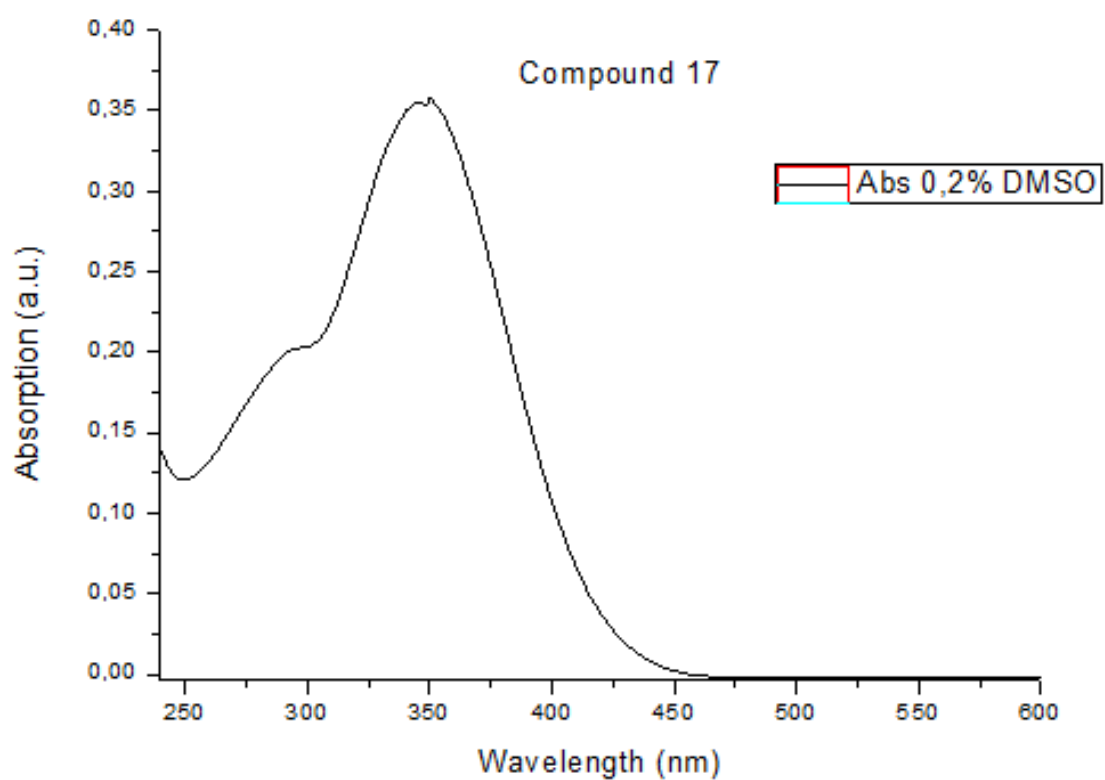


Figure A.7: Absorption spectrum of compound **17**, 10  $\mu\text{M}$  at 0.2% DMSO

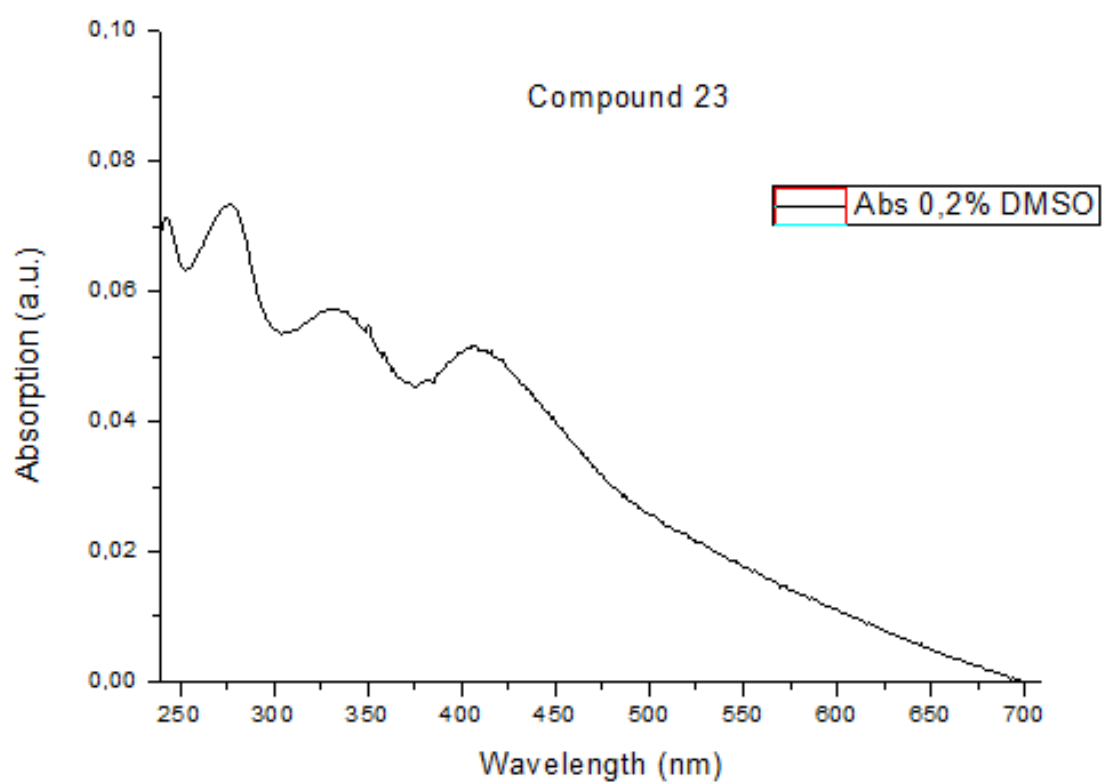


Figure A.8: Absorption spectrum of compound **23**, 10  $\mu\text{M}$  at 0.2% DMSO

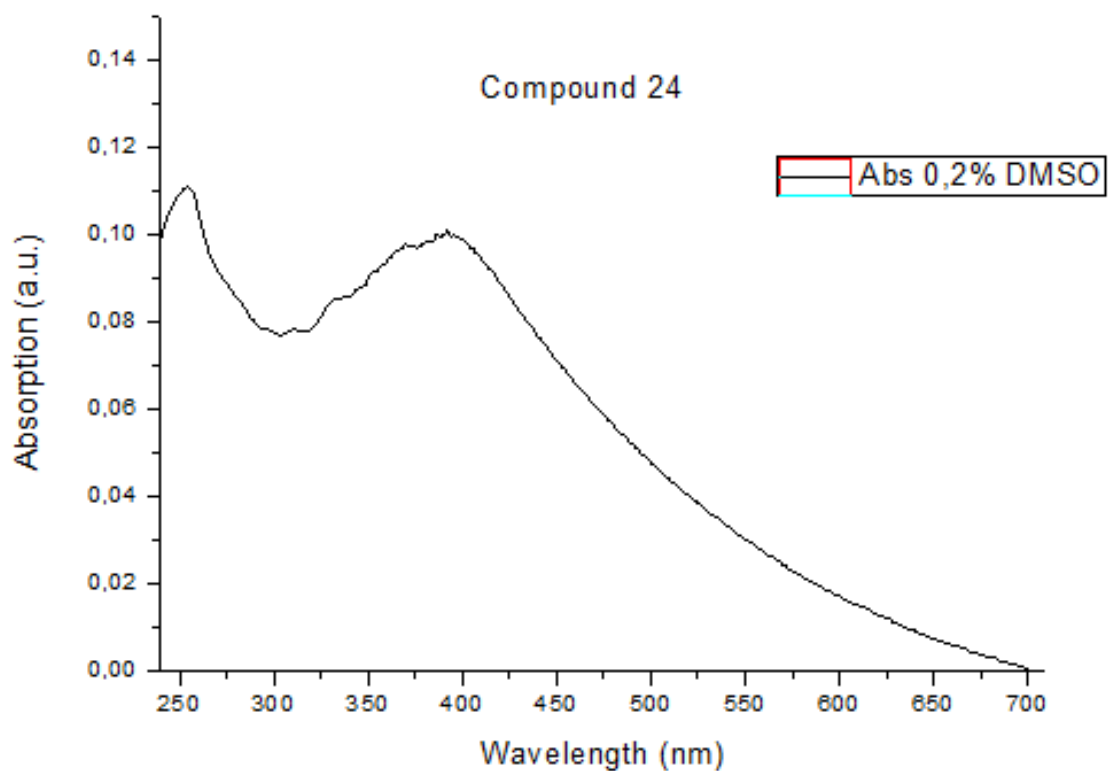


Figure A.9: Absorption spectrum of compound **24**, 10  $\mu$ M at 0.2% DMSO

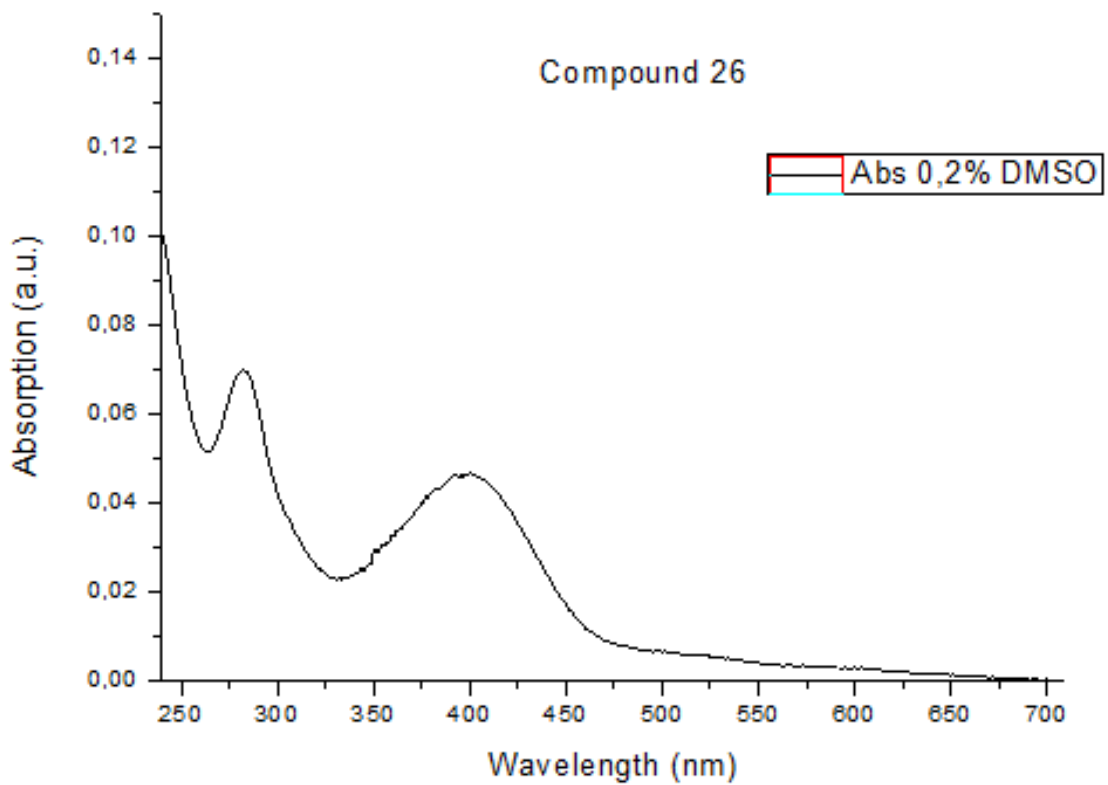


Figure A.10: Absorption spectrum of compound **26**, 10  $\mu$ M at 0.2% DMSO

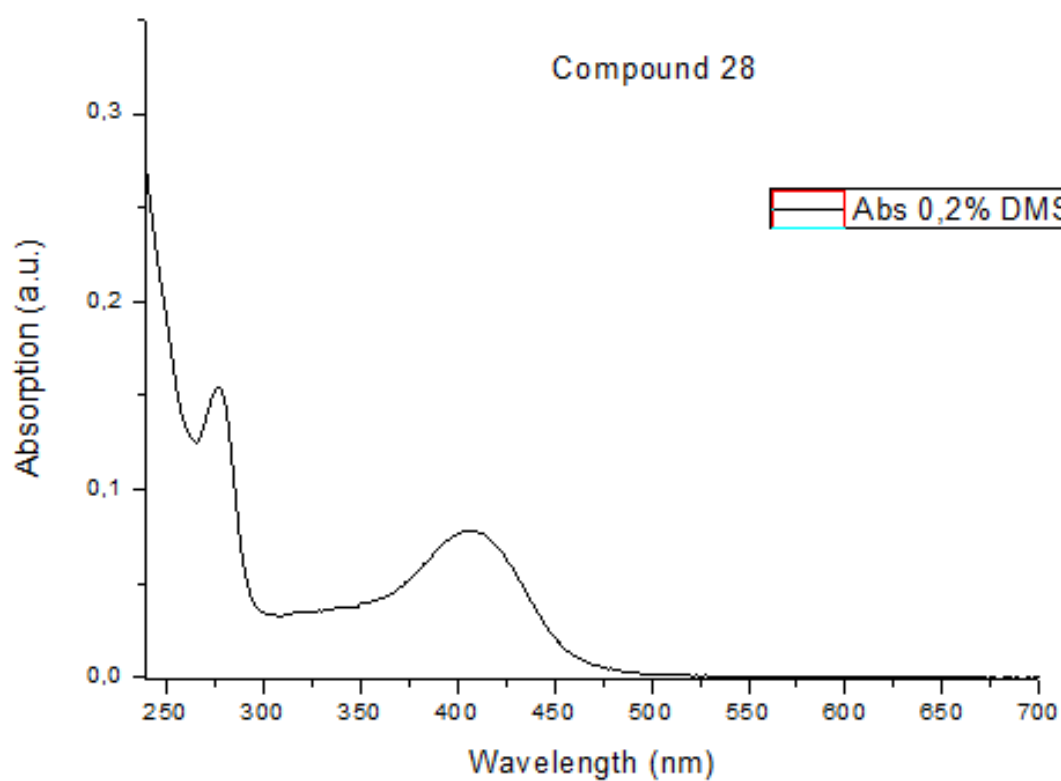


Figure A.11: Absorption spectrum of compound **28**, 10  $\mu\text{M}$  at 0.2% DMSO

### A.3 Compounds not Soluble in 5% DMSO

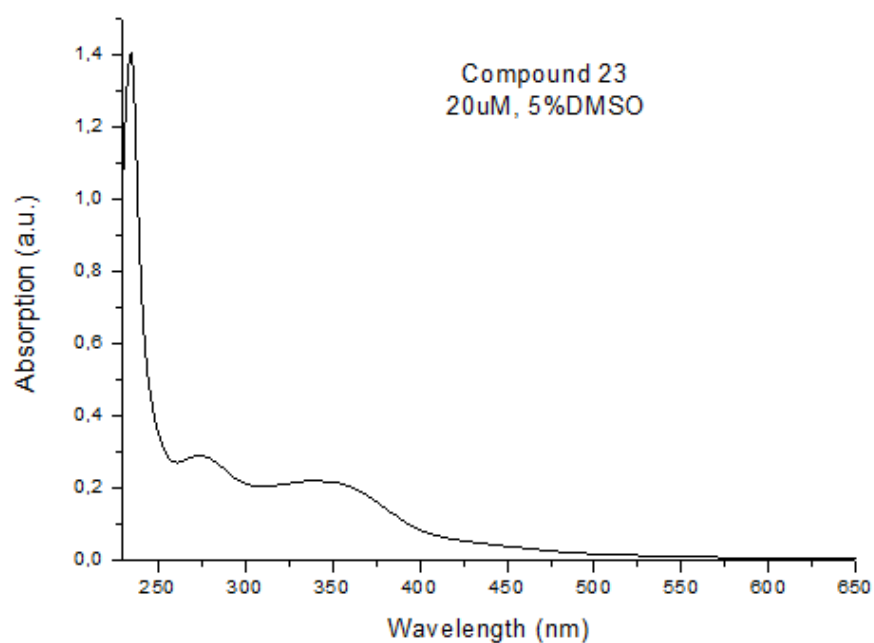
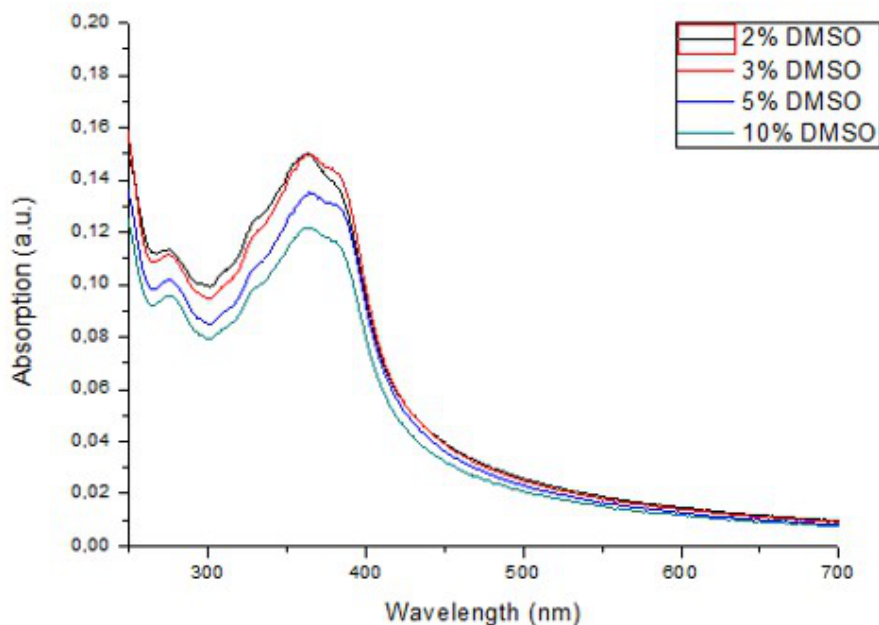
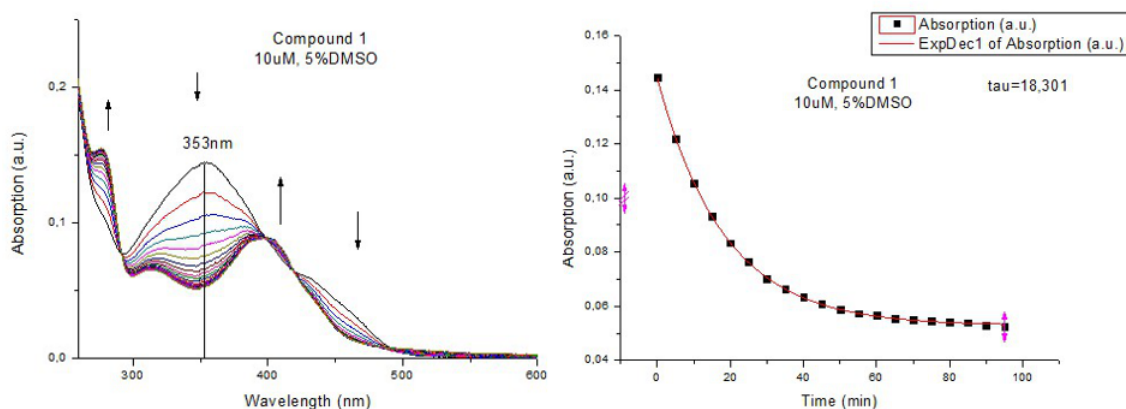


Figure A.12: Absorption spectrum of compound **23**, 20  $\mu\text{M}$  at 5% DMSO



**Figure A.13:** Absorption spectrum of compound **24**, 15  $\mu\text{M}$  at various percentages of DMSO

## A.4 Absorption Kinetics



**Figure A.14:** Molecular transition of compound **1** (10  $\mu\text{M}$ ) in 5% DMSO monitored using UV-vis spectroscopy at room temperature (*ca.* 22°C) immediately after compound addition from a concentrated DMSO stock into 50 *mM* Tris-HCl (100 *mM* NaCl) buffer. Left panel: Temporal spectral evolution. Right panel: Absorption at 353 *nm* (black squares) as a function of time. A first-order exponential fit (red line) rendered a time constant ( $\tau = 18.301$  *min*) for the reaction.

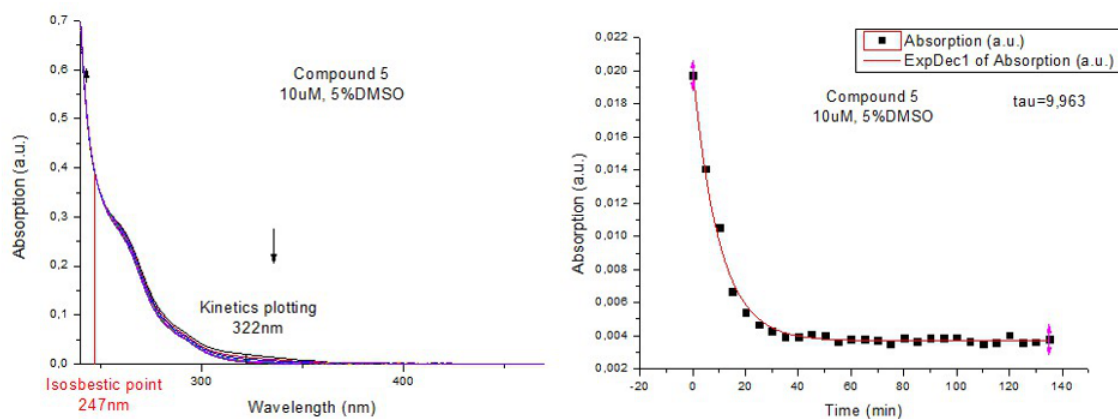


**Figure A.15:** Molecular transition of compound **5** ( $10 \mu\text{M}$ ) in 5% DMSO monitored using UV-vis spectroscopy at room temperature (*ca.*  $22^\circ\text{C}$ ) immediately after compound addition from a concentrated DMSO stock into  $50 \text{ mM}$  Tris-HCl ( $100 \text{ mM}$  NaCl) buffer. Left panel: Temporal spectral evolution. Right panel: Absorption at  $322 \text{ nm}$  (black squares) as a function of time. A first-order exponential fit (red line) rendered a time constant ( $\tau = 9.963 \text{ min}$ ) for the reaction.

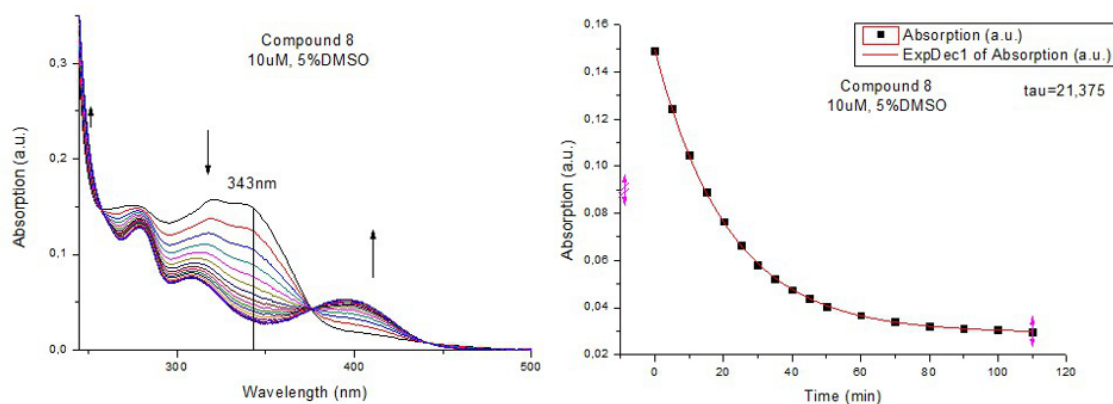


**Figure A.16:** Molecular transition of compound **8** ( $10 \mu\text{M}$ ) in 5% DMSO monitored using UV-vis spectroscopy at room temperature (*ca.*  $22^\circ\text{C}$ ) immediately after compound addition from a concentrated DMSO stock into  $50 \text{ mM}$  Tris-HCl ( $100 \text{ mM}$  NaCl) buffer. Left panel: Temporal spectral evolution. Right panel: Absorption at  $343 \text{ nm}$  (black squares) as a function of time. A first-order exponential fit (red line) rendered a time constant ( $\tau = 21.3751 \text{ min}$ ) for the reaction.

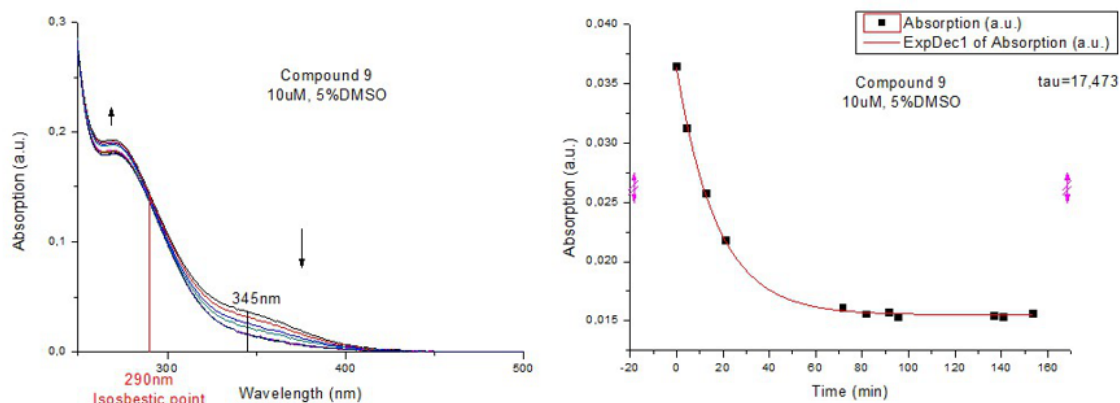


**Figure A.17:** Molecular transition of compound **9** (10  $\mu$ M) in 5% DMSO monitored using UV-vis spectroscopy at room temperature (*ca.* 22°C) immediately after compound addition from a concentrated DMSO stock into 50 *mM* Tris-HCl (100 *mM* NaCl) buffer. Left panel: Temporal spectral evolution. Right panel: Absorption at 345 *nm* (black squares) as a function of time. A first-order exponential fit (red line) rendered a time constant ( $\tau=17.473$  *min*) for the reaction.

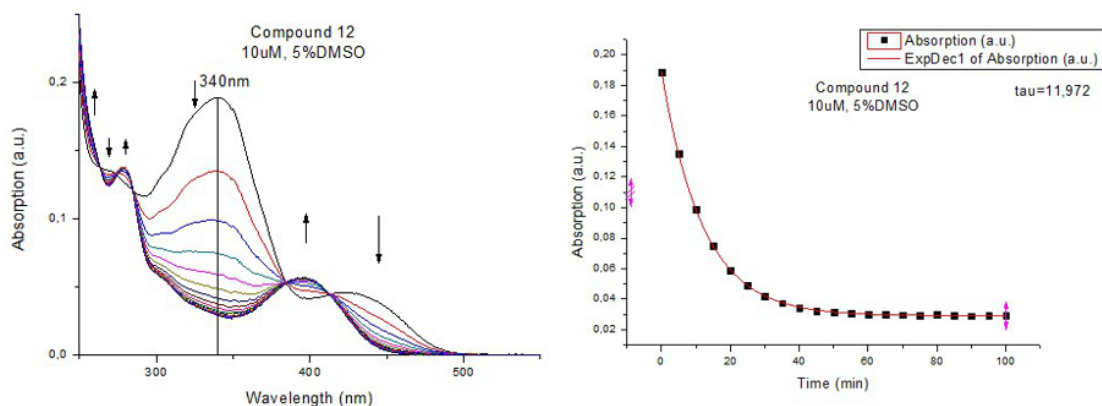


**Figure A.18:** Molecular transition of compound **12** (10  $\mu$ M) in 5% DMSO monitored using UV-vis spectroscopy at room temperature (*ca.* 22°C) immediately after compound addition from a concentrated DMSO stock into 50 *mM* Tris-HCl (100 *mM* NaCl) buffer. Left panel: Temporal spectral evolution. Right panel: Absorption at 340 *nm* (black squares) as a function of time. A first-order exponential fit (red line) rendered a time constant ( $\tau=11.972$  *min*) for the reaction.

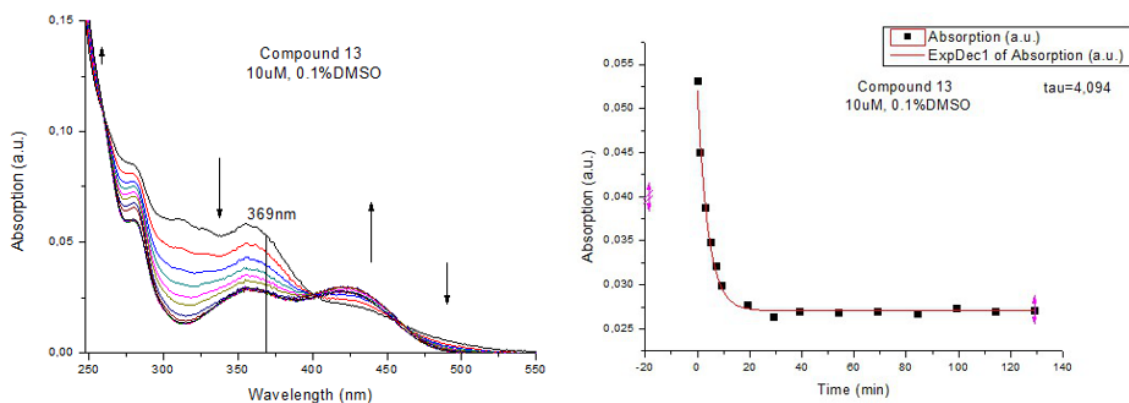


**Figure A.19:** Molecular transition of compound **13** (10  $\mu$ M) in 0.1% DMSO monitored using UV-vis spectroscopy at room temperature (*ca.* 22°C) immediately after compound addition from a concentrated DMSO stock into 50 *mM* Tris-HCl (100 *mM* NaCl) buffer. Left panel: Temporal spectral evolution. Right panel: Absorption at 369 *nm* (black squares) as a function of time. A first-order exponential fit (red line) rendered a time constant ( $\tau=4.094$  *min*) for the reaction.

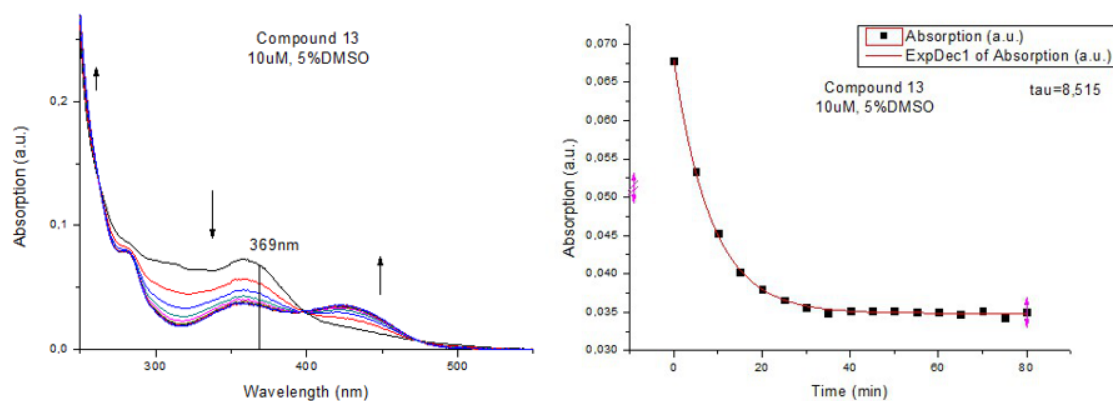


**Figure A.20:** Molecular transition of compound **13** (10  $\mu$ M) in 5% DMSO monitored using UV-vis spectroscopy at room temperature (*ca.* 22°C) immediately after compound addition from a concentrated DMSO stock into 50 *mM* Tris-HCl (100 *mM* NaCl) buffer. Left panel: Temporal spectral evolution. Right panel: Absorption at 369 *nm* (black squares) as a function of time. A first-order exponential fit (red line) rendered a time constant ( $\tau=8.515$  *min*) for the reaction.

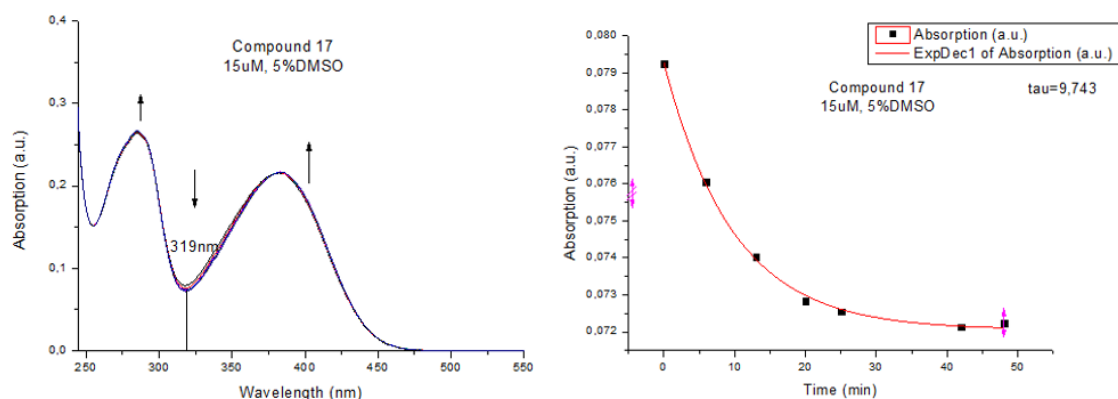


**Figure A.21:** Molecular transition of compound **17** (15  $\mu\text{M}$ ) in 5% DMSO monitored using UV-vis spectroscopy at room temperature (*ca.* 22°C) immediately after compound addition from a concentrated DMSO stock into 50  $m\text{M}$  Tris-HCl (100  $m\text{M}$  NaCl) buffer. Left panel: Temporal spectral evolution. Right panel: Absorption at 319  $\text{nm}$  (black squares) as a function of time. A first-order exponential fit (red line) rendered a time constant ( $\tau = 9.743$   $\text{min}$ ) for the reaction.

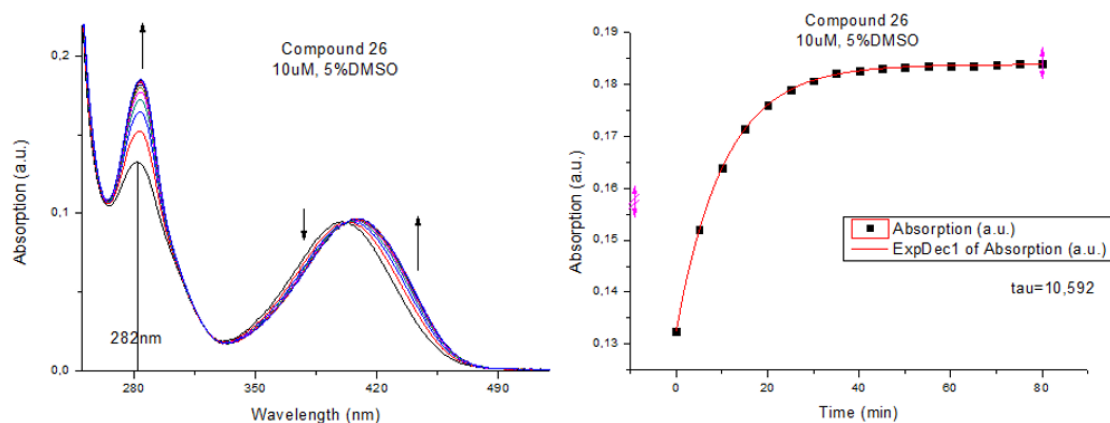


**Figure A.22:** Molecular transition of compound **26** (10  $\mu\text{M}$ ) in 5% DMSO monitored using UV-vis spectroscopy at room temperature (*ca.* 22°C) immediately after compound addition from a concentrated DMSO stock into 50  $m\text{M}$  Tris-HCl (100  $m\text{M}$  NaCl) buffer. Left panel: Temporal spectral evolution. Right panel: Absorption at 282  $\text{nm}$  (black squares) as a function of time. A first-order exponential fit (red line) rendered a time constant ( $\tau = 10.592$   $\text{min}$ ) for the reaction.

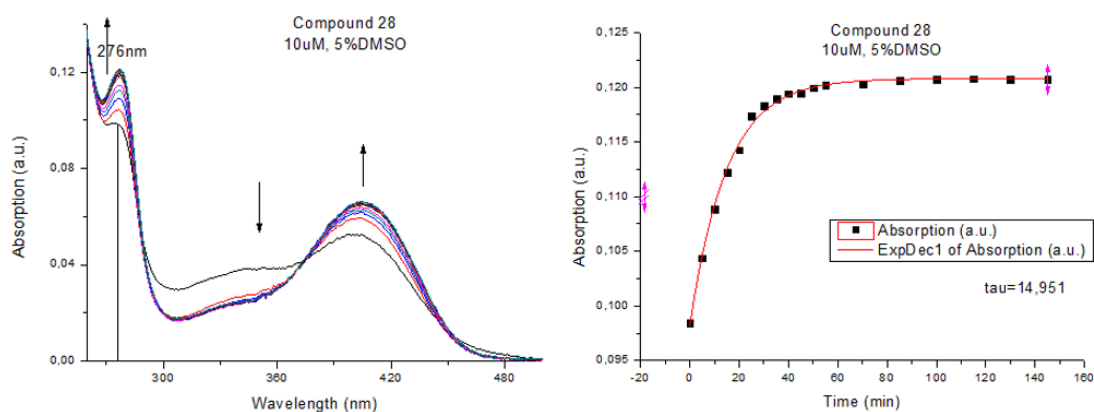


**Figure A.23:** Molecular transition of compound **28** ( $10 \mu\text{M}$ ) in 5% DMSO monitored using UV-vis spectroscopy at room temperature (*ca.*  $22^\circ\text{C}$ ) immediately after compound addition from a concentrated DMSO stock into  $50 \text{ mM}$  Tris-HCl ( $100 \text{ mM}$  NaCl) buffer. Left panel: Temporal spectral evolution. Right panel: Absorption at  $276 \text{ nm}$  (black squares) as a function of time. A first-order exponential fit (red line) rendered a time constant ( $\tau = 14.951 \text{ min}$ ) for the reaction.

## A.5 Absorption Emission

**Table A.2:** Fluorescent properties of all compounds

Compound	Absorption at $\lambda_{exc}$ [a.u.]	$\lambda_{exc}$ [nm]	$\lambda_{em}$ [nm]	Maximum intensity [a.u.]	Exc. & emis. slits' opening [nm]	% DMSO
1	0.0815	398	546	100,8	10	5
5	0.0471	293	358	92	10	5
8	0.0747	308	392	908	5	5
9	0.1439	288	350	141,96	10	5
12	0.0500	381	501	18,8	10	5
13	0.0382	357	493	32	10	5
14	0.0414	357	493	37	10	5
15	0.0565	398	511	43	10	5
17	0.2164	383	-	-	10	5
23	0.2188	336	547	11,5	10	100
24	0.3848	352	534	31,4	10	100
26	0.0935	400	517	239,2	10	5
28	0.0614	393	510	65	10	5

## A.6 Molar absorptivity

Table A.3: Molar absorptivity values for compounds **9**, **14**, **17**, **26**, **28**

Substance	Molar Absorptivity, $\epsilon$ [ $M^{-1}cm^{-1}$ ]	Wavelength [nm]
9	10745	269
14	2233	425
17	9778	382
26	5685	404
28	4621	406

## A.7 Nuclear Magnetic Resonance

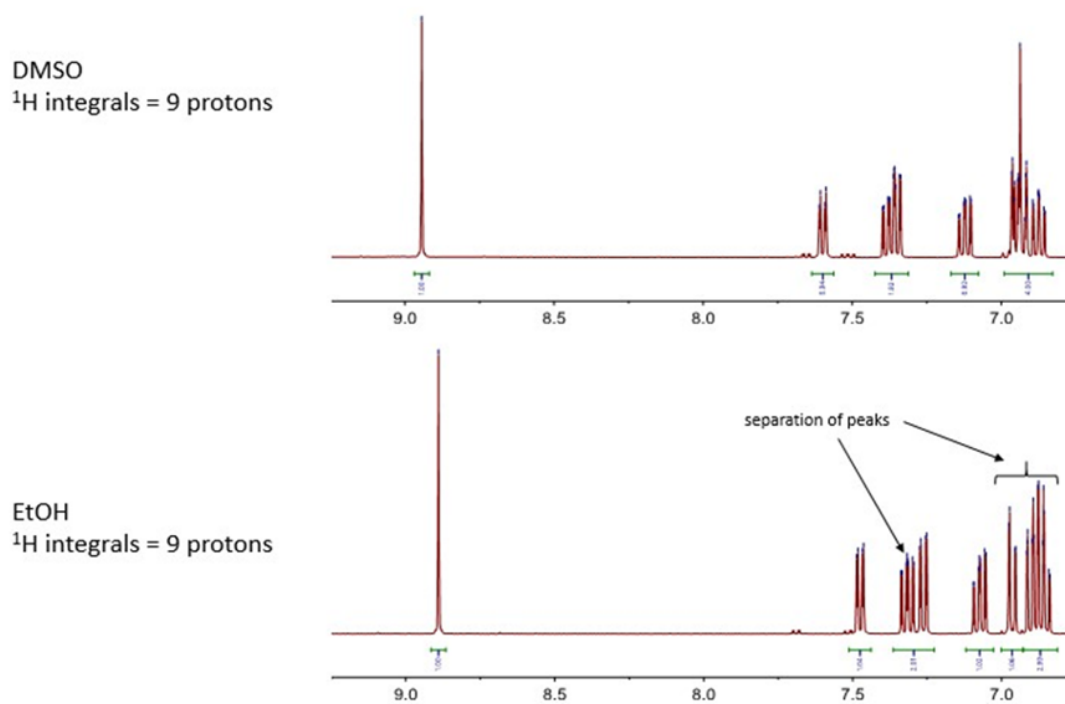
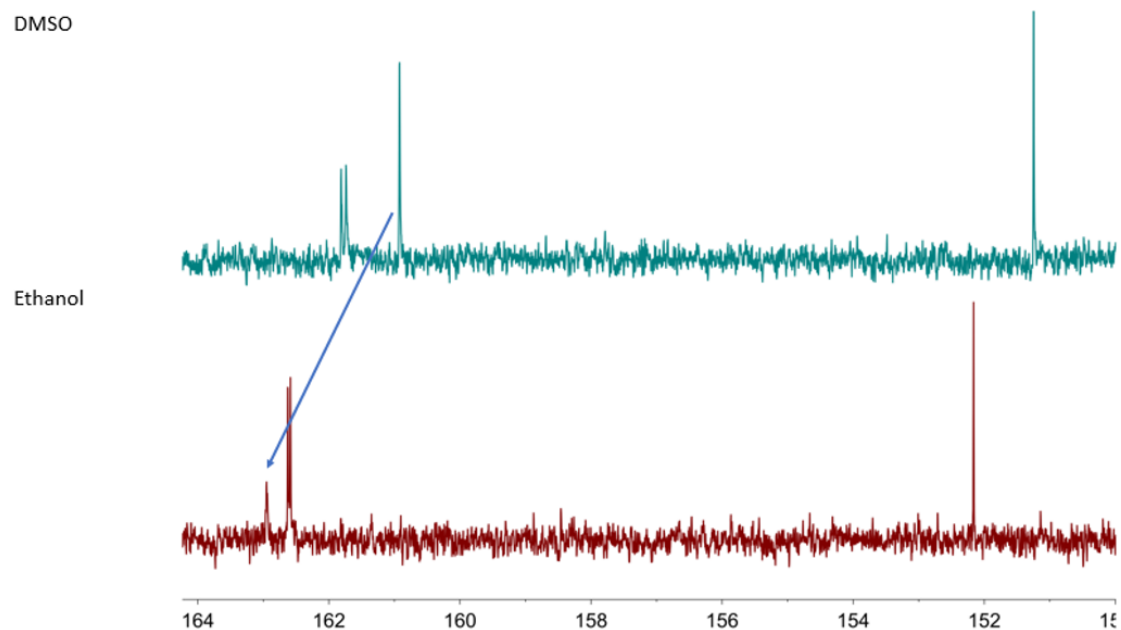


Figure A.24: Proton NMR integration of peaks



**Figure A.25:** Carbon NMR chemical shift maximized

**Table A.4:** Carbon and HSQC NMR peak values for compound **15** in DMSO

a/a.	<sup>13</sup> C-NMR	HSQC	
	<sup>13</sup> C (ppm)	<sup>13</sup> C (ppm)	<sup>1</sup> H (ppm)
1	116,67	116,76	6,95
2	116,89	116,92	6,92
3	118,96	118,96	6,93
4	119,64	119,73	7,34
5	119,86	119,89	6,87
6	128,3	128,3	7,12
7	132,44	132,52	7,6
8	133,12	133,1	7,38
9	135,03	161,79	8,94
10	151,25		
11	160,92		
12	161,74		
13	161,81		

**Table A.5:** Carbon and HSQC NMR peak values for compound **15** in ethanol

a/a.	<sup>13</sup> C-NMR	HSQC	
	<sup>13</sup> C (ppm)	<sup>13</sup> C (ppm)	<sup>1</sup> H (ppm)
1	117,29	117,3	6,97
2	117,88	117,85	6,91
3	119,27	119,3	6,88
4	120,58	120,6	6,86
5	120,84	120,84	7,26
6	128,55	128,56	7,07
7	133,08	133,09	7,49
8	133,49	133,49	7,32
9	135,99	162,48	8,9
10	151,99		
11	162,42		
12	162,45		
13	162,78		

## A.8 DNA binding

### A.8.0.1 Emission Kinetics of compound 15

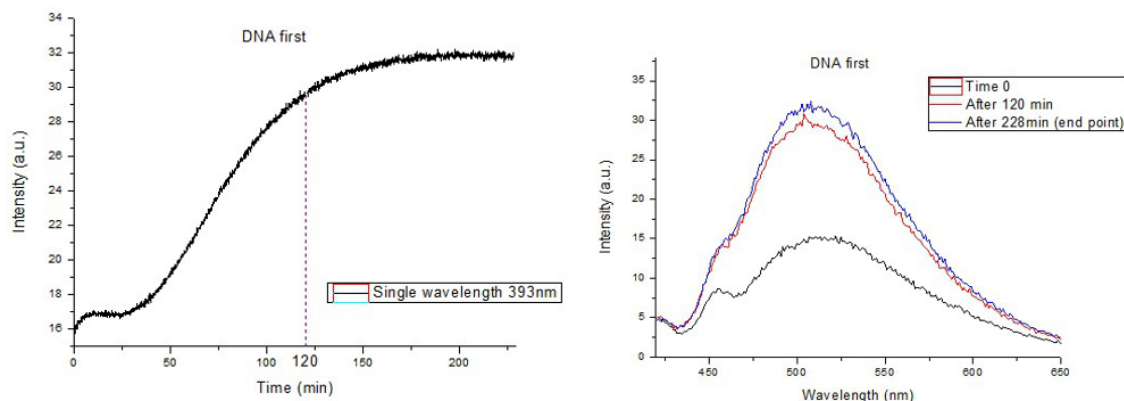


**Figure A.26:** Left panel: Emission kinetics adding DNA prior to compound **15** addition (*i.e.* "DNA first"), 15  $\mu\text{M}$ , exciting at  $\lambda_{exc} = 393 \text{ nm}$  and recording emission at  $\lambda_{em} = 512 \text{ nm}$ . Right panel: Emission spectra at: time 0 (before the emission kinetics recording started, black line), 120 *min* after the emission kinetics initiated (red line) and after 228 *min* (endpoint, blue line). Emission peak at  $\lambda_{em} = 512 \text{ nm}$

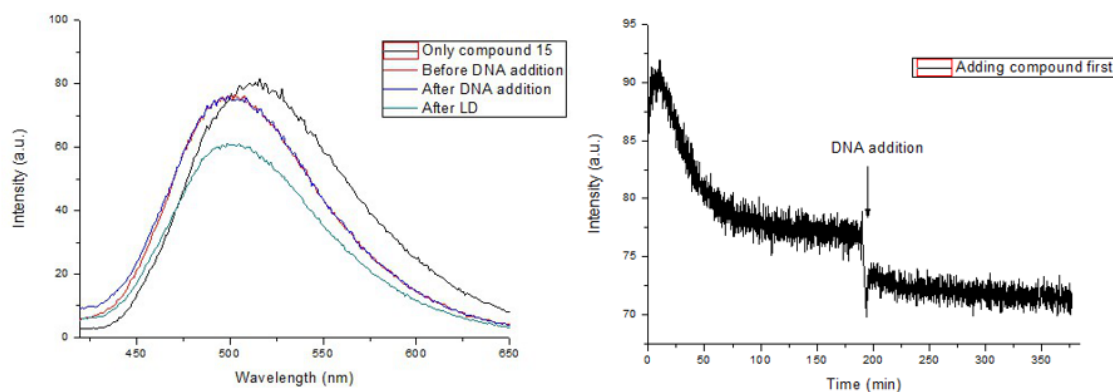


**Figure A.27:** Left panel: Emission spectra: *i*) black line: only compound **15** was present in 50 *mM* Tris HCl (100 *mM* NaCl) buffer. Emission peak at  $\lambda_{em} = 512 \text{ nm}$ , *ii*) red line: only compound **15** in buffer after thermodynamical equilibrium was established ( $t = 185 \text{ min}$ , Shift in emission peak is observed from  $\lambda_{em} = 512 \text{ nm}$  to  $\lambda_{em} = 501 \text{ nm}$ , *iii*) blue line: 200  $\mu\text{M}$  of DNA was added. No changes in emission intensity are observed. Emission peak at  $\lambda_{em} = 501 \text{ nm}$ , *iv*) after linear dichroism spectroscopy took place (approximately 200 *min* after DNA was added in solution. Emission peak at  $\lambda_{em} = 501 \text{ nm}$ . Right panel: Emission kinetics adding compound **15**, 100  $\mu\text{M}$  prior to DNA addition, exciting at  $\lambda_{exc} = 393 \text{ nm}$  and recording at  $\lambda_{em} = 512 \text{ nm}$

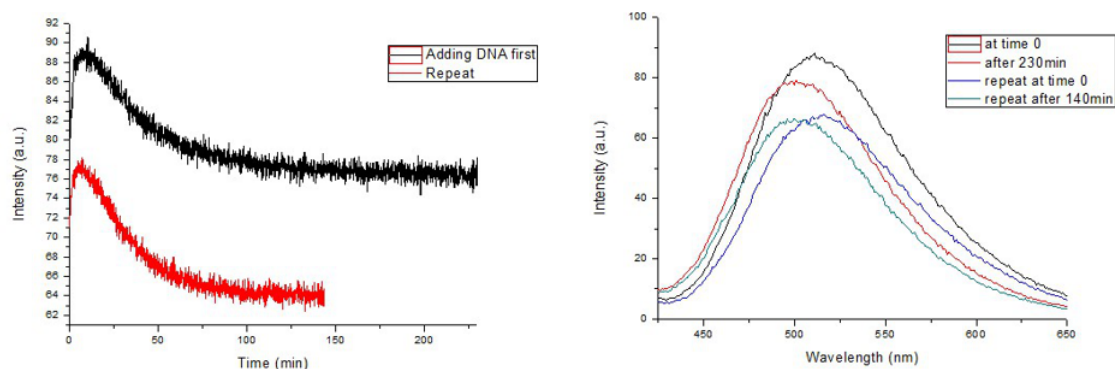


**Figure A.28:** Left panel: Emission kinetics adding  $200 \mu\text{M}$  DNA, prior to  $100 \mu\text{M}$  (black line) and *ca.*  $85 \mu\text{M}$  (red line) of compound **15** addition. Exciting at  $\lambda_{exc} = 393 \text{ nm}$  and recording at  $\lambda_{em} = 512 \text{ nm}$ . The experiment was performed twice to confirm the repeatability of the results. The same pattern in emission intensity changes is recorded, as an initial increase and afterwards a gradual decrease in intensity is observed, until the thermodynamical equilibrium is established after *ca.*  $100 \text{ min}$ . Right panel: Emission intensity spectra of the two samples. The black and red lines correspond to the sample with concentration equal to  $100 \mu\text{M}$  of **15**, at time 0 (before the emission kinetics were initiated) and  $230 \text{ min}$  after the kinetics were initiated and the thermodynamical equilibrium was established (endpoint), respectively. Shift in emission peak from  $\lambda_{em} = 512 \text{ nm}$  to  $\lambda_{em} = 501 \text{ nm}$  and decrease in emission intensity are observed. The blue and green lines correspond to the sample with concentration equal to approximately  $85 \mu\text{M}$  of **15**, at time 0 (before the emission kinetics were initiated) and  $140 \text{ min}$  after the kinetics were initiated and the thermodynamical equilibrium was established (endpoint), respectively. Shift in emission peak from  $\lambda_{em} = 512 \text{ nm}$  to  $\lambda_{em} = 501 \text{ nm}$  and decrease in emission intensity are observed.

### A.8.1 Linear Dichroism Spectra

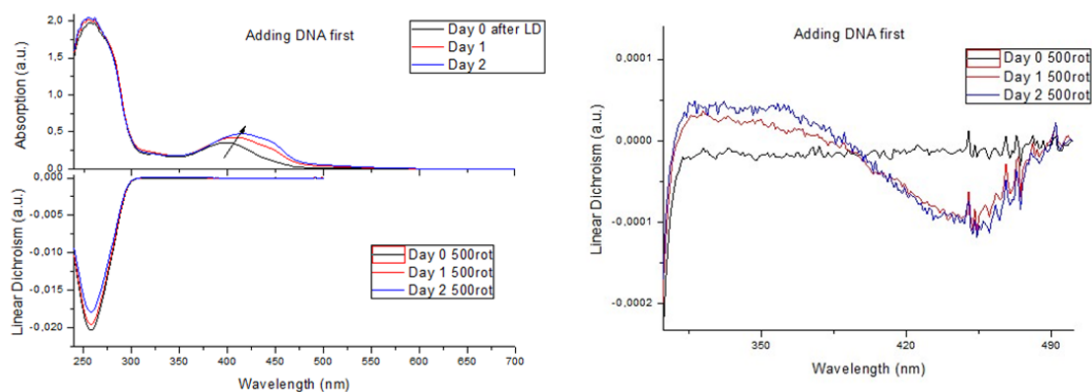


**Figure A.29:** Absorption and LD spectra of compound **15**, 100  $\mu\text{M}$  adding 200  $\mu\text{M}$  DNA prior to compound addition. Left panel: Shift in absorption is observed 2 days after the sample was prepared. Right panel: Magnified image of LD spectra illustrated on the left panel, wavelengths range from 320  $\text{nm}$  to 410  $\text{nm}$

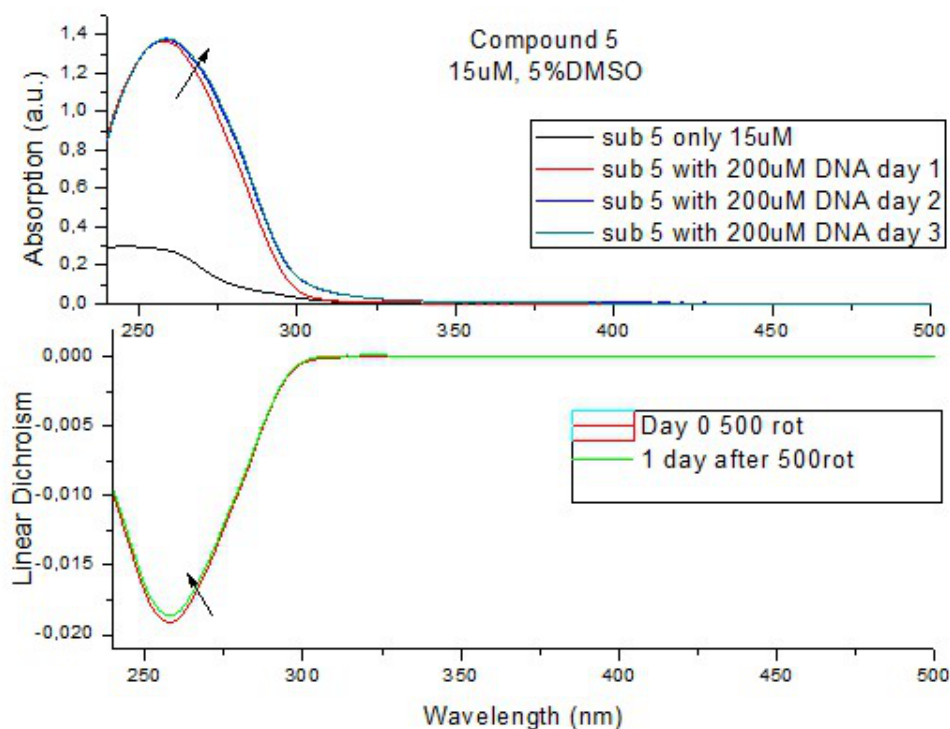


**Figure A.30:** Absorption and LD spectra of compound **5**, 15  $\mu\text{M}$ , in Tris-HCl buffer, 5% DMSO and 200  $\mu\text{M}$  of DNA

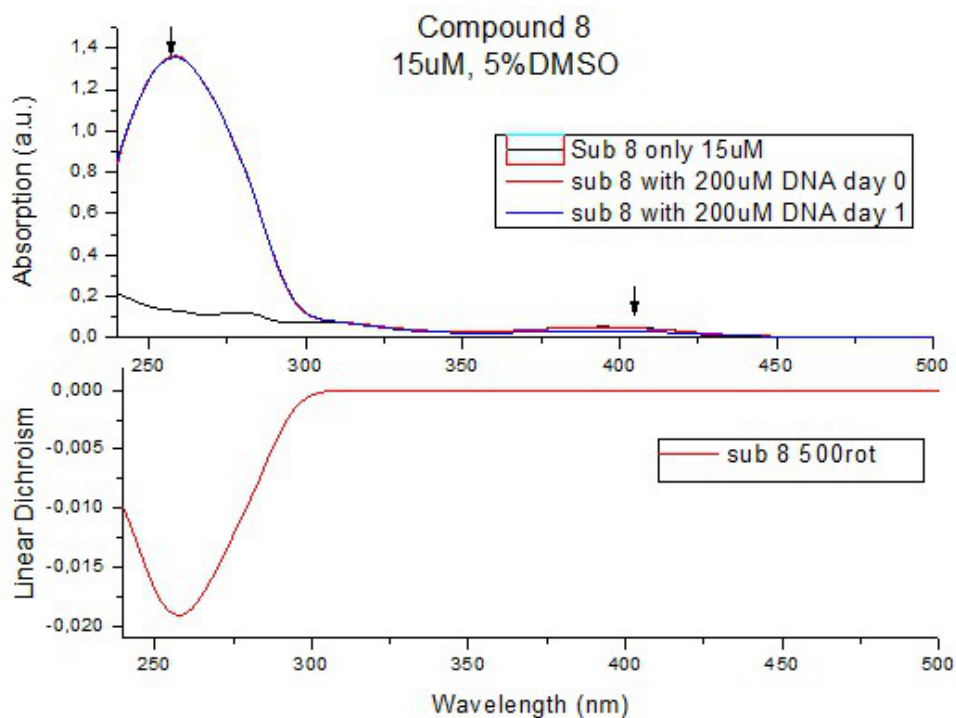


**Figure A.31:** Absorption and LD spectra of compound **8**, 15  $\mu\text{M}$ , in Tris-HCl buffer, 5% DMSO and 200  $\mu\text{M}$  of DNA

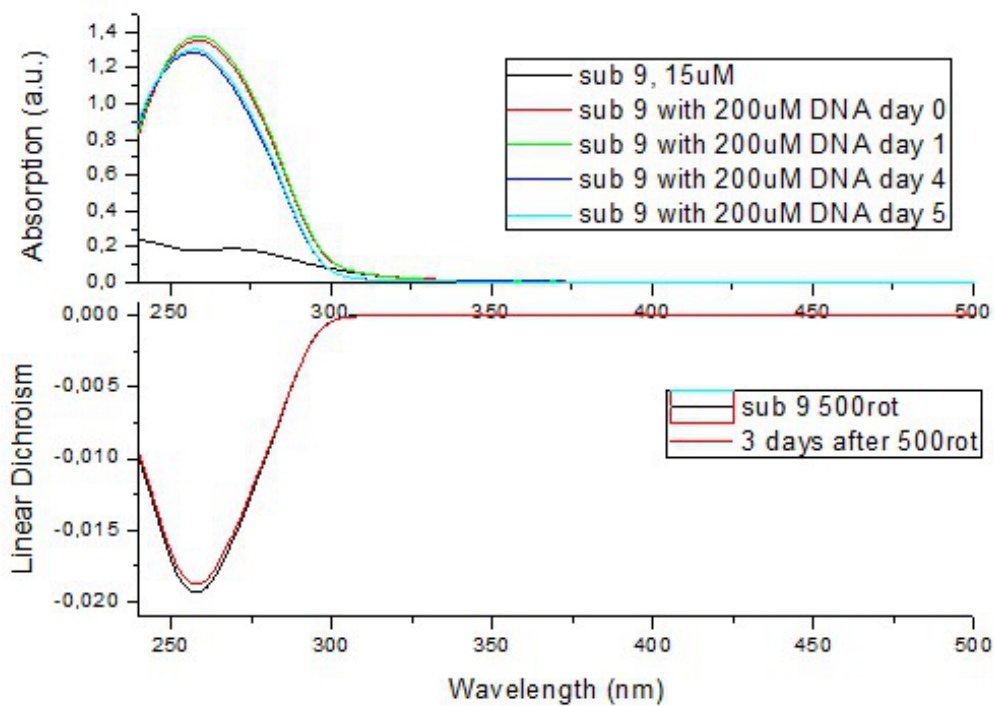


**Figure A.32:** Absorption and LD spectra of compound **9**, 15  $\mu\text{M}$ , in Tris-HCl buffer, 5% DMSO and 200  $\mu\text{M}$  of DNA

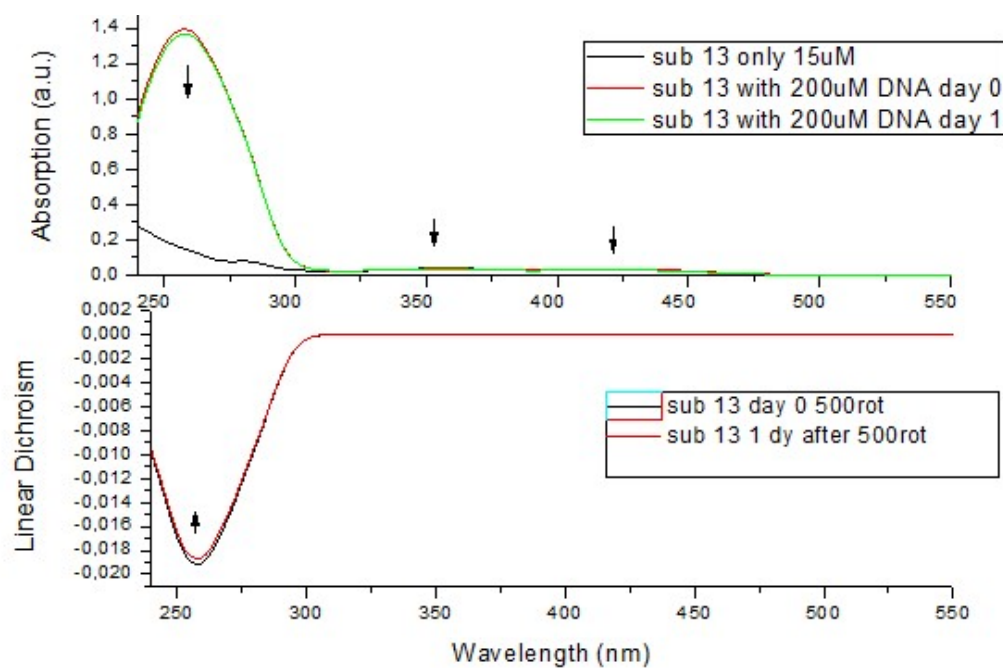


**Figure A.33:** Absorption and LD spectra of compound **13**, 15  $\mu\text{M}$ , in Tris-HCl buffer, 5% DMSO and 200  $\mu\text{M}$  of DNA

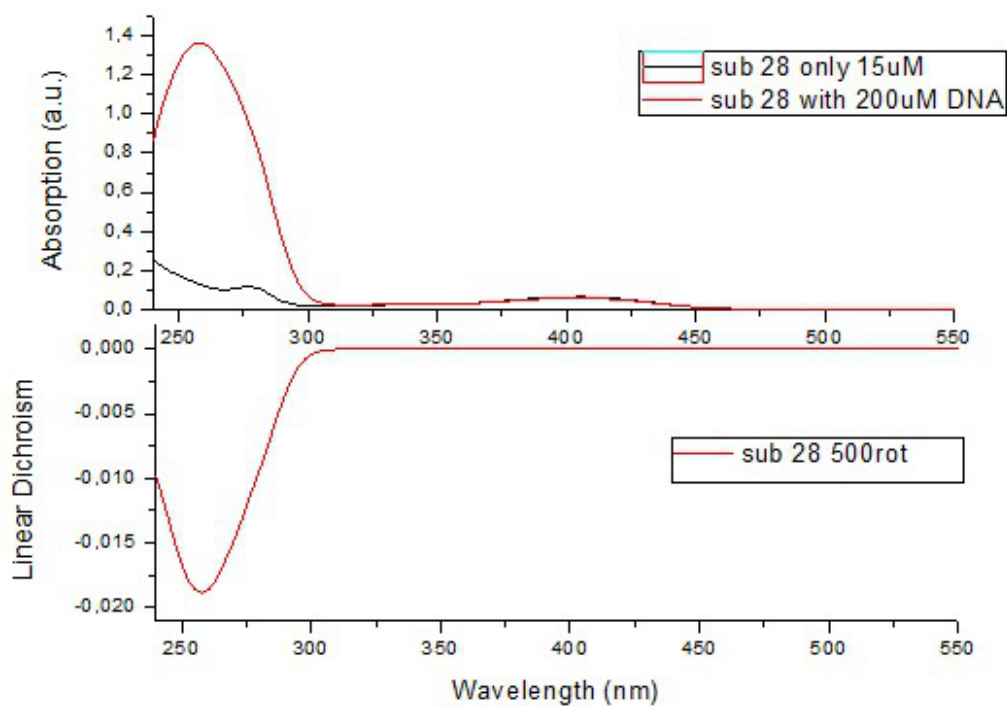


**Figure A.34:** Absorption and LD spectra of compound **28**, 15  $\mu\text{M}$ , in Tris-HCl buffer, 5% DMSO and 200  $\mu\text{M}$  of DNA